



Publicly Accessible Penn Dissertations


1-1-2014

A Microfluidic Approach for Investigating the Role of Intrathrombus Transport in Thrombosis and Hemostasis

Ryan W. Muthard

University of Pennsylvania, rwm5024@gmail.com

Follow this and additional works at: <http://repository.upenn.edu/edissertations>

 Part of the [Biophysics Commons](#), [Chemical Engineering Commons](#), and the [Physiology Commons](#)

Recommended Citation

Muthard, Ryan W., "A Microfluidic Approach for Investigating the Role of Intrathrombus Transport in Thrombosis and Hemostasis" (2014). *Publicly Accessible Penn Dissertations*. 1382.
<http://repository.upenn.edu/edissertations/1382>

This paper is posted at ScholarlyCommons. <http://repository.upenn.edu/edissertations/1382>
For more information, please contact libraryrepository@pobox.upenn.edu.

A Microfluidic Approach for Investigating the Role of Intrathrombus Transport in Thrombosis and Hemostasis

Abstract

Biological and physical factors interact to modulate blood response in a wounded vessel, resulting in a hemostatic clot or an occlusive thrombus. Wall shear stress (τ_w) and pressure differential (ΔP) across the wound from the lumen to the extravascular compartment may impact hemostasis. This thesis describes the design of a microfluidic device capable of flowing human blood over a side channel plugged with collagen (\pm tissue factor) while independently controlling ΔP and τ_w . Using this device we were able to investigate the impact of physiologic hemodynamics on the growth and architecture of human blood clots. Our results revealed that both wall shear rate and the transthrombus pressure gradient govern clot development leading to the formation of two distinct intrathrombus regions; a core of highly-activated platelets and fibrin covered by a shell of less-activated platelets. These regions mimic the activation gradients of clots formed *in vivo*. We demonstrated that core development was dependent on the transthrombus pressure gradient restricting thrombin localization while shell development was dependent on wall shear rates. We also found that fibrin polymerization inhibited thrombin activity at both arterial and venous shear rates. However, the mechanism of this inhibition is shear dependent. At venous shears thrombin activity is inhibited by γ -fibrin(ogen) binding. While at arterial and pathological shear rates the clot forms a more dense structure leading to physical trapping of thrombin independent of γ -fibrin(ogen) binding. Taken together our data supports a model where clot architecture is maintained under various conditions by shear-specific thrombin inhibition mechanisms. Lastly, we demonstrated that the prevailing hemodynamics dilute ADP and thromboxane to regulate platelet contractility, a newly defined flow sensing mechanism to regulate clot function.

The field of *in vitro* hemostasis and thrombosis research has lacked an assay capable of independently studying the effects of ΔP and local τ_w on clot development and function. Our microfluidic device bridges this gap, while providing new insights into the mechanisms of hemostasis and thrombosis, where hemostatic clot development must balance both thrombotic and hemorrhagic risks in order to rapidly and controllably cease bleeding.

Degree Type

Dissertation

Degree Name

Doctor of Philosophy (PhD)

Graduate Group

Chemical and Biomolecular Engineering

First Advisor

Scott L. Diamond

Subject Categories

Biophysics | Chemical Engineering | Physiology

A MICROFLUIDIC APPROACH FOR INVESTIGATING THE ROLE OF INTRATHROMBUS TRANSPORT IN THROMBOSIS AND HEMOSTASIS

Ryan William Muthard

A DISSERTATION

in

Chemical and Biomolecular Engineering

Presented to the Faculties of the University of Pennsylvania

in

Partial Fulfillment of the Requirements for the

Degree of Doctor of Philosophy

2014

Supervisor of Dissertation

Scott L. Diamond

Professor, Chemical and Biomolecular Engineering

Graduate Group Chairperson

Raymond J. Gorte, Professor, Chemical and Biomolecular Engineering

Dissertation Committee

Lawrence F. Brass, Professor, Department of Medicine

Talid R. Sinno, Professor, Department of Chemical and Biomolecular Engineering

Matthew J. Lazzara, Assistant Professor, Department of Chemical and Biomolecular Engineering

A MICROFLUIDIC APPROACH FOR INVESTIGATING
THE ROLE OF INTRATHROMBUS TRANSPORT IN
THROMBOSIS AND HEMOSTASIS

COPYRIGHT

2014

Ryan W. Muthard

ACKNOWLEDGEMENT

For over four years I have been privileged to be mentored, taught, and supported by so many wonderful people. I would like to begin by thanking and recognizing my advisor, Dr. Scott Diamond. I am forever grateful to him for teaching and mentoring me to be a successful and professional researcher. He has the rare ability to conduct research, teach, and mentor at a world renowned level. I have been fortunate to grow as both an engineer and person under his tutelage. I would also like to thank my committee, Dr. Lawrence Brass, Dr. Matthew Lazzara, and Dr. Talid Sinno. I am privileged to have had the opportunity to learn from these three respected leaders in their fields. Their diverse and expert skillsets will continue to have a positive influence on my future as a chemical engineer. I also owe a lot of thanks to all past and current Diamond lab members, particularly those that I have been fortunate to work with closely, Dr. Thomas Colace, Dr. Roman Voronov, John Welsh, Viraj Kamat, Richard Li, and Huiyan Jing. Your guidance and advice has contributed to the success of a lot of the projects in this thesis. The same thanks to Dr. Tim Stalker and Dr. Maurizio Tomaiuolo, with whom I have had many insightful and productive conversations.

A special mention must be made to all of my family and friends that have supported me throughout my academic journey. In particular, I would like to thank my parents. I would not be the person I am today without the care and love they have given me. They taught me how to be responsible, work hard and respect others. I would also like to extend thanks to my aunts, uncles, and fiancé's parents. Their generosity and encouragement have never faltered through the good and bad times. I have been

incredibly fortunate to have them and my parents as a part of my support system. For that, I am eternally grateful. Finally, I would like to give a special thank you to my fiancé Dallas for her overwhelming support. Her work ethic, affectionate personality, and compassion for others have been an inspiration for me since the day that I met her. She continues to motivate me to be a better person. I can never thank her enough for being there when I needed her as a listener, distraction, or best friend.

ABSTRACT

A MICROFLUIDIC APPROACH FOR INVESTIGATING THE ROLE OF INTRATHROMBUS TRANSPORT IN THROMBOSIS AND HEMOSTASIS

Ryan W. Muthard

Scott L. Diamond

Biological and physical factors interact to modulate blood response in a wounded vessel, resulting in a hemostatic clot or an occlusive thrombus. Wall shear stress (τ_w) and pressure differential (ΔP) across the wound from the lumen to the extravascular compartment may impact hemostasis. This thesis describes the design of a microfluidic device capable of flowing human blood over a side channel plugged with collagen (\pm tissue factor) while independently controlling ΔP and τ_w . Using this device we were able to investigate the impact of physiologic hemodynamics on the growth and architecture of human blood clots. Our results revealed that both wall shear rate and the transthrombus pressure gradient govern clot development leading to the formation of two distinct intrathrombus regions; a core of highly-activated platelets and fibrin covered by a shell of less-activated platelets. These regions mimic the activation gradients of clots formed *in vivo*. We demonstrated that core development was dependent on the transthrombus pressure gradient restricting thrombin localization while shell development was dependent on wall shear rates. We also found that fibrin polymerization inhibited thrombin activity at both arterial and venous shear rates. However, the mechanism of this inhibition is shear dependent. At venous shears thrombin activity is inhibited by γ^2 -fibrin(ogen) binding. While at arterial and pathological shear rates the clot forms a more dense structure leading to physical trapping of thrombin independent of γ^2 -fibrin(ogen)

binding. Taken together our data supports a model where clot architecture is maintained under various conditions by shear-specific thrombin inhibition mechanisms. Lastly, we demonstrated that the prevailing hemodynamics dilute ADP and thromboxane to regulate platelet contractility, a newly defined flow sensing mechanism to regulate clot function.

The field of *in vitro* hemostasis and thrombosis research has lacked an assay capable of independently studying the effects of ΔP and local τ_w on clot development and function. Our microfluidic device bridges this gap, while providing new insights into the mechanisms of hemostasis and thrombosis, where hemostatic clot development must balance both thrombotic and hemorrhagic risks in order to rapidly and controllably cease bleeding.

TABLE OF CONTENTS

ACKNOWLEDGEMENT	III
ABSTRACT	V
TABLE OF CONTENTS	VII
LIST OF ILLUSTRATIONS	X
CHAPTER 1 : INTRODUCTION	1
1.1 Hemostasis	1
1.1.1 Platelets	1
1.1.2 Blood Coagulation	3
1.1.3 Vasculature.....	4
1.2 Thrombosis	5
1.3 Transport in Hemostasis	6
1.3.1 Hemodynamics.....	6
1.3.2 Porous Media Transport	9
1.4 Experimental Techniques for Hemostasis Under Physiologic Conditions	11
CHAPTER 2 : SIDE VIEW THROMBOSIS MICROFLUIDIC DEVICE WITH CONTROLLABLE WALL SHEAR RATE AND TRANSTHROMBUS PRESSURE GRADIENT	13
2.1 Introduction	13
2.2 Materials and Methods	14
2.2.1 Device Fabrication and Design	14
2.2.2 Device Operation	18
2.2.3 Device Validation	23
2.2.4 Blood Collection	23
2.2.5 Finite Element Analysis	24
2.3 Results	25
2.3.1 Controllable transcollagen scaffold ΔP in a side view thrombosis device	25
2.3.2 Transthrombus permeation reduces the intrathrombus zone of thrombin activity	30
2.3.3 Pressure gradients affect thrombus composition and size	35
2.3.4 Fluorescent dye transport allows thrombus permeability measurement.....	38
2.4 Discussion	41

2.5 Conclusions	43
------------------------------	-----------

CHAPTER 3 : BLOOD CLOTS ARE RAPIDLY ASSEMBLED HEMODYNAMIC SENSORS: FLOW ARREST TRIGGERS INTRALUMINAL THROMBUS CONTRACTION

3.1 Introduction	44
-------------------------------	-----------

3.2 Materials and Methods	45
--	-----------

3.2.1 Reagents	45
3.2.2 Blood Collection	46
3.2.3 Permeation device design and manufacture	46
3.2.4 Microfluidic device for thrombus permeation.....	49
3.2.5 Permeability Measurements	50
3.2.6 Contraction Measurements.....	50
3.2.7 Finite Element Analysis	51
3.2.8 Statistics	52

3.3 Results	53
--------------------------	-----------

3.3.1 Microfluidic device for measuring clot permeability and contractility	53
3.3.2 Stopping flow caused platelet and clot retraction.....	55
3.3.3 Permeability of collagen, platelet deposits, and platelet-fibrin thrombus without flow interruption	60
3.3.4 Clot retraction in a rigid wall flow device with flow reduction or cessation	63
3.3.5 Intracellular calcium mobilization is triggered by ADP and TXA ₂ after flow cessation	67

3.4 Discussion	71
-----------------------------	-----------

CHAPTER 4 : FIBRIN, γ '-FIBRINOGEN, AND TRANS-CLOT PRESSURE GRADIENT CONTROL HEMOSTATIC CLOT GROWTH DURING HUMAN BLOOD FLOW OVER A COLLAGEN/TISSUE FACTOR WOUND

4.1 Introduction	78
-------------------------------	-----------

4.2 Materials and Methods	80
--	-----------

4.2.1 Materials	80
4.2.2 Blood Collection	80
4.2.3 Microfluidic device for control of wall shear rate and trans-clot ΔP	81
4.2.4 Fibrin polymerization and γ ' fibrin(ogen) inhibition	85
4.2.5 Mouse cremaster arteriole laser injury model	85
4.2.6 Image processing.....	87
4.2.7 Statistics	87

4.3 Results	87
--------------------------	-----------

4.3.1 Microfluidic device for investigating clot architecture at controlled wall shear rates and transthrimbus pressure gradients	87
4.3.2 Transthrimbus pressure gradients influence thrombin mediated clot growth at 400 s ⁻¹	90
4.3.3 Fibrin polymerization reduces both total platelet and core area at 400 s ⁻¹	92
4.3.4 Wall shear rate does not influence the core or thrombin area but does influence the role of fibrin .96	

4.3.5 γ' fibrin(ogen) reduces thrombin mediated clot growth at venous shear rates but not arterial shear rates.....	99
4.3.6 Arterial shear rates promote increased platelet packing, greater thrombin retention, and more fibrin generation per area than venous shear rates	102
4.3.7 Fibrin polymerization reduces clot growth at pathological shear rates	104
4.4 Discussion.....	107
 CHAPTER 5 : RAPID ON-CHIP RECALCIFICATION AND DRUG DOSING OF CITRATED WHOLE BLOOD USING MICROFLUIDIC SHEATH FLOW	
5.1 Introduction	114
5.2 Materials and Methods	116
5.2.1 Fabrication	116
5.2.2 Design	116
5.2.3 Blood Collection	118
5.2.4 Operation.....	118
5.2.5 Finite Element Analysis	120
5.3 Results	121
5.3.1 Diffusion controlled recalcification of citrated whole blood.....	121
5.3.2 Recalcification of citrated whole blood under flow recovers platelet and coagulation function....	126
5.3.3 Intrinsic generation of factor XIIa primed platelet and coagulation activity in citrated whole blood	131
5.3.4 Single channel IC50 measurement of MRS-2179 under flow.....	133
5.4 Discussion.....	136
5.4 Conclusions	138
 CHAPTER 6 : FUTURE WORK.....	
6.1 Effect of platelet contraction on clot growth	140
6.2 Model for evaluating the effect of inflammation on clotting	143
 BIBLIOGRAPHY	 149

LIST OF ILLUSTRATIONS

Figure 2-1	A microfluidic device with controllable trans-scaffold pressure gradients.	17
Figure 2-2	A LabVIEW program to measure and control microfluidic pressure gradients. ...	20
Figure 2-3	A customized LabVIEW interface for controlling syringe pump flow rates to maintain a pressure gradient set point.	21
Figure 2-4	A LabVIEW block diagram utilized to control a Harvard Apparatus PHD 2000 syringe pump.	22
Figure 2-5	Human type I, polymerized collagen localized in the scaffold region.	28
Figure 2-6	Syringe pump control allows rapid responses to changes in pressure set point and fluid viscosity.	29
Figure 2-7	Perfusion of anti-coagulated whole blood provides reproducible thrombus development at the collagen-blood interface.....	32
Figure 2-8	Increasing transthrimbus pressure gradients caused a reduction in thrombin.	33
Figure 2-9	Clots formed in the microfluidic injury model we present illustrate remarkable correspondence to in vivo hierarchical clot architectures found in mouse.....	34
Figure 2-10	Transthrimbus pressure gradients effect dynamic measurements such as clot structure, wall shear stress and height.	37
Figure 2-11	Platelet and platelet/fibrin clot permeability was measured by pulsing fluorescent dyes.....	40
Figure 3-1	Microfluidic device to independently control blood flow and transthrimbus pressure drop.	48
Figure 3-2	A microfluidic device to control transthrimbus pressure drop independent of shear rate.	54
Figure 3-3	Flow arrest triggers clot contraction.....	57

Figure 3-4	Clot permeability.....	58
Figure 3-5	Spatiotemporal variation of contraction with flow arrest.....	59
Figure 3-6	Transthrombus pressure drop affects platelet deposition.....	62
Figure 3-7	Contraction after flow arrest requires myosin and released ADP/TXA ₂	65
Figure 3-8	Platelet flow sensing occurs when arterial flow is reduced to venous flow.....	66
Figure 3-9	Flow cessation triggers platelet intracellular calcium mobilization via ADP/TXA ₂ autocrine signaling.....	69
Figure 3-10	Treating platelet deposits with ADP and TXA ₂ antagonist caused a significant decrease in contraction rate following the cessation of flow.....	70
Figure 3-11	Blebbistatin, a myosin IIA inhibitor, reduced contraction rates before and after flow cessation.....	75
Figure 3-12	Platelet contraction is dependent on local hemodynamic flow conditions.....	76
Figure 3-13	Reestablished flow dampens contraction mediated by temporary flow interruption.....	77
Figure 4-1	Independent pressure control was achieved in three channels simultaneously.....	84
Figure 4-2	Thrombus architecture was investigated in a microfluidic device capable of independently controlling transthrombus pressure gradients and wall shear rates.....	89
Figure 4-3	Transthrombus pressure gradients reduce clot size by diminishing thrombin boundary growth.....	91
Figure 4-4	Fibrin polymerization reduces clot growth at a wall shear rate of 400 s ⁻¹ and ΔP=20 mm Hg.....	94
Figure 4-5	GPRP has no effect on the total clot or P-selectin (core) area when thrombin is inhibited.....	95

Figure 4-6	Wall shear rate does not change the core or thrombin area but does influence thrombin mediated clot growth in the absence of fibrin polymerization.....	98
Figure 4-7	γ' -fibrinogen binds more thrombin and is inhibited to a greater extent than γ A-fibrinogen (free of the γ' -chain).	100
Figure 4-8	Inhibition of γ' fibrin(ogen) with a γ' specific monoclonal antibody results in larger clots at venous but not arterial shear rates.....	101
Figure 4-9	Clots formed at arterial shear rates pack tighter, cleave more thrombin sensitive peptide per area, and generate more fibrin per area than venous clots.....	103
Figure 4-10	Clot growth at pathological shear rates was abated by fibrin polymerization.....	106
Figure 4-11	Human thrombi develop a core and shell architecture that mimic the architecture of clots developed in vivo.....	113
Figure 5-1	A trifurcated microfluidic device to recalcify citrated whole blood under flow.	123
Figure 5-2	Whole blood sheathed in buffer experienced a constant wall shear rate.....	124
Figure 5-3	FITC and BSA line scans within the trifurcation channel.....	125
Figure 5-4	Whole blood recalcified under flow recovers platelet and coagulation function.	128
Figure 5-5	Buffer sheath flows eliminate corner effects on clot formation.	129
Figure 5-6	Recalcification is required for proper platelet and coagulation function.	130
Figure 5-7	Incubation of citrated whole blood primed platelet and coagulation activity via factor XIIa.	132
Figure 5-8	Single channel IC50 measurement.	135
Figure 6-1	Clot contraction reduces total clot height and increases the % P-selectin positive area of the clot.	142
Figure 6-2	Plasma perfusion through blood clots is required for white blood cell chemotaxis towards the injury site.	147

Figure 6-3 LPS embedded in a collagen/TF scaffold induces larger clot growth at venous shear rates. 148

Chapter 1 : Introduction

1.1 Hemostasis

1.1.1 Platelets

Platelets are anucleate cells that are responsible for hemostasis, or the cessation of bleeding. The process in which platelets are produced is termed megakaryopoiesis. In this process, megakaryocytes are derived from hematopoietic stem cells primarily within the bone marrow. Following proliferation and differentiation, megakaryocytes go through a maturation process that ends with the release of new platelets into the circulation [1]. Healthy whole blood typically contains 150,000-400,000 platelets per microliter [2]. Human platelets in an unactivated state are typically 2-3 μm in diameter and have a disk shape [3]. In the presence of platelet agonists, such as collagen or thrombin, platelets become activated through agonist specific surface receptors. Activation causes an increase in intracellular calcium resulting in a conformational change in the platelet cytoskeleton due to interactions between myosin II and actin filaments [4]. In addition to shape change, platelet activation also initiates secretion of soluble agonists such as adenosine diphosphate (ADP) and thromboxane A₂ (TXA₂) [5]. This autocrine process is important for the recruitment of additional platelets and the stabilization of deposited platelets during the formation of a stable clot. The timeline of platelet activation, shape change, and agonist secretion have been studied extensively in both single platelet and clot formation.

In terms of hemostatic clot growth, initial platelet adhesion and subsequent aggregation are required for platelet plug formation. Under flow conditions, platelets

initially adhere to the site of injury by binding to collagen and/or von Willebrand factor (vWF). The initial adhesion of platelets is mediated through receptors $\alpha_2\beta_1$ and GPVI for collagen and $\alpha\text{IIb}\beta_3$ and GPIb for vWF [6]. Following firm adhesion and platelet activation, secretion of ADP and TXA_2 help recruit additional platelets to the site of injury. The release of these agonist also help activate integrin $\alpha\text{IIb}\beta_3$, a critical integrin for platelet aggregation. The conformational change of $\alpha\text{IIb}\beta_3$ to its active state facilitates the binding of fibrinogen and vWF. These proteins have multiple binding sites for activated $\alpha\text{IIb}\beta_3$ which enable more than one platelet to bind the same protein. This stage is known as aggregation and is vital for the extension of the clot and the cessation of bleeding [7]. While platelets are aggregating, the local accumulation of agonists increase the activation level of firmly adhered platelets. This increase in activation results in cytoskeleton rearrangement into a conformational state that anchors adjoining platelets tightly together. The contraction of both single platelets and platelets within regions of high activation securely fastens the clot to the injury site. This prevents additional bleeding by fortifying the clot, thus preventing it from being torn from the surface.

Another important aspect of platelets is their ability to provide a surface for protein binding. When platelets are activated, the surface of the platelet becomes negatively charged due to the phospholipids that are transferred from the inner membrane to the outer membrane [8]. This charge is important for the association of several proteins that are required for thrombin generation. This step is known as coagulation.

1.1.2 Blood Coagulation

Blood coagulation, another important branch of hemostasis, is required for the generation of thrombin and the formation of fibrin. In this process, proteins known as coagulation factors work in series and parallel to converge on a common pathway in order to cleave prothrombin into thrombin. The two paths in the coagulation cascade that lead to the common pathway are the intrinsic and extrinsic pathways. Both of these pathways lead to the generation of activated factor X (Factor Xa) [9, 10].

The intrinsic pathway, also known as the contact pathway, is initiated with a negatively charged surface. At the injury site, activated platelets or damaged smooth muscle cells/endothelial cells provide a negatively charged phospholipid surface that converts Factor XII to Factor XIIa. This activation step then facilitates the cleavage of Factor XI to Factor XIa. Following these events, the intrinsic tenase complex is formed by Factor IXa and its cofactor, Factor VIIIa. This complex rapidly cleaves Factor X to Factor Xa [9]. If any of these factors are deficient or are defective, the production of thrombin via the intrinsic pathway is significantly hindered. Examples of this include hemophilia A, hemophilia B, and hemophilia C, diseases in which blood is deficient in or contain defective factors VIII, IX, and XI respectively [11]. While these disorders often present with a bleeding phenotype if they are severe, the extrinsic pathway can often alleviate some of these issues.

The extrinsic pathway, also known as the tissue factor pathway, is well regarded as the dominating pathway for thrombin generation *in vivo*. The exposure of tissue factor (TF) on the cell surface initiates the extrinsic pathway at the site of vascular injury.

Circulating Factor VII associates with the cell bound TF and is then activated by one of several coagulation proteases (IIa, Xa, IXa, XIIa, VIIa-TF). Once activated, the extrinsic tenase facilitates a burst of thrombin production by rapidly cleaving Factor X to Factor Xa. In addition to Factor Xa generation, the extrinsic tenase also facilitates the cleavage of Factor IX to Factor IXa. This cleavage helps bypass the requirement of intrinsic coagulation Factors XIIa and XIa [10].

The common pathway requires Factor Xa which is generated by either or both the intrinsic and extrinsic tenase. Factor Xa associates with the activated protein cofactor, Factor Va on a negatively charged membrane surface. This complex is known as the prothrombinase complex. Following assembly, the prothrombinase can efficiently cleave prothrombin into thrombin [12]. The generation of thrombin facilitates the enzymatic cleavage of fibrinogen into fibrin monomer. As fibrin monomer is produced, it then polymerizes both laterally and longitudinally to form fibers which are important for additional clot strength and support [13]. The formation of fibrin is the primary goal of the coagulation cascade and is critical for stabilizing the developing clot and ceasing bleeding.

1.1.3 Vasculature

The vasculature also plays an important role in hemostasis. During vessel injury, smooth muscle cells contract to limit blood flow through the injured vessel. This response is mediated by endothelial cells and platelets near the site of injury. These cells release stimuli such as endothelin and TXA₂ to induce vessel constriction [14]. The drop

in flow through the vessel prevents unnecessary blood loss while maintaining a supply of platelets and coagulation proteins to facilitate proper hemostasis.

1.2 Thrombosis

An important part of the hemostatic process is the regulation of the platelet and coagulation response. If either one of these regulatory responses are dysfunctional, clot growth and/or thrombin generation may result in thrombosis, the prevention of blood flow through a vessel by an occlusive thrombus. There are two types of thrombosis, one which occurs within a vein (venous thrombosis) and one which occurs within an artery (arterial thrombosis). One of the most prevalent forms of venous thrombosis is deep vein thrombosis (DVT). Risk factors for DVT typically include immobilization, surgery, or cancer [15]. Prophylaxis is often effective and is typically achieved with anticoagulant drugs such as heparin or vitamin K antagonists [16]. Arterial thrombosis is similar to venous thrombosis with the distinction that the occlusive event occurs within an artery. The primary example of arterial thrombosis is myocardial infarction or a heart attack. This is an event which prevents blood flow to a part of the heart. Patients experiencing myocardial infarctions usually present with atherosclerosis, a chronic disease associated with a plaque buildup in the arteries [17]. The accumulation of plaque in the arterial blood vessel wall can lead to a lesion within a stenosed vessel that will eventually rupture. At the point of rupture, the narrow channel quickly becomes occluded with platelets and fibrin, preventing blood flow to the heart. Typical prophylaxis for myocardial infarctions include antiplatelet drugs, stents, and bypass surgery [18, 19].

In both conditions, one of the major concerns is that the occlusive clot may embolize, an event known as thromboembolism. This type of event is caused by a clot that breaks free from an upstream injury site and eventually becomes lodged in a downstream vessel. Thromboembolism is particular concerning in patients with DVT or myocardial infarction. If the thrombus embolizes and travels to the lungs or to the brain, the patient is at risk for pulmonary embolism or stroke respectively. Both of these conditions can be fatal. Understanding the physical and biochemical properties that regulate thrombosis and/or thromboembolism may lead to improved patient care and outcome, making this field of study critical in the research community.

1.3 Transport in Hemostasis

1.3.1 Hemodynamics

Hemodynamics is the study of circulation and the physical forces that govern blood flow. These forces vary throughout the vasculature, creating diverse environments in which platelets must respond and thrombin must be generated in order to achieve proper hemostasis. Blood is composed of red blood cells, platelets, white blood cells, and plasma. In a healthy individual, the plasma portion of blood normally makes up 55-60% of the total volume. The cells and plasma proteins in blood give it characteristics that make it a non-Newtonian fluid. In particular, blood is a shear-thinning fluid. As shear rates increases, the viscosity of blood is decreases. For simplicity, blood is often treated as a Newtonian fluid where viscosity is constant for all shear rates. This assumption is valid when shear rates are greater than 50 s^{-1} [20]. Wall shear rate is an important term in hemodynamics because it is dependent on the blood velocity and the vessel diameter.

The Navier-Stokes equation describes the velocity field for a Newtonian fluid at motion in a cylindrical vessel:

$$\text{Eqn. 1-1} \quad \rho \left(\frac{\partial v_z}{\partial t} + v_r \frac{\partial v_z}{\partial r} + \frac{v_\theta}{r} \frac{\partial v_z}{\partial \theta} + v_z \frac{\partial v_z}{\partial z} \right) = -\nabla p + \mu \left(\frac{1}{r} \frac{\partial}{\partial r} \left(r \frac{\partial v_z}{\partial r} \right) + \frac{1}{r^2} \frac{\partial^2 v_z}{\partial \theta^2} + \frac{\partial^2 v_z}{\partial z^2} \right)$$

where ρ is the fluid density, v_z is the fluid velocity in the flow direction, v_r is the fluid velocity in the radial direction, v_θ is the fluid velocity in the tangential direction, p is the pressure, and μ is the dynamic viscosity.

In the case of blood flow, the velocity of the blood through a given vessel diameter is driven by the pressure drop along the length of the vessel. An exact solution for Eqn. 1-1 can be derived to determine the mean blood velocity in terms of vessel pressure drop. The first requirement is that the flow must be fully developed, meaning that velocity is not changing in the flow direction ($\frac{\partial v_z}{\partial z} = 0$). This assumption holds true due to the laminar characteristics of blood flow. Laminar flows are more predictable and have more of a dependence on viscous force than turbulent flows, which depend more on inertial forces. When flow is laminar the entrance length containing velocity changes in the flow direction is on the order of the vessel radius [21]. This is typically much smaller than the length of the vessel. The second requirement is that the flow is steady. This means that the velocity field is not changing with time ($\frac{\partial}{\partial t} = 0$). This assumption is valid in smaller vessels such as the arterioles and venules where the pulsatility of the circulatory system is minimized [22]. In larger vessels such as the aorta or inferior vena cava, the pumping of the heart results in pulsatile flow due to the transient pressure

supply. The final assumptions are that the radial ($v_r = 0$) and tangential components ($v_\theta = 0$) of the fluid velocity are zero and flow is axisymmetric ($\frac{\partial}{\partial \theta} = 0$). These assumptions are valid for unidirectional flow, where there is no rotational component of the velocity. The laminar flow characteristics within smaller blood vessels minimizes the rotational component of velocity. Alternatively, this assumption fails in flows near the heart and at bifurcations where flow characteristics begin to transition from the laminar regime to the turbulent regime. In small vessels such as arterioles and venules, blood velocity can be calculated with the Hagen-Poiseuille equation:

$$\text{Eqn. 1-2} \quad \Delta P = \frac{32\mu Lv}{D^2}$$

where ΔP is the pressure difference from the beginning to the end of the vessel, μ is the dynamic viscosity, L is the vessel length, v is the mean blood velocity, and D is the vessel diameter. In this equation, the blood velocity depends on the diameter, length and pressure drop in the vessel. Lumen pressure and diameter vary in both the arterial and venous circulation. Typically, blood velocity is higher in the arterial circulation than the venous circulation leading to higher shear rates in the arterial vessels rather than the venous vessels. The increase in shear is caused by the increased pressure drop. Literature values for arterial shear rates normally are given in the range of 700-2000 s^{-1} while venous shear rates are usually around 200 s^{-1} [23]. In pathophysiology, narrowed or stenosed vessels can experience shear rates in excess of 100,000 s^{-1} [24].

While shear rate is important in terms of the convective delivery of platelets to the injury site, the pressure gradient between the lumen and the interstitial space drives

bleeding out of the vessel. In physiology, these pressure gradients can vary depending on the location of the injured vessel. For example, capillary blood pressure can range from 25 mm Hg to 90 mm Hg between the head and feet due to gravity [25]. Depending on lumen diameter, arterioles usually range from 50-85 mm Hg while venules range from 20-30 mm Hg [23]. The interstitial pressure is not as sensitive, usually ranging from -2 mm Hg to 10 mm Hg [26]. This places the range of pressure gradients between the lumen and extravascular space roughly between 10-85 mm Hg. In order to cease bleeding, clots must prevent these pressure gradients from driving blood loss. They accomplish this by tightly packing together to create a porous media that increases the resistance to flow.

1.3.2 Porous Media Transport

Porous materials are composed of a solid matrix with a pore or void space filled with fluid. These materials are typically characterized by their porosity and permeability. Porosity is defined as the ratio of empty or void volume divided by the total volume of both the fluid and solid. Depending on the structure of the solid matrix, porosity can range from 0 to 1. *In vivo* clot porosity has been calculated experimentally and is typically within a range between 0.4-0.7 depending on the location of the measurement within the clot [27]. The other characteristic used to define porous media is permeability. The permeability of a porous material is defined by the material's ability to permit fluid flow through the structure. Permeability has been estimated to be within the range of $10^{-11} - 10^{-13} \text{ cm}^2$ for compacted coronary thrombi [28].

Porosity and permeability can be used to predict protein and fluid transport within and through blood clots. Protein transport is influenced by the protein's diffusivity within the clot and the fluid velocity through clot. The diffusion coefficient, or the diffusivity for the molecule or protein of interest, is a constant used to describe the proportionality between the molar flux and the concentration gradient of the species. In porous media, diffusivity of a protein or molecule can be reduced. This is determined by the effective diffusivity which is dependent on the material porosity, the free diffusion coefficient, the tortuosity of the material and the constrictivity. The other mode of transport within clots is the fluid velocity, which can be predicted by Darcy's Law:

$$\text{Eqn. 1-3} \quad Q = \frac{\kappa A \Delta P}{\mu L}$$

where Q is the volumetric flow rate, κ is the material's permeability, A is the cross-sectional area to flow, ΔP is the pressure drop across the media, μ is the dynamic viscosity of the fluid, and L is the length in which the pressure drop is achieved. Darcy's Law was derived from the Navier-Stokes equation (Eqn 1-1) by assuming that the flow through the clot is an incompressible, creeping flow and the porous media is isotropic. In a creeping flow, inertial forces are small compared to the viscous forces and $\frac{D(\rho v_i)}{Dt} \sim 0$. This assumptions is valid due to the slow flow velocities and small length scales for porous media transport in clots.

While both advection and diffusion can drive protein transport, it is often beneficial to understand if one of these forces dominates the transport of protein in porous media. This can be characterized by the Péclet number:

Eqn. 1-4

$$Pe = \frac{LU}{D}$$

where L is the characteristic length, U is the velocity, and D is the diffusion coefficient. The Péclet number is a dimensionless number that compares the ratio of advective transport to the diffusive transport. A low Péclet number ($Pe \ll 1$) is representative of transport that is dominated by diffusion while a high Péclet number ($Pe \gg 1$) is representative of transport that is dominated by advection forces. The permeability, porosity, and the resulting Péclet number are important parameters needed to better understand how protein and agonist are transported within clots as they develop under flow. New methods are required to accurately measure these parameters under hemodynamic conditions and at the micron scale.

1.4 Experimental Techniques for Hemostasis Under Physiologic Conditions

With the advances in technology, hemostasis measurements under physiologic conditions have become more reliable both *in vitro* and *in vivo*. Two *in vivo* methods that have become the standard for hemostatic measurements are the tail bleed assay and the mouse cremaster laser injury model [27, 29]. The tail bleeding assay has existed for over 60 years [30]. This assay focuses on the time that it takes for bleeding to cease from the tip of a mouse tail that has been amputated or incised. More recently, the mouse cremaster laser injury model has been utilized [27]. This model facilitates the microscopic observation of platelet and coagulation function as they work together to form a stable clot on the injured vessel wall. In both of these injury models, the hemostatic response is measured by the platelets, coagulation, and vasculatures ability to cease bleeding under physiologic conditions.

In vitro models of hemostasis have drastically improved with the development of both photo and soft lithography techniques. These techniques have facilitated the production of geometrically controllable chips with micron scale resolution. The channels within the chips, also known as microfluidic devices, are designed to control and manipulate small volumes of fluid. This makes them ideal for studying hemodynamics. Previous work has pioneered the use of blood and study of thrombus formation within microfluidic channels [31]. In these studies, the wall shear rate was controlled to better understand the significance of these rates on thrombus formation. The ability to control hemodynamic conditions and localize thrombus formation, for microscopic imaging, makes microfluidics an ideal system for characterizing the role that physical forces have on clot development.

While these models all have their strengths and weaknesses, we were motivated to design and validate a new microfluidic assay to independently control both wall shear rate and transthrombus pressure gradients. The merging of previous microfluidic techniques with control of the hemodynamics represented in the laser injury model would provide us with a platform to understand the role of protein transport within clots formed under physiologic conditions. Insights into the transport mechanisms that are utilized by clots formed under hemodynamic conditions will be crucial for improved drug design and treatment of thrombotic events.

Chapter 2 : Side view thrombosis microfluidic device with controllable wall shear rate and transthrombus pressure gradient

2.1 Introduction

At the onset of vessel injury, collagen and subendothelial matrix become exposed to flowing blood. Hemostasis is maintained by platelet adhesion and aggregation at the site of injury [32], along with thrombin production triggered by extravascular tissue factor. The local physical and biological stimuli present during this development play a critical role in the final clot structure and function. One important physical parameter that has long been recognized is the prevailing wall shear stress (τ_w) [33], with the venous system having lower wall shear stresses than the arterial system [23]. Often absent in the design of *in vitro* models is the transthrombus pressure gradient (ΔP) that exists between the intraluminal space and the interstitial compartment of vascularized tissue. Incorporating this feature into thrombus development could quickly change the profile of soluble species, resulting in altered clot structures.

In recent years, several *in vivo* studies have demonstrated the importance of interstitial pressure and flow on angiogenesis [34, 35]. This research has benefited from the ability to control physical factors such as pressure gradients and shear rates using *in vitro* microfluidic devices. Previous work illustrated control of these parameters but at levels not representative of the arterial vasculature [36]. Others have shown control of τ_w or ΔP , but decoupling their dependence at high and low shear stress is a difficult task [31, 37]. Independently controlling both pressure gradients and wall shear stresses at arterial or venous conditions would provide an important understanding of hemostasis in blood

vessel microenvironments. There have not been any devices that incorporate this level of control.

We were able to design and validate a microfluidic device capable of independently controlling the wall shear stress and trans-scaffold pressure gradient. Localization of collagen \pm tissue factor (TF) in the scaffold region of the device allowed side view imaging of thrombosis under controlled transthrombus pressure drops. At arterial wall shear stress, small increases in transthrombus pressure gradients significantly reduced average platelet and platelet/fibrin clot heights. Similarly, the periphery and quantity of thrombin within the clot was reduced in the presence of increased transthrombus permeation. Permeability measurements were obtained under flow by utilizing dye pulsing. The collagen scaffold permeability was validated with previous literature values and new measurements of platelet and platelet/fibrin clot permeability were calculated at various pressure drops. We demonstrate the ability to independently control trans-scaffold pressure gradients and wall shear stresses for studying the permeation effects and rates on or through thrombi.

2.2 Materials and Methods

2.2.1 Device Fabrication and Design

Polydimethylsiloxane (PDMS) (Ellsworth Adhesives) microfluidic devices were fabricated using previously described soft lithography techniques [38]. In brief, photolithography was used to preferentially pattern negative photoresist (KMPR 1050, MicroChem Corp.) on a silicon wafer (D = 100 mm, WRS Materials). The photoresist was spun to a height of 60 μm then soft baked for 20 min. Following baking, the

substrate was placed beneath a photomask and exposed to UV illumination. Prior to development (AZ® 300 MIF, AZ Electronic Materials USA Corp.), the substrate was baked for 4 minutes at 100 °C. PDMS, with a base to curing agent ratio of 10:1, was then molded on the substrate for 2 hr at 80°C. Inlet/outlet and pressure ports (**Figure 2-1A**) were cut out using 0.75 and 0.5 mm I.D. corers (Harris Uni-Core™, Ted Pella, Inc.), respectively. PDMS-tubing (0.020” ID x 0.060” OD, Cole-Parmer) connections were made via 90°, 23 gauge x 1/2” length blunt needles (Small Parts).

The device was designed with a primary channel (60 μm high x 250 μm wide) connected to two inlets (upstream, downstream), two outlets (scaffold, channel), and three pressure ports (P₁, P₂, P₃). The upstream inlet was used for fluid that will come in direct contact with the scaffold while the downstream inlet, prior to the compressed channel (200 μm wide), was added to create resistance to flow upstream (**Figure 2-1A**). The added resistance caused increased pressure due to the constant volume syringe pumps. Two pressure ports were added upstream (P₂) and downstream (P₁) of the scaffold region to accurately measure the pressure at the scaffold-channel interface. An additional pressure port (P₃) was placed next to the scaffold outlet port to determine the pressure drop across the region. The scaffold was designed with an array of posts (D = 50 μm) spaced 20 μm apart with a narrowed opening from L = 250 μm at the interface to L=50 μm at the exit (**Figure 2-1B**). The posts positions were ideal for uniformly loading collagen fibers and the compressed exit forced the majority of the pressure drop across the scaffold rather than the exiting channel. Post arrays were placed surrounding each of the channel setups to support the negative pressure due to vacuum sealing to glass slides

(Figure 2-1C). All of the design features in this device made it possible to monitor and control the pressure gradients across the scaffold, while maintaining constant wall shear stress at the interface.

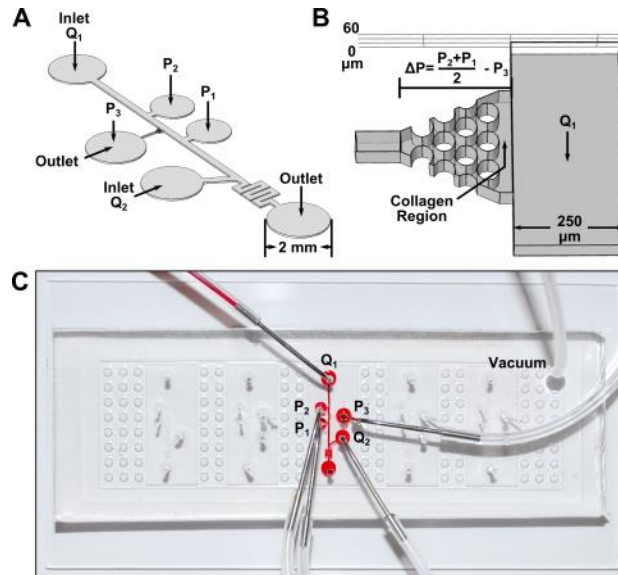


Figure 2-1 A microfluidic device with controllable trans-scaffold pressure gradients.

Syringe pump inlet Q_1 provided a constant volume flow that exited through the downstream outlet or transversed the collagen region towards the outlet monitored by P_3 (A). The main flow channel ($H=60\ \mu\text{m}$, $W=250\ \mu\text{m}$) provided a collagen-fluid flow interface between pressure sensors P_2 and P_1 (B). A LabVIEW control panel interpreted the pressure measurements (P_1 , P_2 , P_3) and proportionately controlled a constant volume syringe pump (Q_2) to maintain constant pressure gradients across the collagen region. Prior to use, the PDMS microfluidic device was vacuum sealed to a glass slide and connections between the tubing and device were made via 90° , 23-gauge blunt needle tips (C).

2.2.2 Device Operation

Devices were vacuum sealed to Sigmacote® (Sigma-Aldrich) treated glass slides and channels were coated with a 10% BSA solution for 30 min. Polymerized fibrillar collagen was prepared overnight by incubating (37 °C) an 8:1:1 ratio of collagen (3 mg/ml monomeric, human Type I) (Vitrocol, Advanced BioMatrix, Inc.), 10x PBS, and 0.09M NaOH respectively. Tissue factor liposomes were prepared as previously described [38, 39]. Briefly, biotinylated anti-collagen (4 µg/ml, Abcam) and streptavidin (10 µg/ml, Sigma-Aldrich) were mixed subsequently in a 1:10 volumetric ratio with polymerized collagen. Following a 5 min room temperature incubation for each, biotinylated/TF liposomes (79:20:1, L- α -phosphatidylcholine (PC):L- α -phosphatidylserine (PS):biotinylated phosphatidylethanolamine (bPE), Avanti Polar Lipids) were mixed in a 1:20 ratio by volume with the polymerized collagen/biotinylated anti-collagen/streptavidin mixture. The solution was incubated for an additional 10 minutes at room temperature. Device scaffolds were then loaded by pulling 2.5 µL of polymerized collagen (\pm TF liposomes) through pressure ports P₁ and P₂ out of the scaffold region exit. Immediately following loading, Ca²⁺ buffer (5mM) was rinsed through the channels to remove any collagen outside of the scaffold. Devices were setup on a slide holder for imaging using a CCD camera (ORCA-ER, Hamamatsu) on an inverted microscope (IX81, Olympus America Inc.).

The loaded channel was then connected to the three pressure sensors (P₁, P₂, P₃) and the upstream and downstream syringe pumps as previously discussed. The flow rate from the upstream pump (PHD Ultra, Harvard Apparatus) provided a constant initial wall

shear stress (33.9 dyne/cm^2) at the scaffold by setting a constant flow rate ($13 \text{ }\mu\text{l/min}$). Pressure transducers (Honeywell Sensing and Control) connected at the P₁, P₂, and P₃ ports transmitted analog voltage signals to a data acquisition device (NI USB-6210, National Instruments) that was used to process the measurements in LabVIEW (National Instruments, **Figure 2-2**). The flow rate from the downstream pump (PHD 2000, Harvard Apparatus) was controlled proportionately according to the real-time pressure measurements (**Figure 2-3 and Figure 2-4**). This control allowed the device to maintain constant pressure drop across the scaffold throughout the experiment.

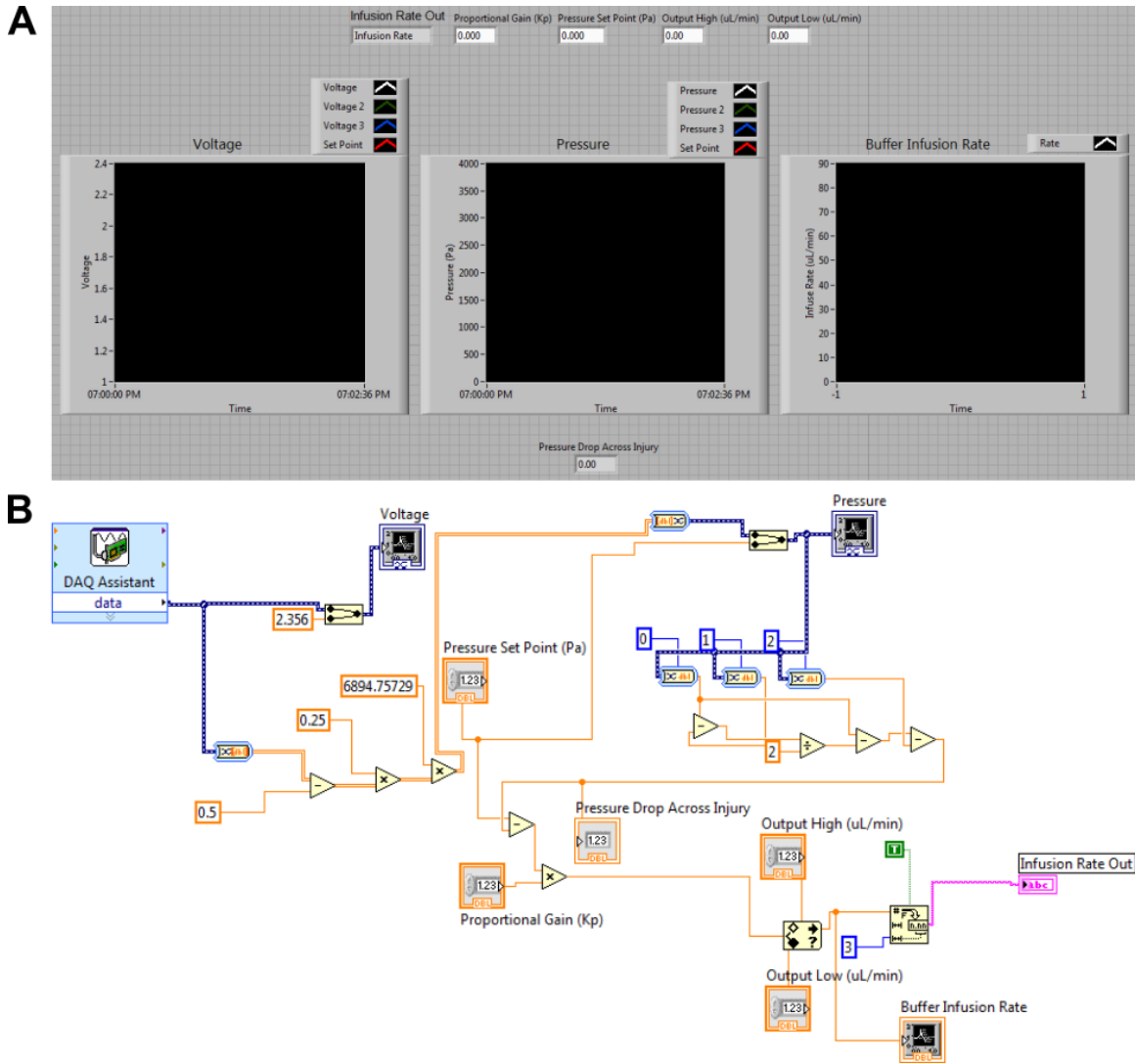


Figure 2-2 A LabVIEW program to measure and control microfluidic pressure gradients.

A user interface was developed to monitor instantaneous pressure measurements inside of the microfluidic channel at three independent pressure sensors. The pressure transducers outputted voltage signals that were then converted into pressure. The pressures were monitored and controlled proportionally by a proportional gain constant (K_p) that produced a resulting flow rate required to maintain the pressure gradient set point. The interface continuously displayed the resulting voltage, pressure, and flow rate (A). The underlying block diagram illustrates the voltage to pressure signal conversion and the proportionate controller used to calculate the required buffer infusion flow rate (B).

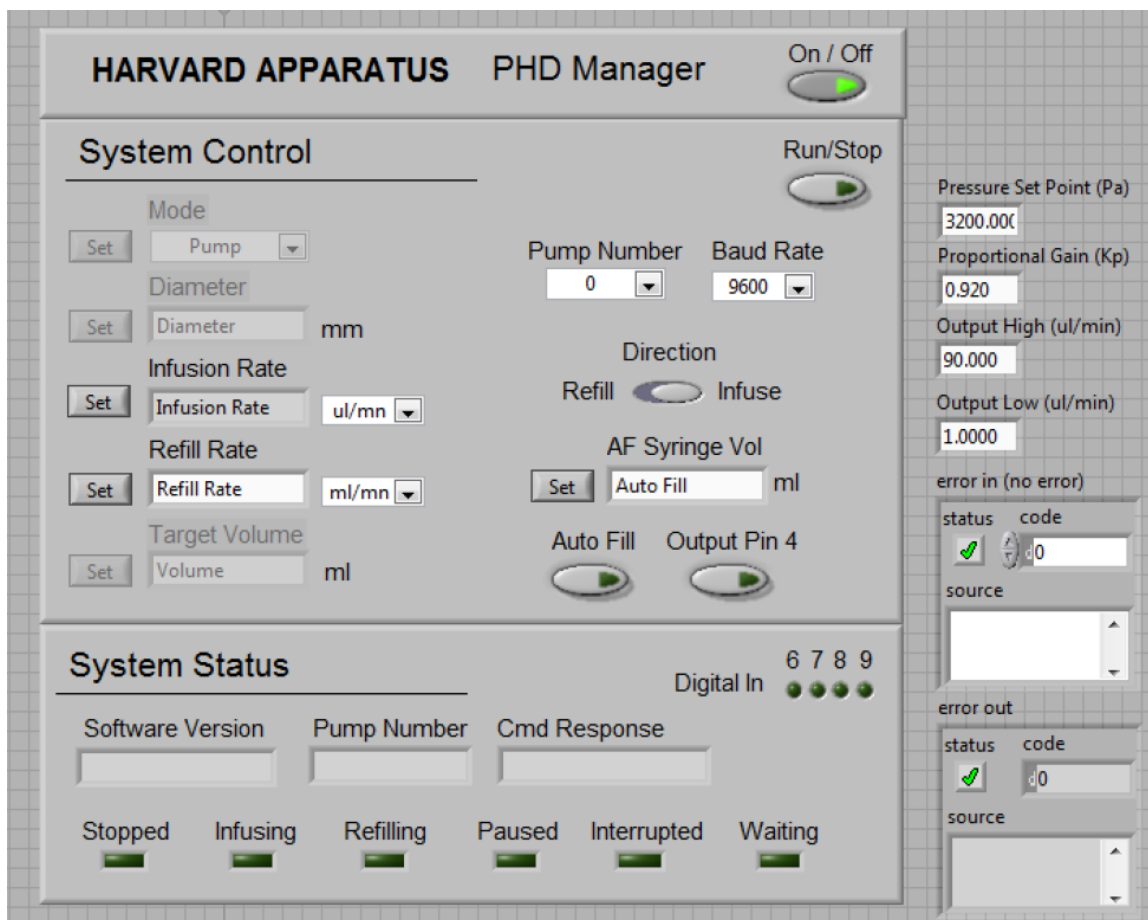


Figure 2-3 A customized LabVIEW interface for controlling syringe pump flow rates to maintain a pressure gradient set point.

This interface directly controls a Harvard Apparatus PHD 2000 syringe pump allowing computer input of the infusion rate, refill rate, syringe diameter, pumping direction, and on/off. For the purpose of controlling microfluidic pressure gradients, the interface was supplemented with inputs for pressure set point, proportional gain, output high, and output low. Prior to imaging under flow, this interface was initiated (Run/Stop) and device pressure gradients were stabilized at the desired set point.

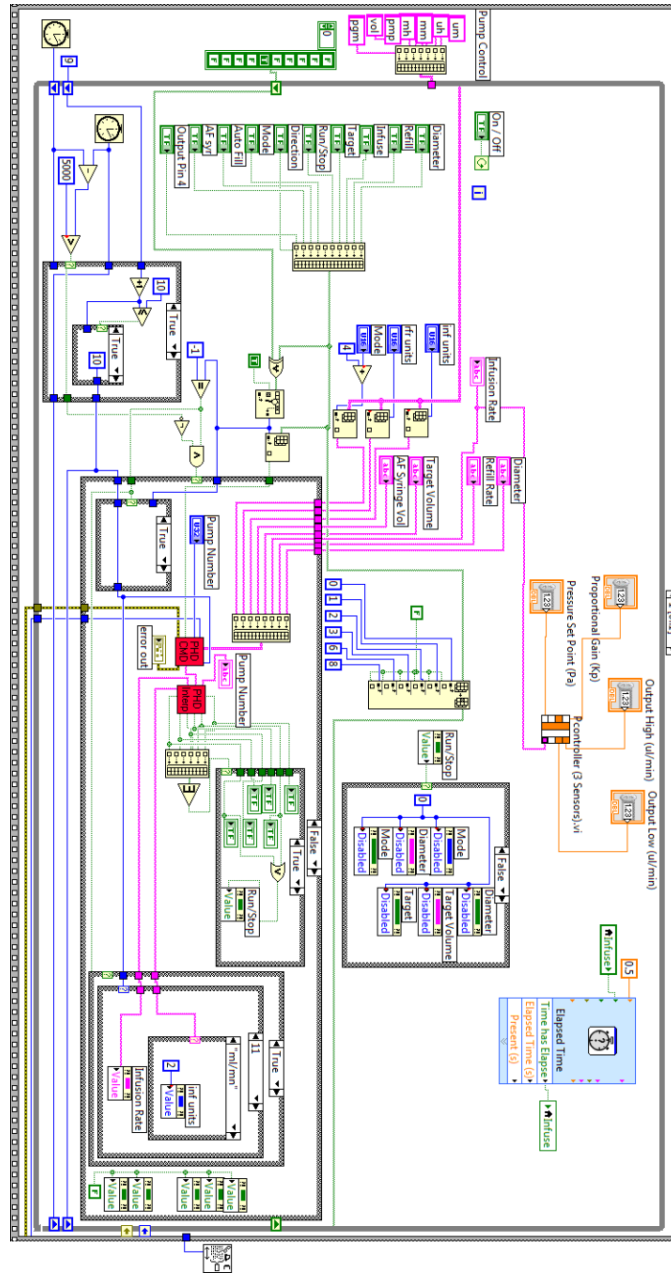


Figure 2-4 A LabVIEW block diagram utilized to control a Harvard Apparatus PHD 2000 syringe pump.

This block diagram was supplemented with code to control the output infusion rate based on an externally designed proportional controller interface using instantaneous microfluidic pressure measurements. The external program measures pressure and calculates an adjusted flow rate necessary to proportionally control the pressure gradient at the desired set point. The flow rate is passed to this interface which continuously updates the pump infusion rate every 0.5 s, allowing the microfluidic pressure gradients to remain constant.

2.2.3 Device Validation

Pressure transducers were calibrated between 0-1 psig in LabVIEW using atmospheric pressure and 27.7 inches of H₂O respectively. The device was validated by measuring the permeability of collagen loaded in the scaffold. An injection valve (V-450, IDEX Health & Science LLC) was placed between the syringe pump and the microfluidic channel (Q₁) to produce a controlled pulse under constant flow. The average velocity through the scaffold was measured by pulsing ~25 μL of sulforhodamine 101 acid chloride (Texas Red, Sigma-Aldrich) in 5 mM Ca²⁺ buffer through the channel and monitoring dye FI at the inlet and outlet of the collagen scaffold. Measuring the average velocity through the collagen allowed permeability to be calculated over the complex domain using COMSOL Multiphysics software. The resulting collagen permeability was validated by comparisons to previously determined literature values [41, 42]. The permeability of platelet and platelet/fibrin deposited layers could then be measured using similar techniques by pulsing ~25 μL of fluorescein isothiocyanate (FITC, Sigma-Aldrich) in Ca²⁺ buffer (5 mM) following 10 minutes of whole blood flow (1130 s⁻¹) at a range of physiologic pressure drops [25, 26].

2.2.4 Blood Collection

Blood draws were in accordance with the University of Pennsylvania's IRB and all healthy volunteers were self reported as alcohol and medication free. Human blood was collected from donors directly into anti-coagulant via venipuncture. Studies examining the absence of thrombin were completed with 100 μM of the anti-coagulant Phe-Pro-Arg-chloromethylketone (PPACK, Haematologic Technologies Inc.) and 1

$\mu\text{g/ml}$ of a fluorescently conjugated anti-CD41 monoclonal antibody (Abd Serotec). Uninhibited thrombin studies were completed in $40 \mu\text{g/ml}$ of the anti-coagulant corn trypsin inhibitor (CTI, Haematologic Technologies Inc.) and $0.125 \mu\text{g/ml}$ of a PE-conjugated anti-CD61 antibody (Becton Dickinson Biosciences). CTI-treated blood was also supplemented with $5 \mu\text{g/ml}$ of a thrombin sensitive antibody (ThS-Ab) for thrombin localization studies [43], $0.0625 \mu\text{g/ml}$ of a PE-conjugated anti-CD62P antibody (Becton Dickinson Biosciences) for P-selectin studies, and $0.5 \mu\text{g/ml}$ of a fluorescently conjugated anti-fibrin antibody (gift from the M. Poncz, Children's Hospital of Philadelphia) for fibrin localization studies [44, 45].

2.2.5 Finite Element Analysis

During the design phase of the microfluidic fabrication, COMSOL Multiphysics was used to predict the localization of collagen in the scaffold. The entire structure was modeled and the pressure ports were a source of collagen ($C=1$) while the remainder of the ports with exception to the scaffold exit were a source of 5 mM Ca^{2+} ($C=0$). The solution was pulled through the scaffold exit at a velocity (1 mL/min) similar to slowly pulling with a 1 mL syringe. Velocity profiles and concentration localization plots were used to predict the best suited scaffold design. COMSOL was also used to calculate clot wall shear stress on experimentally defined clot structures at two minute time intervals. Three-dimensional simulations were modeled using experimental clot structures in a $250 \mu\text{m}$ wide x $60 \mu\text{m}$ high channel. The inlet flow rate was set to $13 \mu\text{L/min}$ and the middle 60% of the clot surface was averaged over 100 equal spaced lines scans for each time dependent structure. In an independent measurement, COMSOL was used to calculate

permeability [45]. Briefly, the pulsed dye buffer was modeled using the stationary Navier-Stokes equation for laminar flow. The collagen, platelet deposit, and platelet/fibrin structures were simulated using Darcy's law:

$$\text{Eqn. 2-1} \quad \mathbf{u} = -\frac{\kappa}{\mu} \nabla p$$

where \mathbf{u} is the fluid velocity, κ is the Darcy's permeability, μ is the buffer viscosity, and p is the pressure. Coupling the Navier-Stokes equation with Eqn. 2-1 allowed Darcy's permeability (κ) to be iteratively calculated by minimizing the squared error between the mean experimental and simulated fluid velocity through the porous media.

2.3 Results

2.3.1 Controllable transcollagen scaffold ΔP in a side view thrombosis device

A microfluidic device was designed with the ability to maintain a computer-controlled trans-scaffold pressure gradient of $\Delta P = (P_2+P_1)/2 - P_3$, while providing constant wall shear stress τ_w (**Figure 2-1**). The pressure gradient and wall shear stress were controlled by utilizing two independent syringe pumps (Q_1 , Q_2), three pressure sensors (P_1 , P_2 , P_3), and a proportional controller in LabVIEW (**Figure 2-2-Figure 2-4**) to control Q_2 based on P_1 , P_2 , and P_3 at constant Q_1 . The syringe pump upstream of the scaffold region dictated the wall shear stress while the downstream syringe pump controlled the channel pressure for independent control of ΔP and τ_w .

The scaffold region was designed with six posts equally spaced in a triangular orientation (**Figure 2-1B and Figure 2-5**) to support the loading of fibrous matrix

materials such as polymerized collagen. Pressure ports upstream (P_2) and downstream (P_1) of the scaffold were used for even infusion of a collagen solution during the loading protocol by withdrawal from port P_3 (**Figure 2-5A**). With Q_1 and $Q_2 = 0$, the velocity profile throughout the posts initially focuses collagen loading in the middle of the scaffold where the velocities are roughly twice as fast as the edges (**Figure 2-5B**). As the middle region is loaded, the edge velocities start to dominate resulting in a uniform distribution of collagen at the interface of the main channel (**Figure 2-5C**). This approach provided a reliable and repeatable method to create a defined protein matrix to trigger reactions during the subsequent perfusion of whole blood using Q_1 .

After collagen was loaded into the device, the ΔP controller algorithm was optimized under diverse conditions. First, the proportionate control parameter K_p was determined to be $0.92 \mu\text{L}/\text{min}\cdot\text{Pa}$ using manual tuning to maximize response speed and minimize overshoot. The maximum buffer flow rate was set to $100 \mu\text{L}/\text{min}$ to prevent overshooting the set point. Robust control of trans-scaffold ΔP set points was obtained under arterial (1130 s^{-1} , $13 \mu\text{L}/\text{min}$) or venous (174 s^{-1} , $2 \mu\text{L}/\text{min}$) wall shear rates (**Figure 2-6A**) using whole blood perfusion. A range of ΔP values from 20.6 to 30 mm Hg were achieved at an arterial shear rate. Similarly, a range of ΔP values from 11.3 to 22.5 mm Hg were achieved at a venous shear rate. The average response rate was $0.26 \text{ mm Hg}/\text{s}$ during set point changes. Lower wall shear stress required higher buffer flow rates to reach larger pressure gradients which caused reduced response rates ($0.20 \text{ mm Hg}/\text{s}$) compared to arterial wall shear stress ($0.31 \text{ mm Hg}/\text{s}$). Throughout these

experiments P_2 and P_1 typically differed by less than 1 mm Hg while P_3 remained relatively constant.

For measurement of clot permeability, pulsing of a fluorescent solute tracer under constant flow rate was required. This feature was examined by measuring the trans-scaffold pressure gradient and buffer flow rate during the injection of a fluorescent dye solution at a lower viscosity ($\mu_{\text{Dye}}=0.001 \text{ Pa}\cdot\text{s}$) than that of whole blood ($\mu_{\text{Blood}}=0.003 \text{ Pa}\cdot\text{s}$) (**Figure 2-6B**) [47]. Prior to the introduction of dye (<1 min), the blood viscosity in the channel and the Q_2 flow rate were constant. As the dye in buffer solution began to exceed the blood concentration (1-3 min, **Figure 2-6C**), the viscosity of the mixture began to drop. This drop in viscosity was met with an increase in the Q_2 flow rate to compensate for the reduction in resistance against the Q_1 syringe pump. When the blood began to exceed the dye/buffer solution (>3 min), the viscosity began to increase and the Q_2 flow rate began to decrease to provide a constant resistance against the Q_1 syringe pump. Throughout all of these viscosity changes the pressure drop in the channel remained constant ($23.5 \pm 0.12 \text{ mm Hg}$) due to the constant downstream resistance maintained by the Q_2 flow rate. The ΔP range that we investigated mimics the range located in capillaries. At the head or heart level lumen pressures are generally 25-30 mm Hg [25] and interstitial pressures are within -2-10 mm Hg [26]. While this is the ΔP (15 mm Hg to 32 mm Hg) we have focused on, higher ΔP values certainly exist in physiology and can be achieved in this device.

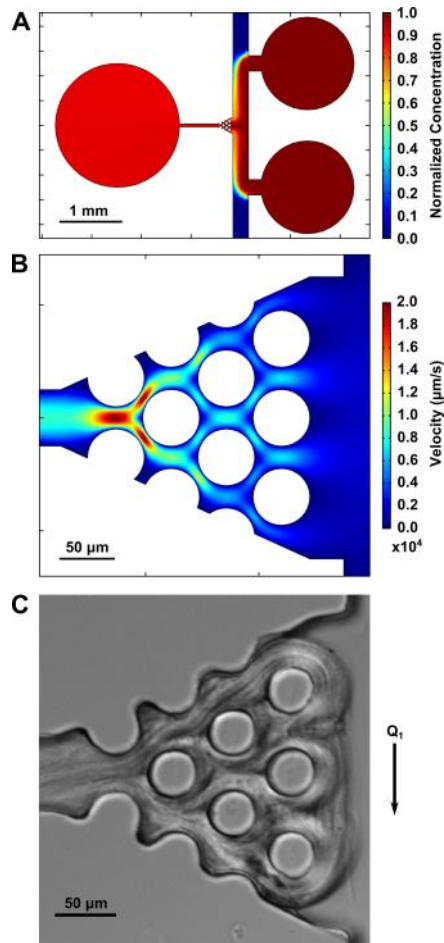


Figure 2-5 Human type I, polymerized collagen localized in the scaffold region.

Polymerized collagen (2.5 μL) was placed on pressure ports P_2 and P_1 . A 1 mL syringe was used to pull the solution through the scaffold region allowing fibers to wrap around the posts. COMSOL simulations demonstrated the normalized concentration and the limited exposure of collagen in the channel during the loading procedure (A). The initial velocity field in the scaffold region produces slightly higher velocities in the middle of the posts which allowed collagen fibers to load the middle of the region before the outer edges (B). This type of loading resulted in an evenly distributed collagen region with a flat collagen-fluid flow interface (C).

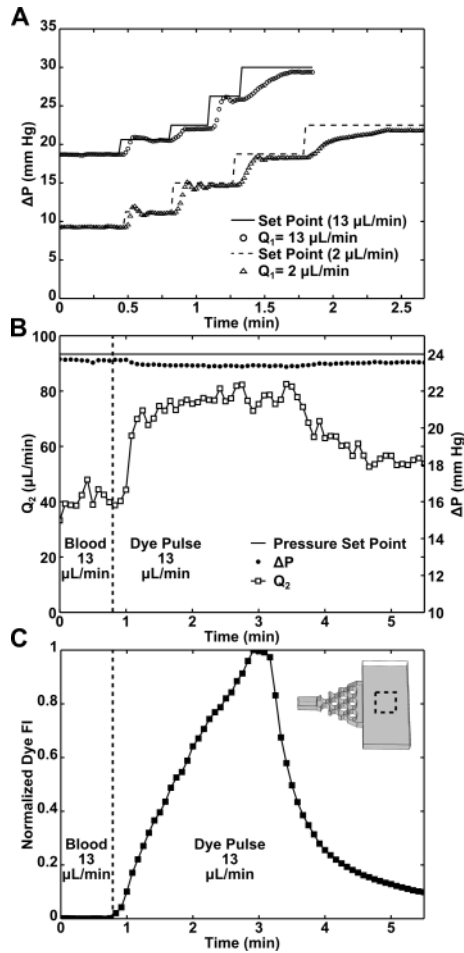


Figure 2-6 Syringe pump control allows rapid responses to changes in pressure set point and fluid viscosity.

Constant Q_1 flow rates provide a constant wall shear rate at the collagen-fluid flow interface. LabVIEW control over Q_2 , via a downstream syringe pump, allowed pressure gradients across the scaffold region to remain constant while responding quickly to set point adjustments (**A**). In a separate experiment, buffer containing dye was pulsed through the device. As the lower viscosity buffer became more concentrated than the blood, the Q_2 flow rate increased to maintain pressure at the desired set point (**B**). The increase in normalized dye fluorescence intensity corresponded to the decrease in viscosity and the increase in the downstream flow rate Q_2 (**C**).

2.3.2 Transthrimbus permeation reduces the intrathrombus zone of thrombin activity

Thrombus development at the collagen or collagen/TF scaffold was followed for 10 min with a trans-scaffold pressure drop of 23.4 mm Hg. During the perfusion of PPACK anti-coagulated whole blood at an initial wall shear stress of 33.9 dyne/cm², the thrombin deficient clot formed a uniform layer at the collagen/blood interface (**Figure 2-7A-C**). When TF was added to the collagen scaffold and PPACK was replaced with CTI, the clot favored larger upstream and downstream platelet deposits rather than the uniformity seen in thrombin deficient clots (**Figure 2-7D-F**). Using a thrombin sensing anti-platelet antibody, we were able to clearly show the thrombin rich layer within the clot near the collagen/TF interface during transthrimbus permeation. The clot structure was then modeled in COMSOL to analyze the resulting wall shear stress at the surface of the clot following 9 minutes of flow. Due to the shape of the thrombus, the maximum shear stress (138 dynes/cm²) was located at the leading edge of the clot and was ~4-fold larger than the average clot shear stress (**Figure 2-7G**).

Using the platelet-targeted thrombin sensor added to CTI-treated whole blood, the thrombin rich region was further analyzed at trans-scaffold $\Delta P = 0$ and 23.4 mm Hg. The thrombin sensor provides a cumulative readout of local thrombin activity. Fluorescent line scans from the collagen interface (width=0 microns) and across the clot into the blood flow (width=45 microns) were averaged over the entire front-to-back length of the clot. In a diffusion-controlled transport process lacking transthrimbus interstitial permeation ($\Delta P=0$ mm Hg), the thrombin concentration and boundary thickness were

~62% and ~59% larger, respectively, compared to that of clots formed with transthrimbus permeation ($\Delta P = 23.4$ mm Hg) (**Figure 2-8A and Figure 2-8B**). This drastic difference demonstrates the importance that transthrimbus permeation has on soluble agonist localization. Since an inert protein the size of thrombin ($D_{\text{Brownian}} \sim 7 \times 10^{-7}$ cm²/s) would be expected to diffuse more than 100 microns in 4 minutes, the restricted ~15-micron thick region of thrombin activity in **Figure 2-8** indicates a combination of rapid inhibition by antithrombin, sequestration within fibrin, restricted diffusion by platelets, and/or platelet binding (eg. platelet GPIIb α). In addition to the thrombin studies, P-selectin positive platelets were also identified. **Figure 2-9** compares hierarchical clot architecture using human blood *in vitro* with previously reported *in vivo* mouse laser injury model [27], demonstrating a remarkable correspondence between these two independent approaches, namely the formation of a P-selectin-positive core and a surrounding P-selectin-negative shell. This is the first microfluidic device to recreate with human blood the core/shell architecture originally characterized in mouse blood vessels.

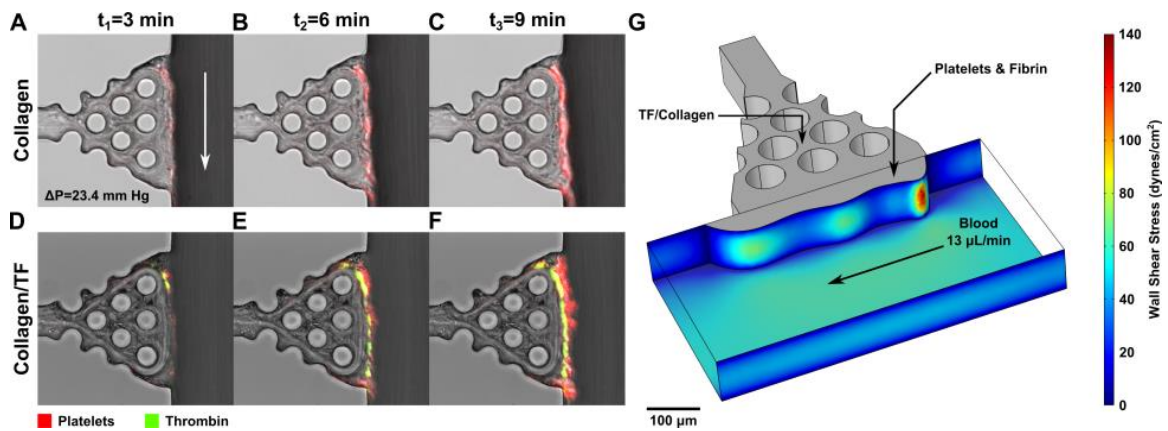


Figure 2-7 Perfusion of anti-coagulated whole blood provides reproducible thrombus development at the collagen-blood interface.

Anti-coagulated whole blood was perfused at an initial wall shear stress (33.9 dyne/cm^2) while a constant ΔP (23.4 mm Hg) was maintained across the collagen-blood interface. Dynamic studies of platelet (red) and thrombin (green) development on collagen (**A-C**) or collagen/TF scaffolds (**D-F**) allowed for spatial-temporal clot measurements. Resulting structures were simulated in COMSOL to study time-dependent wall shear stress at the clot boundary (**G**).

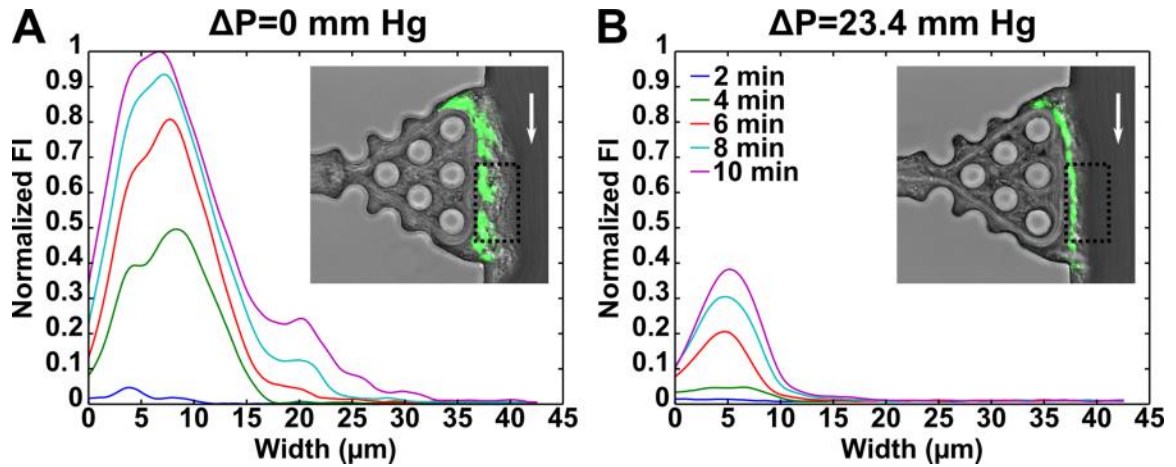


Figure 2-8 Increasing transthrombus pressure gradients caused a reduction in thrombin.

Average line scans of the thrombin boundary layer were taken every two minutes during clot formation on a collagen/TF surface. Whole blood anti-coagulated with CTI was perfused for 10 minutes and transthrombus pressure gradients were maintained at $\Delta P=0$ mm Hg (A) or $\Delta P=23.4$ mm Hg (B). The increased convection through the clot caused a reduction in the presence and velocity of thrombin towards the clot surface.

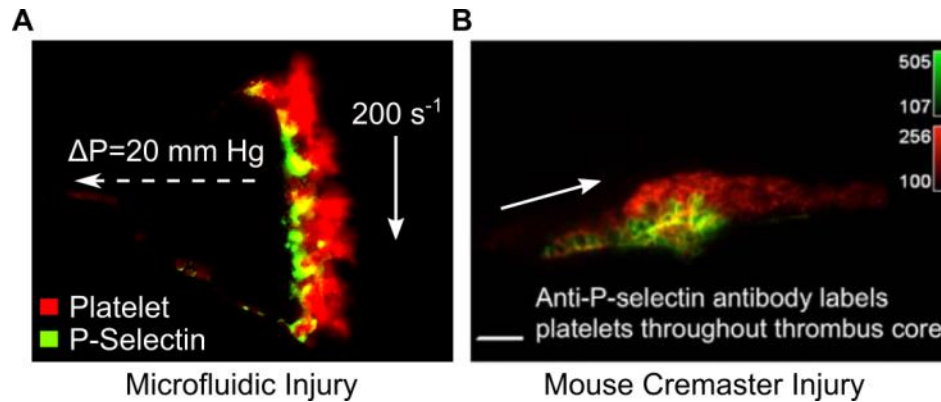


Figure 2-9 Clots formed in the microfluidic injury model we present illustrate remarkable correspondence to *in vivo* hierarchical clot architectures found in mouse.

Fluorescent P-selectin antibodies (green) were used to determine platelet α -granule release. Following 10 minutes of whole blood perfusion (200 s^{-1}) with a $\Delta P = 20$ mm Hg, a distinct core of P-selectin positive platelets was covered by a shell of P-selectin negative platelets (red) in the microfluidic injury assay (A). The clot architecture of a thrombus in a mouse cremaster injury (21, with permission) demonstrates remarkable similarities (B). In both assays only the core or P-selectin positive platelets release their α -granules. This illustrates a level of activation that only the core region of the clot can reach during transthrombus permeation.

2.3.3 Pressure gradients affect thrombus composition and size

Using CTI-treated whole blood perfusion, the dynamics of clot composition, wall shear stress, and average clot height, in the presence (collagen/TF) or absence (collagen) of thrombin, were investigated at transthrombus pressure gradients of 20.8 mm Hg (**Figure 2-10A-D**), 23.4 mm Hg (**Figure 2-10E-H**), or 0 mm Hg (**Figure 2-10I-K**). As the clot grew into the flow field, the wall shear stress increased under the constant flow rate conditions of the experiment. Since the average clot thickness (up to 50 μm) was small relative to the channel width (250 μm), the wall shear stress only increased modestly at constant flow rate. The calculated clot wall shear stress was averaged in the middle 60% of the clot length.

Comparison of structures formed on collagen versus collagen/TF scaffolds at constant transthrombus pressure gradients revealed dramatically different structures. At $\Delta P = 20.8$ mm Hg, the upstream portion of clots on collagen remained larger than the trailing edge whereas the trailing edge outgrew the upstream edge when whole blood was exposed to collagen/TF surfaces (**Figure 2-10A and Figure 2-10B**). In the case of $\Delta P = 23.4$ mm Hg, the clots developed on collagen were relatively uniform along the length of the clot (**Figure 2-10E**). At the same pressure, the incorporation of thrombin caused an initially larger upstream edge that eventually became uniform with the trailing edge following 10 minutes of perfusion (**Figure 2-10F**). Noticeably, clots formed without transthrombus permeation (**Figure 2-10I**) looked more similar to clots formed on collagen/TF surfaces at $\Delta P = 20.8$ mm Hg, where the trailing edges protruded further into

the flow. This phenomenon has been observed previously in a parallel channel microfluidic device at arterial wall shear stress [48].

Throughout all experiments, clot height decreased when transthrbus pressure drop was increased. Interestingly, only an 11% increase in pressure drop (20.8 mm Hg to 23.4 mm Hg) resulted in large percent reductions in final clot height for both collagen (27.9%, $p<0.001$) and collagen/TF structures (20.2%, $p=0.012$) (**Figure 2-10C and Figure 2-10G**). This trend continued when clots were formed without permeation. Final average clot height at $\Delta P = 0$ mm Hg (TF/Collagen surface) was ~ 12 μm larger than clots exposed to transthrbus pressure gradients of 23.4 mm Hg (**Figure 2-10J**). As previously discussed in **Figure 2-8**, the thrombin boundary height was reduced with increasing ΔP (**Figure 2-10G and Figure 2-10J**). With the increases in clot heights came corresponding increases in wall shear stresses from an initial stress of 33.9 dynes/cm² to 42.3 dynes/cm² (platelet structures) or 46.9 dynes/cm² (platelet/fibrin structures) (**Figure 2-10D and Figure 2-10H**).

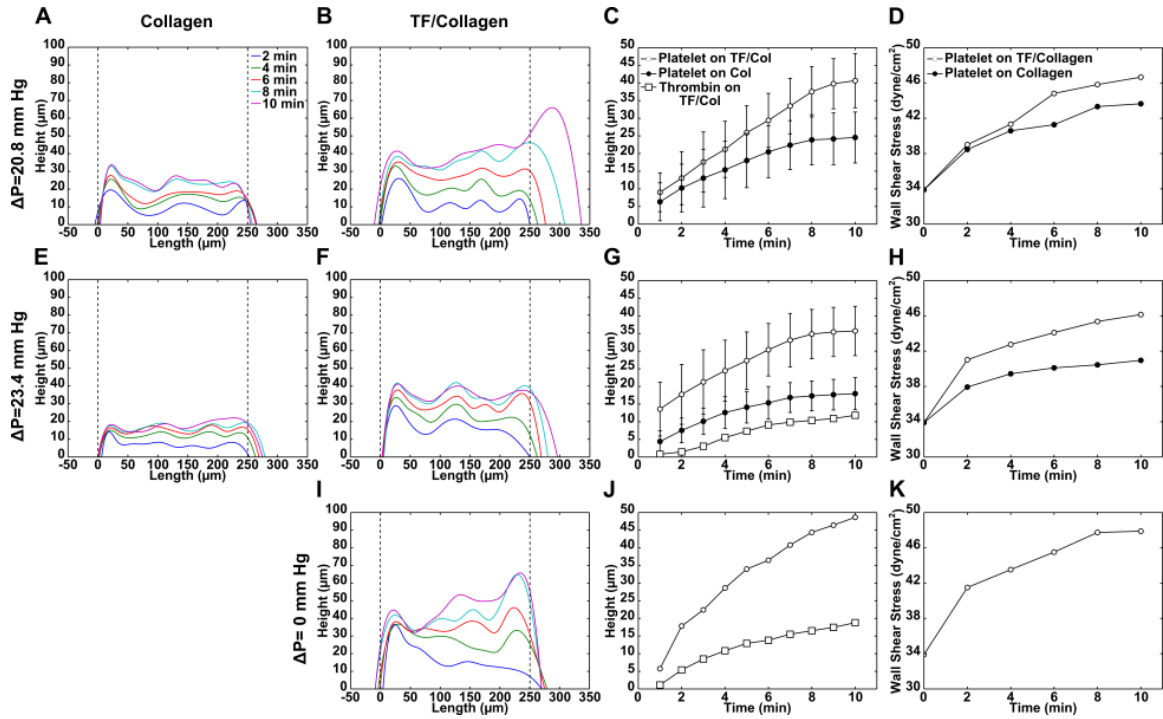


Figure 2-10 Transthrombus pressure gradients effect dynamic measurements such as clot structure, wall shear stress and height.

Clots formed on collagen (\pm TF) with transthrombus pressure gradients of 20.8 mm Hg (A-D), 23.4 mm Hg (E-H), or 0 mm Hg (I-K) resulted in structural differences based on the pressure and the presence or absence of TF. Thrombus development on collagen without TF typically produced smaller clot heights and reduced wall shear stresses. Reductions in transthrombus pressure gradients resulted in increased thrombin and platelet deposition heights.

2.3.4 Fluorescent dye transport allows thrombus permeability measurement

The designed microfluidic device not only allowed a side view analysis of thrombus development under transthrombus pressure gradients, but it was also a versatile tool for permeability measurements. In order to analyze permeability measurements for platelet and platelet/fibrin clots formed under flow, the device was validated comparing collagen permeability measurements to previous literature values. Measurements were made by injecting a fluorescent dye into the main channel under continuous flow and following the progression of the dye at the inlet and outlet of the collagen scaffold. From these curves, an average velocity was calculated by dividing the distance between measurements by the time between peak fluorescent intensities on both the inlet and outlet measurements. The calculated average velocities were then matched by minimizing the sum squared error between the predicted velocities through the structure in COMSOL. The measured permeability for the collagen scaffold was $1.98 \times 10^{-11} \pm 0.64 \times 10^{-11} \text{ cm}^2$. This value was within the range of collagen permeabilities ([41]: $8.9 \times 10^{-11} \text{ cm}^2$; [42]: $1 \times 10^{-11} \text{ cm}^2$) previously reported. This measurement was calculated for trans-scaffold pressure drops of 11.95 mm Hg, 14.15 mm Hg, and 23.43 mm Hg respectively.

With a validated measurement for the collagen scaffold, the next step was to measure the permeability of clots formed with and without thrombin. The addition of TF liposomes to the collagen and substitution of CTI for PPACK allowed us to study platelet/fibrin clots. Measurements were made identical to the techniques previously discussed with collagen and the concentration curves were validated by the COMSOL

model (**Figure 2-11A and Figure 2-11B**). Without thrombin in the system, the platelet clot permeability was $5.45 \times 10^{-14} \pm 0.89 \times 10^{-14} \text{ cm}^2$ for $\Delta P = 20.70 \text{ mm Hg}$ and 23.53 mm Hg (**Figure 2-11C**). When thrombin was uninhibited, the time between peak dye intensities from the inlet to the outlet increased from 115s to 280s for the representative pulse curves. This increase resulted in a platelet/fibrin permeability of $2.71 \times 10^{-14} \pm 0.38 \times 10^{-14} \text{ cm}^2$ for $\Delta P = 20.76 \text{ mm Hg}$ and 23.34 mm Hg (**Figure 2-11C**). The 50% reduction in permeability ($p = 4.6 \times 10^{-4}$) can be seen by the relative increase in the time between peak dye intensities in the representative platelet ($\Delta t_{\text{platelet}} = 115 \text{ s}$) and platelet/fibrin ($\Delta t_{\text{platelet/fibrin}} = 280 \text{ s}$) clot curves. COMSOL was utilized to express these curves and the normalized dye concentration in the device at $t = 3.33 \text{ min}$ (**Figure 2-11D**), $t = 5.33 \text{ min}$ (**Figure 2-11E**), and $t = 7.33 \text{ min}$ (**Figure 2-11F**) for the representative platelet/fibrin clot.

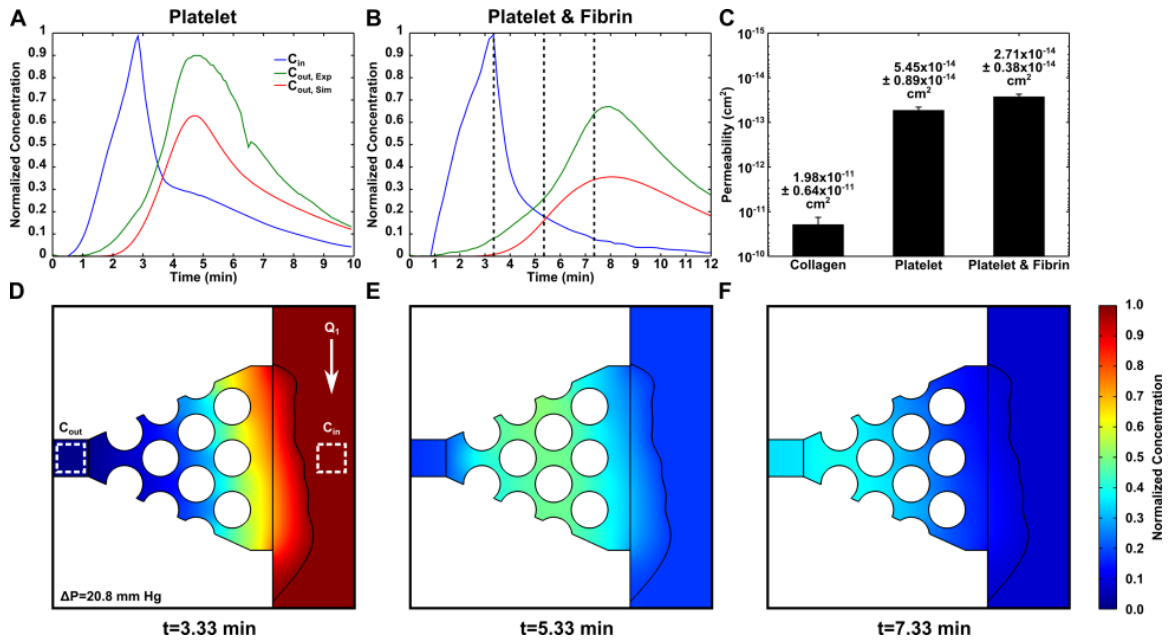


Figure 2-11 Platelet and platelet/fibrin clot permeability was measured by pulsing fluorescent dyes.

Following platelet deposition, whole blood flow was continuously switched to fluorescent dye injection. Dye fluorescence intensity was measured at the platelet (A) or platelet/fibrin (B) interface and collagen exit to predict average fluid velocities across the structure. The permeability of the collagen scaffold, platelet clot, and platelet/fibrin clot were calculated using COMSOL to solve for average velocity (C). Normalized dye fluorescence intensity was demonstrated in COMSOL at the time points indicated (D-F). The pulse was observed as it permeated through the collagen and platelet/fibrin structure.

2.4 Discussion

The development of in vitro microfluidic assays and in vivo mouse injury models have provided many insights into thrombosis and hemostasis under physiologic flow conditions [31, 48]. While each assay has advantages, a challenge that remains is the ability to study clot development and permeation at higher and lower physiologic transthrimbus pressure gradients. In the designed microfluidic device, clot development occurs under permeation while being visualized from the side as in the mouse laser injury models. The advantage of incorporating these characteristics into a microfluidic model is the ability to control transthrimbus pressure gradients and wall shear stress. This is the first reported device that facilitates the independent control of both of these important regulators of clot development at physiologic vessel conditions.

Studies of interstitial flow and its importance in angiogenesis and other cellular environments have steadily increased over the last decade. Incorporating controllable pressure gradients and wall shear stress in a model of angiogenesis may provide a more realistic in vitro representation of the process as it pertains to human physiology. In the case for thrombosis and hemostasis, minimal changes of transthrimbus pressure gradients revealed a significant change in clot size and structure. The increase in transthrimbus permeation caused by an increase in pressure gradients resulted in decreased clot height. The diffusivity of agonists such as thrombin, ADP, and TXA₂ play an important role in these observations. In a thrombin deficient scenario, platelet aggregation is primarily achieved by the release of ADP and TXA₂ after the initial adhesion to the exposed collagen. The diffusivity of these molecules is much faster than

thrombin and as a result, more easily affected by transthrimbus permeation [50]. When thrombin is present, the reduction in clot size is still noticeable at increased pressure gradients but slightly reduced compared to the previous scenario. This interpretation was supported by the reduction in thrombin boundary height in clots formed in the presence of transthrimbus permeation. Without pressure gradients, the thrombin was allowed to diffuse further towards the surface of the clot. This suggests that ADP or TXA₂ would easily reach the clot surface under these conditions but quickly be convected away under permeation [51]. Studying the dynamics of thrombosis and hemostasis under transthrimbus permeation has allowed for a more thorough investigation of the platelets response to the physical and biological stimuli present in physiology.

While clot structure and size were affected by pressure gradients, the permeability of platelet and platelet/fibrin thrombus formed under these conditions remained constant. Permeability measurements in microfluidic devices are not novel [52], but the measurement of thrombus permeability under flow certainly is. Previous measurements have fallen short in their attempt to predict physiologic clot permeability due to the omission of clot structure and composition only observed under flow [53]. In this device, these critical features were preserved and clot permeability measurements were obtained in the presence and absence of thrombin. The permeability observed in these measurements compares closely to previous measurements made in rabbit endothelium [54], suggesting that these clots may be a rapidly developing replacement tissue for the denuded endothelium. This would allow the necessary wound healing molecules and cells access to the site of injury while maintaining vessel hemostasis. Incorporation of

tissue factor allowed clots to quickly intertwine fibrin into their structure and resulted in a significant reduction in permeability as compared to thrombin/fibrin deficient clots. This is important because clots formed in low tissue factors areas such as joints may rely solely on thrombin production from the intrinsic pathway [55]. The reduction in their permeability allows increased access to the site of injury. The increase in access may be correlated to cases of joint bleeding in hemophiliacs where thrombin production via the intrinsic pathway is limited [56]. The device implemented in these studies has proved to be a great way to measure permeability and the role of pressure gradients on clot development. Moving forward, this device would provide valuable data to the fields of angiogenesis and thrombosis, where interstitial permeation plays a critical role in the functionality of the assay.

2.5 Conclusions

While investigating thrombus development on a collagen or collagen/TF scaffold we were able to conclude that small reductions in transthrombus pressure drop caused significant increases in average clot height. This observation was also observed during a study of agonist localization. In the presence of clot permeation the thrombin boundary height and intensity were substantially reduced compared to a scenario where diffusion dominated clot transport. Additionally, measurements for collagen permeability were validated with previous literature values and clot permeabilities were easily measured under continuous flow conditions at varying pressure drops. This device provides a novel system that is translatable to studies requiring independent control of physiologic trans-scaffold pressure gradients and/or wall shear stresses.

Chapter 3 : Blood clots are rapidly assembled hemodynamic sensors: flow arrest triggers intraluminal thrombus contraction

3.1 Introduction

During thrombosis or hemostasis under flow conditions, platelets rapidly deposit at a site of vascular injury. The vessel wall and subendothelium quickly become connected mechanically to the developing thrombus [57]. During vessel wound closure, this interwoven assembly prevents further blood loss by platelet-mediated clot contraction and stiffening [58]. Platelets generate contractile forces to allow clots to match the stiffness of the endothelium [59]. Interactions between myosin II and actin filaments govern this contraction and are regulated by the activation of myosin light chain kinase through calcium/calmodulin and/or Rho kinase signaling [60, 61]. During contraction, force transmission ultimately occurs via talin and $\alpha_{IIb}\beta_3$, which binds platelets via fibrinogen and fibrin [62, 63]. Following clot retraction, the tight seal that is formed around the injured tissue significantly reduces clot permeability, consequently limiting the leakage of cells and plasma. Also, the permeability of occlusive clots is critical to thrombolytic therapy for acute myocardial infarction since permeation dictates penetration of plasminogen activators [28]. The effects of local hemodynamics on clot contraction and permeability are poorly understood, yet highly relevant to thrombus growth, stability, or susceptibility to embolism, fibrinolysis, or bleeding.

Prior studies of clot permeability have used whole blood clots that do not achieve the 50 to 100-fold increase in platelet concentration on a surface that occurs under flow conditions [64, 65]. While clot contraction has been studied for decades using clots

formed in test tubes, there exists a large gap in the fundamental understanding of mechanisms that initiate and control the response under hemodynamic conditions. In terms of force-loading of thrombotic structures, platelets respond with larger stall forces when exposed to stiffer fibrinogen-coated atomic force microscopy (AFM) cantilevers [59]. Studies of whole clot contraction forces may not necessarily predict clot contraction dynamics under flow conditions.

We measured, for the first time, clot contractility and permeability under hemodynamic conditions. The presence of tissue factor caused a significant decrease in thrombus permeability. Unexpectedly, flow arrest caused enhancement of permeability for platelet deposits due to a triggered clot contraction and consequent collagen restructuring. To further examine platelet contraction after flow cessation, a rigid wall flow device was used. Platelet deposits were developed and antagonized using blebbistatin, a myosin II inhibitor and ADP/thromboxane receptor antagonists. Flow arrest caused an intracellular increase in Ca^{2+} that preceded contraction and was dependent on the autocrine signaling of ADP and TXA_2 . These studies provide new insight into the ability of platelets to sense local hemodynamic flow based on the convective-diffusive transport of autocrine signaling molecules.

3.2 Materials and Methods

3.2.1 Reagents

The following reagents and instrumentation were obtained and stored according to manufacturers' instructions: polydimethylsiloxane (PDMS) (Ellsworth Adhesives); sigmacote, streptavidin, sulforhodamine 101 acid chloride (Texas Red), fluorescein

isothiocyanate (FITC), and 2-MeSAMP (Sigma-Aldrich); human type-1 monomeric collagen (VitroCol, 3 mg/ml) (Advanced Biomatrix); equine tendon-derived type-1 fibrillar collagen (Chrono-log); biotinylated goat anti-collagen type I polyclonal antibody (Abcam); 0.05 μm Fluoresbrite® microspheres (Polysciences Inc.); fluo4-NW (Life Technologies); blebbistatin (EMD Millipore); SQ 29,548 (Cayman Chemical); MRS-2179 (Tocris Bioscience); anti-fibrin antibody (gift from the M. Poncz, Children's Hospital of Philadelphia); L- α -phosphatidylserine (PS), L- α -phosphatidylcholine (PC), and biotinylated phosphatidylethanolamine (bPE) (Avanti Polar Lipids); analog pressure transducers (Honeywell Sensing and Control).

3.2.2 Blood Collection

All donors were reported as medication free for the previous 10 days and blood collection was in accordance with the University of Pennsylvania's IRB. Human blood from healthy volunteers was collected into 100 μM Phe-Pro-Arg-chloromethylketone (PPACK, Haematologic Technologies Inc.) or 40 $\mu\text{g/ml}$ corn trypsin inhibitor (CTI, Haematologic Technologies Inc.). PPACK-treated whole blood was also treated with fluorescently conjugated anti-CD41 monoclonal antibody purchased (1 $\mu\text{g/ml}$; Abd Serotec). PE-conjugated anti-CD61 (0.125 $\mu\text{g/ml}$; Becton Dickinson Biosciences) and fluorescently conjugated anti-fibrin antibodies (0.5 $\mu\text{g/ml}$) were added to CTI-treated blood as previously described [44, 45].

3.2.3 Permeation device design and manufacture

PDMS was used to construct microfluidic devices following soft lithography protocols [38] as previously described [31, 40, 48]. The primary blood flow channel (250

μm wide x $60 \mu\text{m}$ high) was designed to create flow over a micropost scaffold region as illustrated in **Figure 3-1A**. At this micropost scaffold junction, blood could continue along the primary channel or exit through the scaffold channel ($50 \mu\text{m}$ wide x $60 \mu\text{m}$ high) to an outlet port maintained at $P3 = \text{atmospheric pressure}$ or blocked so that $P3$ equals the pressure within the blood flow channel. Real-time pressure measurements were collected in LabVIEW (National Instruments) using 0-1 psig pressure transducers upstream (P2), downstream (P1) and exiting the scaffold region (P3) as shown in **Figure 3-1**. Channel pressure was controlled using two constant volume syringe pumps (Harvard Apparatus). A syringe pump located upstream of the collagen scaffold delivered anti-coagulated whole blood at an independently controlled initial inlet wall shear rate (1130 s^{-1}), while a downstream pump perfused Ca^{2+} buffer (5 mM) at a rate set by a proportionate controller programmed in LabVIEW.

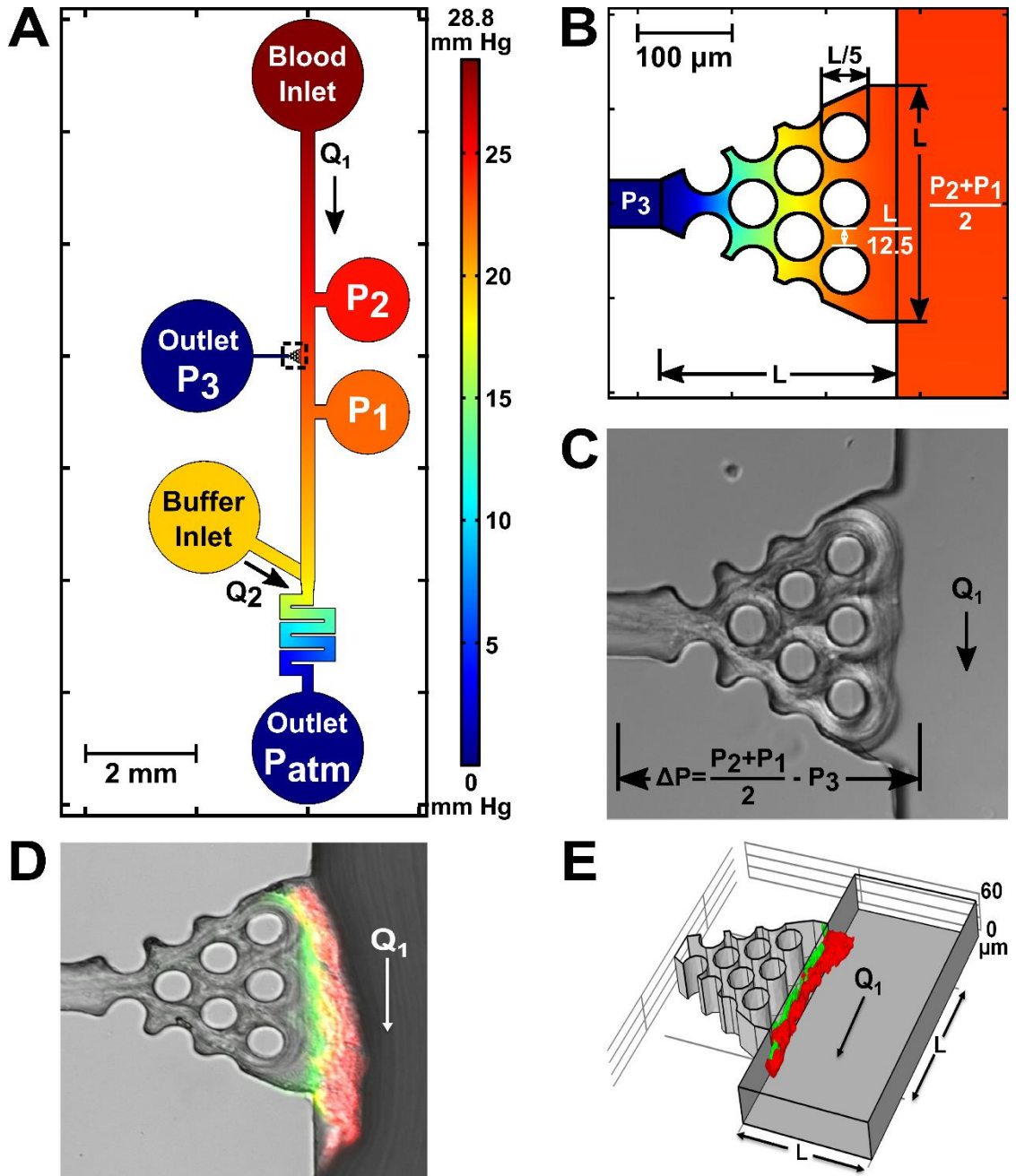


Figure 3-1 Microfluidic device to independently control blood flow and transthrombus pressure drop.

COMSOL was used to determine the pressure throughout the microfluidic device (A) including the collagen scaffold region (B), where $L=250\ \mu\text{m}$. Human type I polymerized collagen was localized in the scaffold region (C). Following 10 min of CTI-whole blood flow at $1130\ \text{s}^{-1}$, platelets (red), fibrin (green) and their overlap (yellow) form a thrombus on the collagen (D). A confocal image of platelets (red) and fibrin (green) shows the 3D structure the microfluidic device (E).

3.2.4 Microfluidic device for thrombus permeation

PDMS devices were sealed to Sigmacote-treated glass slides using vacuum-assisted bonding. Type I human monomeric collagen solution was polymerized at 2.4 mg/ml overnight using 8 parts collagen, 1 part 0.09 M NaOH, and 1 part 10x PBS. Prior to loading the scaffold with collagen, all channels were incubated with 10% BSA for 30 min at room temperature. Following incubation, well mixed polymerized collagen solution was pipette on the upstream and downstream pressure ports and localized into the micropost scaffold region by pulling the solution (2.5 μ L) through the scaffold exit channel with syringe withdraw for \sim 15 s. A fixed amount of collagen (\sim 3.3 ng) was thus deposited on the micropost scaffold. Collagen solution remaining in the channel region (between P2 and P1) was removed by infusion of Ca^{2+} buffer (5 mM) from the blood inlet port prior to instillation of blood for the experiment. For experiments using collagen with linked tissue factor (TF), biotinylated and TF liposomes (20:79:1, PS/PC/bPE) were prepared as previously described [40, 48] following the method of Smith et al. [39]. Polymerized collagen (2.4 mg/ml) was mixed in a 10:1 ratio by volume with biotinylated anti-collagen (4 μ g/ml) and incubated at room temperature for 5 minutes. Streptavidin (10 μ g/ml) at a 1:10 volumetric ratio and TF liposomes at a 1:20 volumetric ratio with collagen were sequentially added and incubated for 5 min and 10 min, respectively. The fibrillar collagen/TF solution was then perfused through the micropost array region as described for fibrillar collagen.

3.2.5 Permeability Measurements

Whole blood was anti-coagulated with PPACK for perfusion over collagen or with CTI for perfusion over collagen/TF. Each whole blood perfusion was conducted at an inlet wall shear rate of 1130 s^{-1} for 10 min. The transthrbus pressure drop was immediately set to the controlled value and side view images of the platelet or platelet/fibrin thrombus were taken at the blood contact region of the collagen scaffold. Following thrombus development, an injection valve (Idex Health & Science) was manually switched to pulse Ca^{2+} buffer (5 mM) containing Texas Red or FITC dye ($\sim 25 \mu\text{L}$) without disruption of the flow. Real-time dye, platelet, and fibrin fluorescent intensities were imaged with an inverted microscope (IX81, Olympus America Inc.) using a CCD camera (ORCA-ER, Hamamatsu). Confocal images of platelet/fibrin thrombus were taken in $2\text{-}\mu\text{m}$ sections, under flow, with a disk-scanning unit (IX2, Olympus America). ImageJ software was used to analyze all images and develop 3-dimensional representations of thrombus.

3.2.6 Contraction Measurements

PPACK-treated whole blood with or without the addition of 50 nm fluorescent microspheres (10^{10} beads/ml blood) was perfused through the permeation device at 1130 s^{-1} . Platelet deposits were formed for 10 min under a constant transthrbus pressure drop (23.5 mm Hg). Whole blood flow was then switched without interruption to Ca^{2+} buffer (5 mM) flow. Following 4.5 min of buffer flow, both syringe pumps were stopped and the transthrbus pressure drop immediately approached zero. Platelet deposits were imaged in 15 sec intervals over 30 min.

Thrombus contraction studies were also performed in a parallel channel microfluidic device [31]. Briefly, a microfluidic device was used to print a 250 μm wide strip of diluted fibrillar collagen lengthwise on a Sigmacote treated glass slide. The patterning device was removed and second device was positioned with ten parallel channels (250 μm wide x 60 μm high) perpendicular to the collagen. All channels were pre-incubated with 0.5% BSA. Anti-coagulated whole blood (PPACK) was treated with or without an intracellular Ca^{2+} dye. Fluo4-NW (2.5 mM probenecid) was loaded into platelets by incubating 1 part dye with 4 parts blood for 45 min. Dye treated or untreated blood was then placed in the inlets of three channels. A syringe pumped allowed simultaneous perfusion of the three channels at an initial wall shear rate of 1160 s^{-1} . After the collagen patches (250 x 250 μm) were covered with platelets, flow was immediately switched to Ca^{2+} buffer (5 mM, 0.01% DMSO) in the presence or absence of antagonist (blebbistatin or mixtures of SQ-29,548, MRS-2179, 2-MeSAMP). In some experiments, buffer flow was stopped (30-sec or 1-min) and then reestablished or completely stopped following 7 min of perfusion. Intracellular Ca^{2+} fluorescence and platelet deposit structures were imaged with a 20x objective, in 15 sec intervals, for the duration of the experiment.

3.2.7 Finite Element Analysis

COMSOL Multiphysics software was used to numerically solve steady state pressure gradients, blood flow velocities and permeation velocities over complex geometries (collagen plus thrombus) with constant permeability in the PDMS permeation device. Blood ($\rho=1060 \text{ kg/m}^3$, $\mu=0.003 \text{ Pa}\cdot\text{s}$) and buffer ($\rho=1000 \text{ kg/m}^3$, $\mu=0.001 \text{ Pa}\cdot\text{s}$)

were both modeled using laminar flow for solution of the Navier-Stokes equation ($Re=0.49$, $Re_{\text{element}}=0.25$). The collagen region was modeled using Darcy's law ($\nabla^2 P=0$) with entrance and exit pressures being coupled to the external laminar flow properties and permeability (κ) set to a previously determined value (eg. $\kappa = 1 \times 10^{-15} \text{ m}^2$) [42]. Flow rates of 13 $\mu\text{L}/\text{min}$ for blood and buffer allowed the downstream resistance length to be modified to achieve $\Delta P=23.5 \text{ mm Hg}$ at the collagen scaffold interface.

Collagen, platelet, and platelet/fibrin permeability were each solved in COMSOL for the complex geometries of the collagen scaffold and developed thrombus. Calculating and comparing the permeability of collagen to previously reported values provided experimental validation of the device [41, 42]. Experimental pressure and calculated average velocity data were used as input parameters. The square difference between the experimental and computational average velocity across the collagen scaffold were iteratively reduced ($<0.001 \mu\text{m}^2/\text{s}^2$) by varying the collagen permeability. With the solved collagen permeability, the process was repeated for the platelet or platelet/fibrin geometry on the collagen. The normalized dye concentration in the channel was used as transient input data into the model. Matching the transient pulse concentration at the collagen output with the experimental output validated the computational model. As expected, calculated values of κ were not dependent on ΔP .

3.2.8 Statistics

Two-tailed Student's *t*-tests were used to calculate all *P* values. Statistically significant differences were reported if $P < 0.05$.

3.3 Results

3.3.1 Microfluidic device for measuring clot permeability and contractility

A microfluidic device was designed to allow pressure-driven transthorbus permeation with simultaneous imaging of clot contractile dynamics under flow. The device has a blood and buffer inlet port, collagen scaffold, and three ports for pressure readings (P1, P2, P3) up to 50 mm-Hg (**Figure 3-1A and Figure 3-2**). The downstream buffer and upstream whole blood flows merge into a narrow channel to create resistance and control the lumen pressure at the collagen site corresponding to $(P2+P1)/2$. The pressure readings in these locations allowed the pressure drop across the collagen to be controlled, thus allowing computer simulation (**Figure 3-1B**) of Darcy flow through the complex geometry assuming constant permeability of the collagen (**Figure 3-1C**). Exposing a 250 μm long x 60 μm wide surface area of collagen (\pm linked lipidated tissue factor) to whole blood flow provided a localized thrombotic site comparable to a previous device without permeation [31]. The side view of collagen made it possible to image the permeation of dyes and the morphology of fibrin and platelet deposits as they contracted (**Figure 3-1D and Figure 3-1E**).

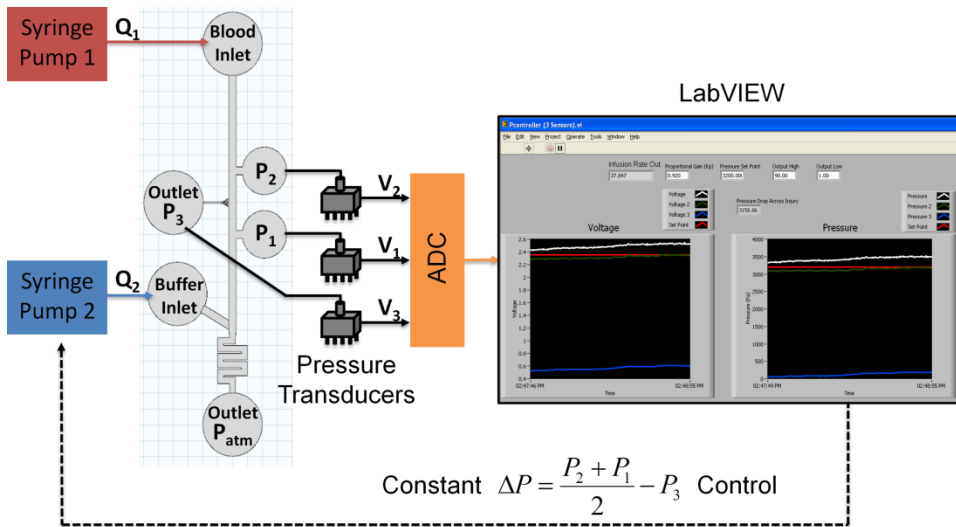


Figure 3-2 A microfluidic device to control trans-thrombus pressure drop independent of shear rate.

Syringe pump 1 and syringe pump 2 are constant volume pumps that perfuse anti-coagulated whole blood and 5 mM Ca^{2+} buffer respectively. The increased downstream resistance due to a narrowed length of channel and the buffer flow causes an increase in upstream pressure. The pressure measurements at P1, P2, and P3 are converted from voltages to digital signals which LabVIEW records and uses to proportionately control pressure drop via an increase or decrease in syringe pump 2 flow rate.

3.3.2 Stopping flow caused platelet and clot retraction

During permeability testing of platelet deposits (no thrombin), the interruption of blood flow resulted in a drastic contractile response of the newly formed clot (**Figure 3-3**). This retraction unexpectedly enhanced permeability due to the reconfiguration of the supporting collagen and opening of flow paths along the sides of the collagen (**Figure 3-4**). To investigate the contraction triggered by flow cessation, platelet deposits were formed for 10 min with embedded 50 nm fluorescent beads as fiduciary markers (inlet wall shear rate of 1130 s^{-1}). A wall shear rate of 1160 s^{-1} was used to reproduce rates found in capillaries where the pressure drops between the vessel lumen and interstitial space are known [25, 26]. This shear rate is also in the range of arterial flows. Following the thrombus formation for 10 min, the flow was switched without interruption to buffer for 4.5 min and then flow was completely stopped. Switching the flow from blood to buffer prevented the arrival of new platelets and release of fresh ADP or TXA_2 [66, 67]. Thrombus structure was mapped before and after stopping the flow (**Figure 3-3A**). The upstream and downstream edge contraction rates were measured throughout the buffer flow period and after flow stoppage (**Figure 3-3B**). Contraction rates 1 to 2 min after flow cessation significantly increased by 6.5-fold (upstream region) and 4.6-fold (downstream region) ($P < 0.05$), compared to the rate during buffer flow. Donor to donor variability ($n=3$ donors) for total clot contraction, 7 minutes after flow arrest, was $8.93 \pm 3.89 \text{ }\mu\text{m}$ and $13.6 \pm 4.42 \text{ }\mu\text{m}$ at the upstream and downstream positions respectively. The restructuring of the thrombus upstream and downstream edges by 2 min post flow cessation resulted in contractile trajectories of embedded beads towards the center of the thrombus mass (**Figure 3-3C and Figure 3-5C**). Comparisons of the time dependent

contraction data in the Y and Z direction at upstream and downstream positions of the clot demonstrated increased contraction rates after flow cessation (**Figure 3-3D**). Movement in the +Z-direction occurred rapidly and simultaneously in the upstream, downstream and middle positions due to an immediate rebound effect caused by a reduced pressure drop and reduced permeation when the flow was stopped (**Figure 3-5**). Total bead distance in the Y and Z direction shows the rates at which the clot contracts in all three locations (**Figure 3-5**). The ~1 min delay in contraction in the Y direction is one indicator of an active signaling mechanism that must be engaged following the cessation in flow.

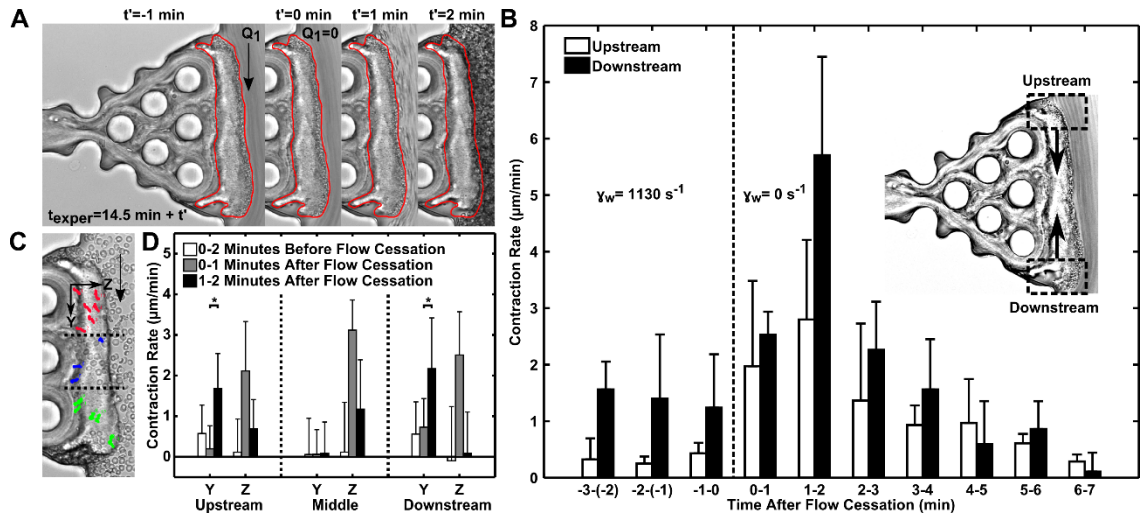


Figure 3-3 Flow arrest triggers clot contraction.

A thrombus formed in the absence of thrombin and presence of fluorescent 50 nm beads was rinsed with Ca^{2+} buffer for 4.5 min before the cessation of flow caused a rapid contraction. The outline of a pre-retracted thrombus ($t'=-1$ min) shows the inward retraction of the thrombus following flow stoppage ($t'=0$ to 2 min) (A). Contraction rate of the upstream and downstream sections of the thrombus were measured before and after flow arrest ($n=3$ donors) (B). Trajectories of the 50 nm beads represent the contractile response of the thrombus at upstream (red, $n=6$), middle (blue, $n=3$), and downstream (green, $n=6$) locations (C). Stopping the flow caused a significant increase in contraction rate in the Y and Z directions. To quantify these rates, the times before (0-2 min) and after flow cessation (0-1 min, 1-2 min) were monitored for bead velocity in the three sections of the thrombus (D). Downstream contraction rate in Y direction is shown as absolute value for contraction toward the middle region. *, $P<0.01$; error bars indicate mean \pm SD.

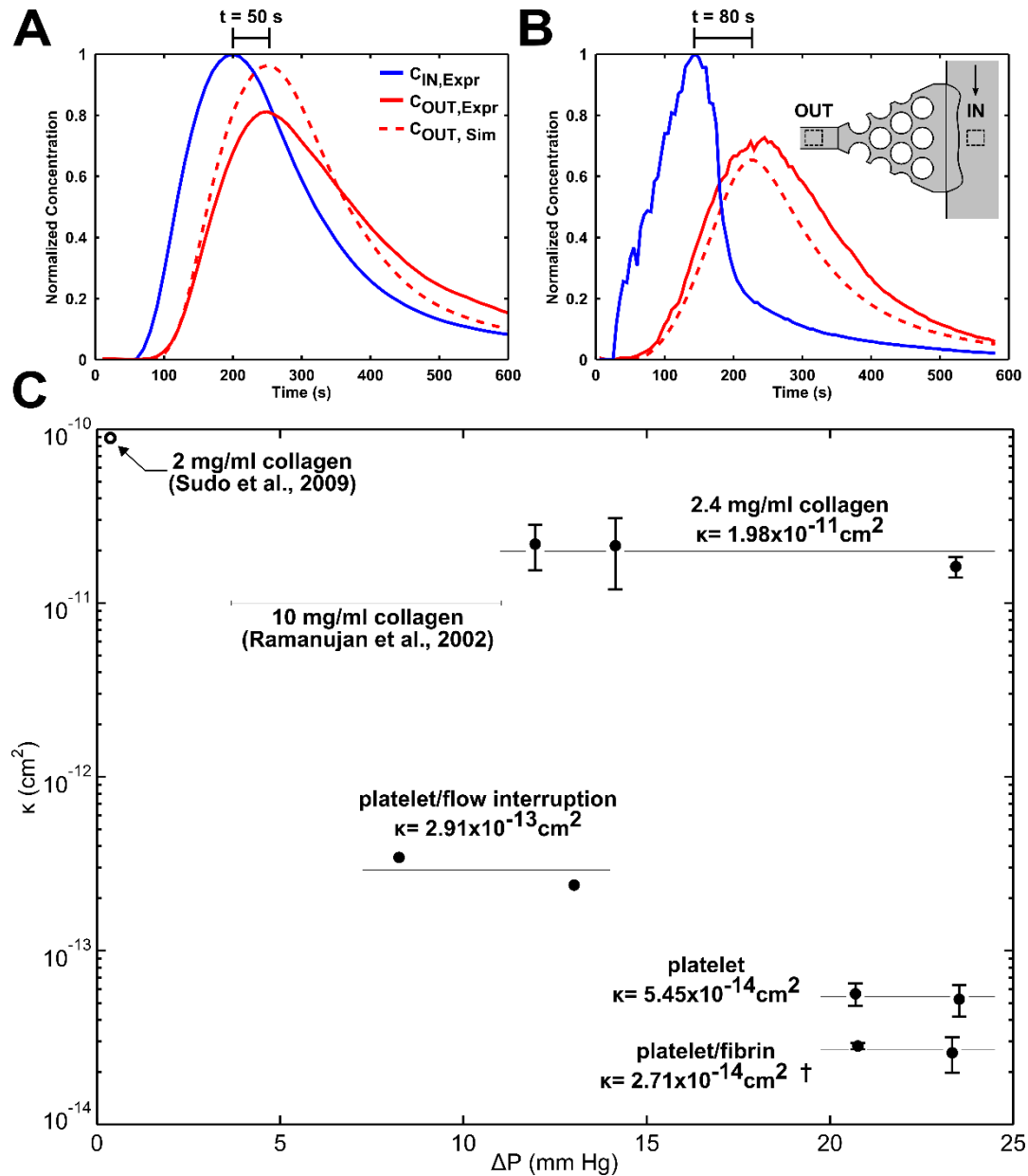


Figure 3-4 Clot permeability.

Thrombi formed under 1130 s^{-1} were pulsed with fluorescent dye at controlled pressure drops. The normalized input and output fluorescent intensities, along with a numerically predicted output from COMSOL were measured over time for clots formed in the absence (A) and presence of TF (B). Thrombus formed without thrombin reduced the residence time of the permeated dye by 30 s compared to platelet/fibrin thrombus. COMSOL simulations were used to numerically calculate permeability over collagen (n=9), platelet (n=6, 5 donors), platelet/fibrin (n=4, 4 donors), and platelet/flow interrupted (n=2, 2 donors) geometries at constant pressure drops (C). †, $P < 0.01$; error bars indicate mean \pm SD.

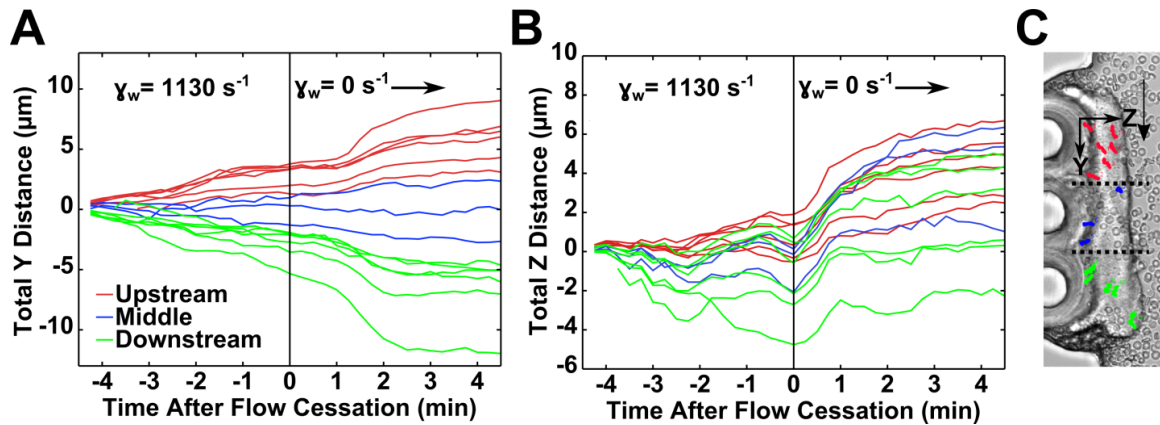


Figure 3-5 Spatiotemporal variation of contraction with flow arrest.

Platelet deposits with 50 nm beads were formed at 1130 s^{-1} and $\Delta P = 23.5 \text{ mm Hg}$. Deposits were rinsed with buffer 4.5 min prior to flow arrest. Total bead distance was measured before and after flow cessation at the upstream, middle and downstream positions within the clot, in both the Y (A), and Z directions (B). The fastest velocity of beads travelling in the Y direction was $\sim 1 \text{ min}$ following flow arrest. Conversely, the immediate decrease in pressure drop and clot permeation caused the bead distance in the Z direction to immediately increase after the cessation of flow. Bead trajectories were mapped in the upstream (red), middle (blue) and downstream (green) portions of the clot throughout the duration of the experiment (C).

3.3.3 Permeability of collagen, platelet deposits, and platelet-fibrin thrombus without flow interruption

To measure permeability without triggered thrombus contraction, dye tracer was pulsed immediately following whole blood flow without interruption of the flow. Inlet and outlet concentrations were measured with time to determine the permeation velocity at several physiologic pressure drops [25, 26]. Permeability was numerically calculated over the complex geometry (**Figure 3-4A and Figure 3-4B**) by reducing the squared error between the experimental and simulation permeation velocity. We validated this approach by comparing our calculated collagen permeability ($\kappa_{\text{collagen}} = 1.98 \times 10^{-11} \pm 0.640 \times 10^{-11} \text{ cm}^2$) with previous literature values (**Figure 3-4C**) [41, 42]. Similarly, permeation velocity was measured across platelet deposits and platelet-fibrin thrombi formed on collagen or TF/collagen scaffolds, respectively. Simulations that accurately predicted the experimentally measured output of dye concentration over the course of these experiments allowed determination of the permeability of the thrombus (**Figure 3-4A and Figure 3-4B**). The resulting permeabilities for platelet deposits ($\kappa_{\text{platelet}} = 5.45 \times 10^{-14} \pm 0.898 \times 10^{-14} \text{ cm}^2$) and platelet-fibrin thrombus ($\kappa_{\text{thrombus}} = 2.71 \times 10^{-14} \pm 0.377 \times 10^{-14} \text{ cm}^2$) formed after 10 min of flow quantify the resistance that each structure provides to resist bleeding. In the absence of thrombin, PPACK-treated whole blood formed a platelet mass that was >350-fold less permeable than collagen alone. The presence of thrombin and formation of fibrin provided a further 50% reduction in permeability under hemodynamic conditions. Comparing the measured platelet deposit permeability (without flow interruption) to that obtained following flow interruption ($\kappa_{\text{interrupted}} = 2.91 \times 10^{-13} \pm 0.745 \times 10^{-13} \text{ cm}^2$) demonstrated the impact that stopping the flow

had on the ability of the platelet deposit to maintain hemostasis in our device. In addition to permeability measurements, we observed decreased platelet accumulation with increased pressure drop (13.8 vs. 23.4 mm Hg) across the intraluminal thrombus in PPACK-treated whole blood (**Figure 3-6**), likely due to increased transthrombus permeation of ADP and TXA₂ into the collagen.

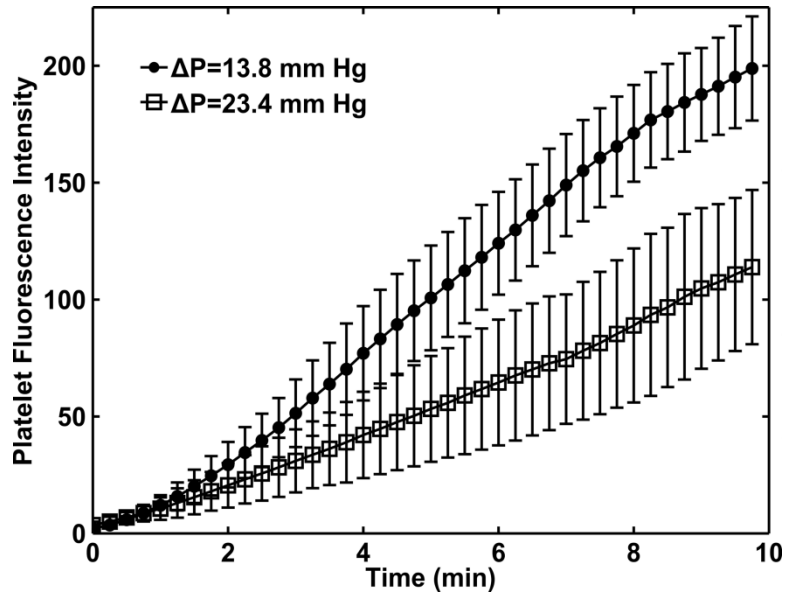


Figure 3-6 Transthrbus pressure drop affects platelet deposition.

PPACK-treated whole blood was perfused over a permeable scaffold of collagen at 1130 s^{-1} for 10 min. Platelet fluorescence intensity was measured for the platelet deposits formed at a low ($\Delta P=13.8 \text{ mm Hg}$, $n=3$) and high ($\Delta P=23.4 \text{ mm Hg}$, $n=3$) pressure drops. Increased transthrbus pressure drops caused a significant decrease in platelet deposition at the site of injury. Data was collected using 5 separate donors; error bars indicate mean \pm SD.

3.3.4 Clot retraction in a rigid wall flow device with flow reduction or cessation

Clot retraction was also examined in a rigid, impermeable parallel-plate microfluidic device lacking transthrombus permeation. Clot development in PPACK-treated whole blood was imaged on a 250 μm x 250 μm area of glass-supported fibrillar collagen at an initial wall shear rate of 1160 s^{-1} . Flow cessation resulted in a ~ 10 μm contraction (upstream region) towards the center of the thrombus as outlined in **Figure 3-7A**. In comparison, by switching to 10 μM blebbistatin perfusion (without flow disruption) for 7 min before the flow cessation, clot retraction after flow cessation was reduced 90% to only ~ 1 μm (**Figure 3-7B**). Blebbistatin is a well established platelet myosin IIA ATPase inhibitor [68]. In a scenario where flow was reduced from arterial (2000 s^{-1}) to venous (100 s^{-1}) shear rates, total contraction was similar to that observed with flow cessation. Also, the contraction was ~ 5 μm larger than stopping the flow following blebbistatin treatment (**Figure 3-8**). This result demonstrates the requirement of platelet myosin IIA activity in the triggered thrombus contraction following flow reduction or cessation.

We also measured clot retraction while stopping and restarting flow after a 30-sec or 1-min interruption (**Figure 3-7C**). Statistical differences between complete cessation of blood or buffer and the 30-sec flow interruption became apparent after 1 min. Interrupting flow for 1 min took 5 min to diverge statistically from complete flow cessation in buffer. While neither of the temporary flow interruptions (30-sec or 1-min) were statistically different from each other, the longer 1-min delay provided enough time to engage the contraction mechanism before eventually being diminished by the return of

flow. The technique of switching to a non-physiologic buffer and measuring contraction was validated by showing no contractile differences between stopping the flow in blood or stopping buffer flow after 7 min of rinsing.

Since flow cessation results in a dramatic change in both wall shear stress and wall shear rate on the thrombus structure, we investigated the role of soluble autocrine mediators whose concentration may change when flow is stopped. To explore the role of TXA₂, we added 1 μM SQ-29,548, a potent TXA₂ receptor antagonist [69]. Additionally, the contribution of ADP was investigated by adding 10 μM MRS-2179 and 50 μM 2-MeSAMP, selective inhibitors of the P2Y₁ and P2Y₁₂ platelet receptors, respectively [70]. The dose response curves for these inhibitors have been well established and the final concentrations used under flow exceeded the experimentally determined IC₅₀ values to ensure complete inhibition [69, 70]. After 7 min of buffer/antagonist perfusion, flow was stopped and total contraction was measured with time (**Figure 3-7D**). Both antagonists significantly reduced the total clot contraction as compared to buffer. ADP antagonists had the largest effect, reducing the total contraction nearly 75% over 7 min, whereas TXA₂ antagonist reduced the contraction by 44%. While uninhibited contraction can vary significantly between donors (~32-44%), the addition of antagonist results in consistent donor to donor percent reductions that vary <7% for ADP and <3% for TXA₂. These findings demonstrate ADP (from dense granules) and TXA₂ from activated cyclooxygenase-1 (COX1) were the mediators of the triggered contraction response upon flow cessation.

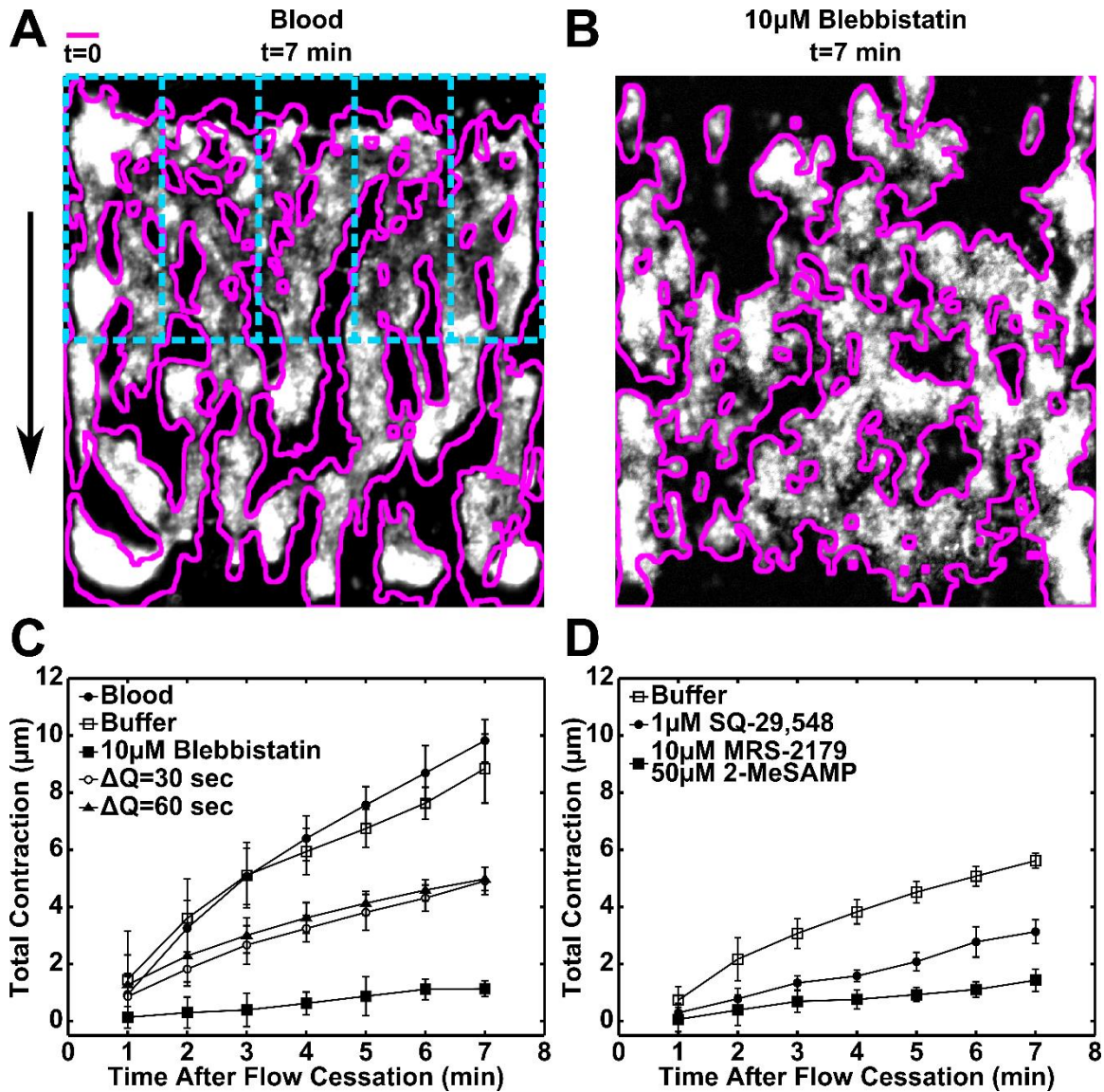


Figure 3-7 Contraction after flow arrest requires myosin and released ADP/TXA₂.

A parallel channel microfluidic device was used to develop thrombus in PPACK, at 1160 s⁻¹. Following the formation of stable thrombi, Ca²⁺ or antagonist buffer was used to rinse the surface for 7 min before stopping flow. Upstream contractions were observed in five sections (blue dashed line) over ten min. Stopping flow without a buffer rinse (**A**) and with a 10 μ M blebbistatin rinse (**B**) show clot retraction compared to a trace (pink line) before flow cessation. Total clot contraction measured over time compares the effects of blebbistatin and intermediate flow stopping with stopping flow with and without a buffer rinse (**C**). TXA₂ and ADP antagonist significantly reduced total contraction after flow cessation as compared to buffer (**D**). n=3 events at 5 discrete points for each time-point indicated, using 5 separate donors; error bars indicate mean \pm SD.

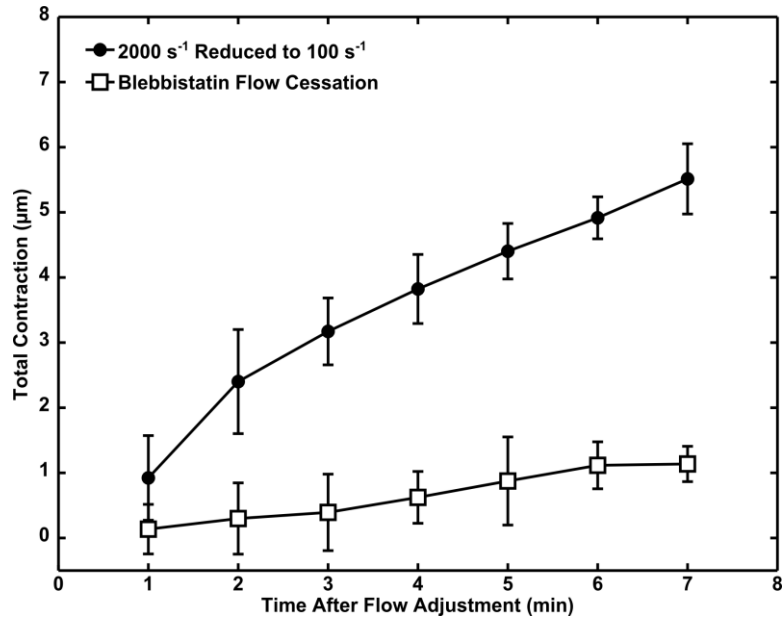


Figure 3-8 Platelet flow sensing occurs when arterial flow is reduced to venous flow.

A parallel channel microfluidic device was used to perfuse PPACK whole blood with labeled platelets over patterned collagen at an initial wall shear rate of 2000 s^{-1} . Arterial shear rates were reduced to 100 s^{-1} (venous) following the deposition of labeled platelets at the site of injury. Total contraction of the platelet deposits for three donors (n=7 total events) were followed immediately after the reduction in shear rate. Significant contraction was observed and can be compared to stopping flow following blebbistatin treatment (n=3). Error bars represent mean \pm SD.

3.3.5 Intracellular calcium mobilization is triggered by ADP and TXA₂ after flow cessation

To explore the role of ADP and TXA₂ in the flow sensing by the thrombus, we loaded platelets in PPACK-treated whole blood with Ca²⁺ sensitive dye fluo-4. Prior to flow cessation, we treated the platelet deposits with buffer in the presence and absence of a triple cocktail of 1 μM SQ-29,548, 10 μM MRS-2179, and 50 μM 2-MeSAMP. To minimize the measured intracellular Ca²⁺ fluctuations prior to flow cessation, initial contraction measurements were made 3 min after treatment and 3 min before flow arrest. The calcium signal increased as the platelet mass accumulated on the collagen between 0 and 4 min. When flow was switched to buffer at 4 min, there was no further deposition of platelets resulting in a slight decrease in signal. In the absence of inhibitors, flow cessation at 10 min caused an immediate and substantial mobilization of intracellular calcium (**Figure 3-9A**) that was completely blocked by the triple inhibitor cocktail to antagonize ADP and TXA₂ (**Figure 3-9B**). The calcium mobilization occurred within seconds following flow cessation and preceded the maximum platelet contraction rate which began 1 to 2 min after flow stoppage (**Figure 3-10**).

The triggered contraction by the platelet mass, following flow cessation, is an active material response requiring myosin (**Figure 3-7C**) and represents a flow sensing mechanism to impede contraction when flow is present. ADP and TXA₂ are the soluble mediators responsible for this response (**Figure 3-7D** and **Figure 3-9B**). Both of these agonists are highly sensitive to convective dilution which controls their concentrations in the boundary layer around the thrombus [51]. Since soluble species mediated Ca²⁺ mobilization and contraction upon flow cessation, the flow sensing involved a transport

mechanism: flow dilutes soluble species and flow cessation allows a rapid accumulation of autocrine ADP and TXA₂ to trigger G_q signaling via platelet P2Y₁, P2Y₁₂, and TP receptors (**Figure 3-9C**).

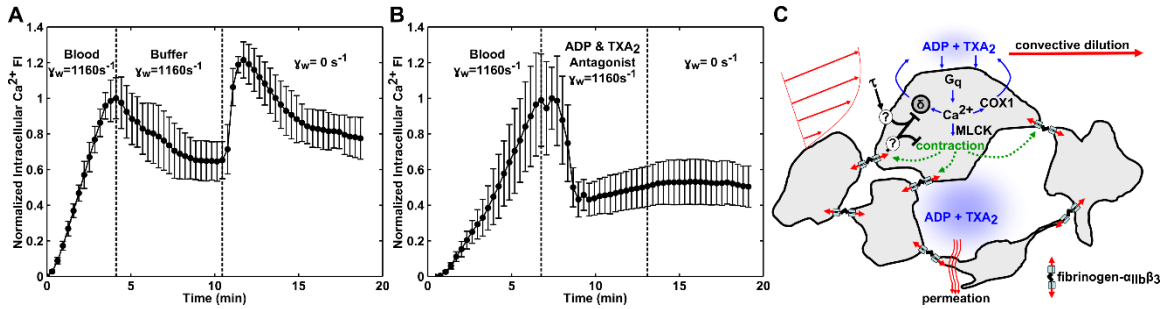


Figure 3-9 Flow cessation triggers platelet intracellular calcium mobilization via ADP/TXA₂ autocrine signaling.

Platelets in PPACK whole blood were loaded with Ca^{2+} dye and perfused over collagen at $1160 s^{-1}$. Following thrombus formation, whole blood perfusion was switched to Ca^{2+} or antagonist buffer for six minutes prior to stopping flow. Intracellular Ca^{2+} was measured via fluorescent intensity over time for either a Ca^{2+} buffer (A) or ADP and TXA₂ antagonist rinse (B). $n=3$ events using 2 donors, error bars indicate mean \pm SD. A schematic illustrates the flow sensing ability of platelets via convective removal of ADP/TXA₂ (C). Shear (τ) acting on the exterior of aggregated platelets accompanied by the strain placed on interconnected $\alpha_{IIb}\beta_3$ may signal the inhibition of contraction or dense granule (δ) release.

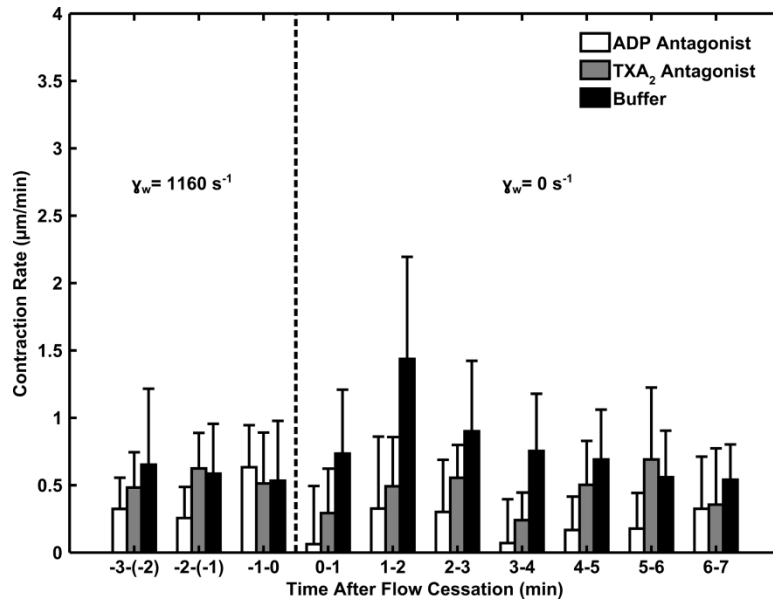


Figure 3-10 Treating platelet deposits with ADP and TXA₂ antagonist caused a significant decrease in contraction rate following the cessation of flow.

Platelet deposits were formed on patterned fibrillar collagen in rigid wall, parallel channel flow devices at 1160 s⁻¹. Following platelet clot development, PPACK blood flow was continuously switched to buffer (5 mM Ca²⁺, n=3), 10 µM MRS-2179 and 50 µM 2-MeSAMP (ADP antagonist, n=3), or 1 µM SQ-29,548 (TXA₂ antagonist, n=3) for 7 min. Flow was stopped and contraction rates were measured before and after. Data was collected using 1 donor and each independent event was analyzed at 5 discrete points; error bars indicate mean ± SD.

3.4 Discussion

We report a novel hemodynamic sensing function of intraluminal blood clots. Flow impedes clot retraction. When flow stops, intraluminal clots retract more rapidly and to a greater extent. This hemodynamic sensing by platelets in thrombus involves a rapid mobilization of calcium that strictly requires released ADP and TXA₂. Myosin activity is also required for the triggered contraction upon flow cessation, indicating that the contraction is not a passive material response to reduced drag forces. This concept of a triggered, active response is also consistent with the ~1 min delay between flow cessation and enhanced contraction.

While platelet contraction of a clot is usually considered in an isotropic context where blood is clotted in a tube and then detached from the glass walls to allow contraction, intraluminal thrombus formation is fundamentally different. In an isotropic assay, platelets have random orientation within a fibrin network whereas platelets depositing under flow conditions spread on collagen and then form many more platelet-platelet interactions due to high platelet concentration in the thrombus. In the thrombus formed under flow, the structure is less isotropic and spread platelets would be expected to exert greater forces along their axis of spreading and lesser forces perpendicular to the plane of spreading. Furthermore, clotted whole blood in a tube contains incompressible red blood cells at the prevailing hematocrit, while thrombus formed under arterial flow are greatly enriched in platelets (50-100X platelet rich plasma levels) and substantially depleted of RBC.

Despite recent advances in microfluidic devices and intravital mouse microscopy, few tools are available to control and study the effects of thrombus permeation under flow conditions. Recent studies examining angiogenesis demonstrated microfluidic devices that hold promise for studying *in vitro* clot permeability under flow conditions [36, 41]. However, these designs lacked the potential to produce controllable pressure drops and shear rates relevant to thrombosis and hemostasis. In the present study, we designed a microfluidic device to develop whole blood clots under physiologic flow and to investigate transthrombus permeation in the presence of a controlled pressure drop. The microfluidic device allowed the first reported *in vitro* clot permeability for clots formed under flow. While a measurement for the permeability of a contracted clot could not be obtained due to the accompanied structural changes in the absence of endothelium, it is expected to be less than that of a non-retracted platelet-fibrin deposit. Our measurement for these deposits represents a quantitatively important upper bound of the contracted clot permeability and the associated inner clot transport of ADP and TXA₂. Interestingly, the permeability of healthy rabbit aortic wall is on the order of 10⁻¹⁴ cm² [54], which is quite similar to our measurement of a platelet-fibrin thrombus. This suggests that a platelet-rich intraluminal thrombus has a permeability that is well matched to the surrounding intact endothelium. In addition to matching rigidity [59], an intraluminal thrombus may match permeability to the surrounding vessel wall. Under flow conditions, we propose flow sensing helps the spread platelet(s) maintain hemostatic function by balancing the contractile apparatus with the applied flow to limit platelet contraction since contraction would potentially create gaps for leakage or alter nearby endothelial function.

In a quantitatively more intense example of hemostasis, a blunt impact that compresses a vessel without rupturing the vessel would be expected to cause more extensive endothelial denudation. This situation is perhaps most analogous to the experimental configuration developed in this study. When blood flow is maintained in such an injured vessel, the flow impedes clot contraction because wound closure would not be needed. Also occlusion might be prevented since clot stabilization via contraction is impeded by flow. Reduced ADP/TXA₂ transport may also facilitate the formation of a dense inner thrombus core [71], while the outer domains of the clot remain loose and friable due to flow sensing. Throughout our studies with multiple donors, this was repeatedly verified by the constant but relatively low contraction rate under flow (**Figure 3-3B and Figure 3-11**). As vessel injury becomes severe enough to cause vessel rupture with blood leaving the vascular space, blood pools around the puncture/rupture/severed site. This results in more isotropic clotting of whole blood, which can exert isotropic contraction on the surrounding tissue to facilitate wound closure and consequently hemostasis (**Figure 3-12**). In this situation, the pooled blood around a leaking vessel is not subjected to substantial hemodynamic flow to dilute ADP/TXA₂ and thus impair platelet actinomyosin-mediated contraction. Additional highly diffusible platelet activators may also play a role in this observed contraction and provide an area of future study.

To further investigate the novel flow sensing abilities of platelets we examined their ability to contract following 30 seconds or 1 minute interruptions in flow. Contraction rates initially followed previous experiments but were drastically dampened

upon the return of flow (**Figure 3-13**). This result suggests that the quasi-steady state that platelet deposits reach under hemodynamic forces preserves their ability to rapidly contract in response to flow arrest. Flow sensing by a thrombus balances the need for wound closure and hemostasis against the risk of intraluminal occlusive thrombosis with dense contracted and lytic-resistant structures [72]. In cases of normal hemostasis, this mechanism would allow clots to contract gradually from their interior towards their exterior as hemodynamic flow is reduced. The extent to which stress present in the thrombus plays a role in signaling (i.e. mechanotransduction) remains a subject of future study. These experiments clearly demonstrate the ability of platelet deposits to rapidly assemble into a hemodynamic sensor and contract upon the arrest of flow.

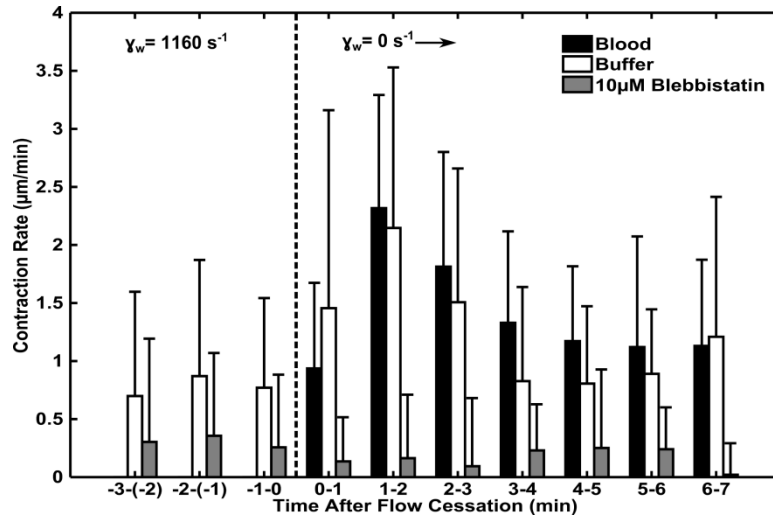


Figure 3-11 Blebbistatin, a myosin IIA inhibitor, reduced contraction rates before and after flow cessation.

Whole blood anti-coagulated with PPACK was perfused at 1160 s^{-1} over impermeable collagen in a parallel channel flow device. Flow was stopped immediately (blood, $n=3$) or following a 7 min rinse with 5 mM Ca^{2+} buffer ($n=3$) or 10 µM blebbistatin ($n=3$). Rinsing platelet deposits with buffer for 7 min was not significantly different than a physiological flow arrest in blood. Data was collected using 2 separate donors and each independent event was analyzed at 5 discrete points; error bars indicate mean \pm SD.

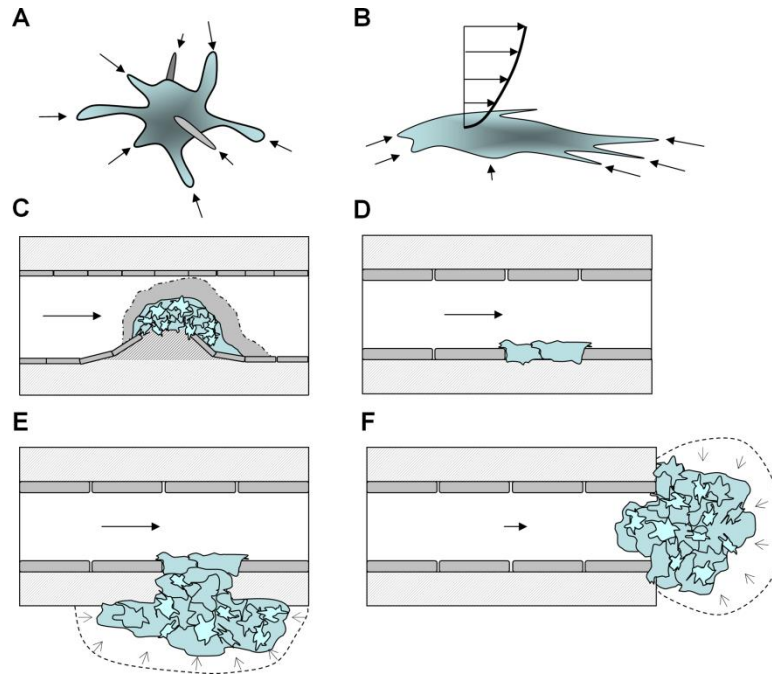


Figure 3-12 Platelet contraction is dependent on local hemodynamic flow conditions.

For blood clotted under static conditions platelets can exert isotropic contraction (A). When platelets spread on a surface, contraction becomes anisotropic due to platelet morphology (B). When non-occlusive intraluminal thrombi form at sites of plaque rupture (C) or denuded endothelium (D), contraction is limited due to the thrombus flow sensing where autocrine agents are controlled by convective transport. However, punctured (E) or severed (F) vessels, where flow is substantially decelerated, allows isotropic contraction of platelets and surrounding tissue to securely close the wound.

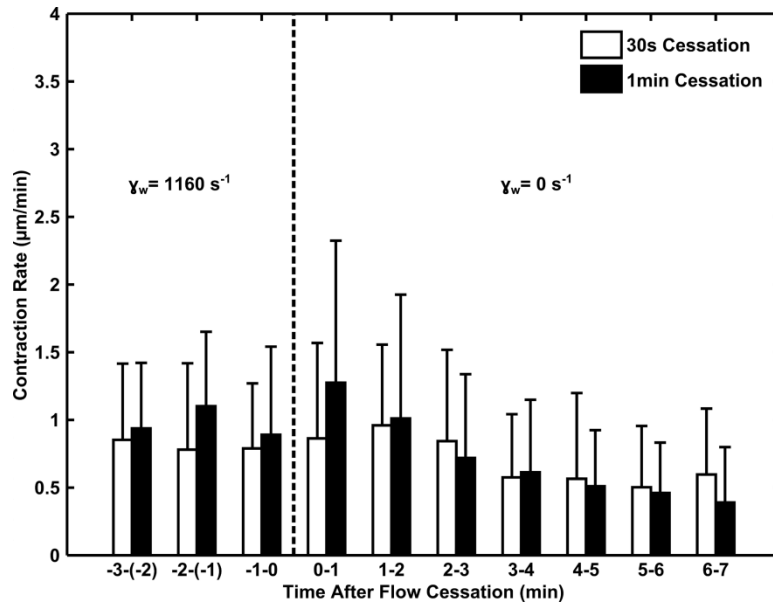


Figure 3-13 Reestablished flow dampens contraction mediated by temporary flow interruption.

Parallel flow channels were used to form platelet deposits in PPACK whole blood at 1160 s^{-1} . Following the development of the deposits, flow was continuously switched to buffer for 7 min. Immediately following the rinse, flow was interrupted and resumed after 30-sec (n=3) or 1-min (n=3). There were no significant differences in the contraction rates between the two interruption times due to the reestablished hemodynamic flow conditions. Data was collected using 1 donor and each independent event was analyzed at 5 discrete points; error bars indicate mean \pm SD.

Chapter 4 : Fibrin, γ '-fibrinogen, and trans-clot pressure gradient control hemostatic clot growth during human blood flow over a collagen/tissue factor wound

4.1 Introduction

During hemostasis, stable clot formation at the site of wounding is facilitated by the growth of a platelet plug and the generation of fibrin. Essential to vascular integrity, this structure must form rapidly under flow at an injury site, withstand hemodynamic forces, and prevent pressure-driven blood loss. With the laser injury mouse model, the *in vivo* architecture of the hemostatic clot has been revealed to contain two distinct regions of platelet activation: an inner tightly packed 'core' with extensive α -granule release and an unstable outer 'shell' with minimal α -granule release [27]. α -granule release is identified by P-selectin display and is characteristic of the core. Recent mouse studies have shown that the core region is thrombin and fibrin rich, platelet-retracted with lower porosity and reduced albumin mobility, and localized to the interior of the clot closest to the injury site. In contrast, the shell region is thrombin and fibrin poor, more porous and localized to the exterior of the clot towards the vessel lumen, and displays significant platelet turnover [27, 73-75].

The regional heterogeneity of platelet activation in clots highlights the complexities of when and where agonists are localized and what biochemical and physical parameters regulate hemostatic clot development. Importantly, the factors that trigger wall-attached clots to become fully occlusive thrombi are not fully understood,

but may include platelet hyper-reactivity, dysregulated thrombin production, and enhanced vWF function in pathological stenotic flows [76-78].

Thrombin is a potent platelet activator at ~1 nM and cleaves fibrinogen to drive fibrin polymerization at ~10 nM or higher. In humans, the γ -chain of fibrinogen has two expression variants: γ A (main form) and γ' (splice variant). The γ' -chain contains a 20-amino acid extension due to alternative mRNA splicing [79]. Unique to γ' -fibrinogen is a high affinity binding site for exosite II on thrombin [80]. While γ A/ γ' fibrinogen only makes up about 8-15% of total fibrinogen, γ' -fibrinogen can serve as a sink for locally produced thrombin [81-83]. Also, Factor XIII has a 20-fold higher affinity for the γ A/ γ' fibrinogen heterodimer than the γ A/ γ A fibrinogen homodimer [84].

Using microfluidics and human blood, our prior studies have demonstrated that fibrin polymerization stabilizes clots by anchoring the clot to the injury site with ~12 to 28-fold greater resistance to shear forces [48]. Our goal was to study the impact of fibrin(ogen)'s antithrombin properties and fibrin polymerization on thrombin mediated clot growth in human blood. Mouse models do not allow precise control of: prevailing shear rates, trans-thrombus pressure drops, or biochemical constituents of the wound. Additionally, mice lack the γ' splice variant of fibrinogen [85]. In order to study fibrin(ogen)'s role in the hemostatic growth of thrombi, it was critical to have reproducible hemodynamics. There are few studies that demonstrate the ability to simultaneously measure and control wall shear rate and trans-clot pressure gradients (Δ P). This limitation motivated our previous work on designing a microfluidic device

capable of independently controlling both wall shear rate and ΔP [46, 86]. Using this device we have now studied the localization of thrombin, the role of thrombin in platelet P-selectin display, and the role of fibrin polymerization and γ' -fibrinogen in regulating fibrin function. We report that fibrin, in addition to stabilizing clot structures against shear forces [48], is critical in localizing and restricting thrombin to the core region of a hemostatic clot.

4.2 Materials and Methods

4.2.1 Materials

The following instrumentation and reagents were used: analog pressure transducers (Honeywell Sensing and Control); human type-1 monomeric collagen (VitroCol, 3 mg/ml) (Advanced Biomatrix); recombinant tissue factor (Dade® Innovin®; Siemens); Sigmacote® (Sigma-Aldrich); polydimethylsiloxane (PDMS) (Ellsworth Adhesives); anti-fibrin antibody (gift from M. Poncz, Children's Hospital of Philadelphia); anti-fibrinogen γ' antibody (clone 2.G2.H9) and H-Gly-Pro-Arg-Pro-OH (GPRP, EMD Millipore); peak 1 fibrinogen (XIII free) and peak 2 fibrinogen (Enzyme Research Laboratories); anti-human CD62P antibody (BD Biosciences); anti-human CD41 antibody (AbD Serotec); anti-human CD32 antibody (STEMCELL Technologies Inc.); Boc-VPR-AMC fluorogenic peptide substrate (R&D Systems®).

4.2.2 Blood Collection

All blood donations were conducted in accordance with the IRB at the University of Pennsylvania. Human blood was drawn via venipuncture from healthy volunteers reported as both alcohol and medication free. Studies conducted in the presence of

thrombin were completed with blood drawn directly into 40 µg/ml corn trypsin inhibitor (CTI, Haematologic Technologies Inc.). Thrombin free investigations were performed with blood anticoagulated with 40 µg/ml CTI, 100 µM Phe-Pro-Arg-chloromethylketone (PPACK, Haematologic Technologies Inc.), and 1 µM Apixaban (Selleck Chemicals, Houston, TX, USA). Platelets were labelled with a fluorescently conjugated anti-CD41 monoclonal antibody (1 µg/ml, Abd Serotec) and P-selectin was labelled with a PE-conjugated anti-CD62P antibody (0.0625 µg/ml, Becton Dickinson Biosciences). Thrombin localization was visualized using either 5 µM Boc-VPR AMC or a thrombin sensitive antibody (5 µg/ml, ThS-Ab) [43]. Fibrin studies were performed with 0.5 µg/ml of a fluorescently conjugated, fibrin specific antibody (gift from the M. Poncz lab, Children's Hospital of Philadelphia) [44, 45].

4.2.3 Microfluidic device for control of wall shear rate and trans-clot ΔP

The microfluidic device fabrication has previously been described [38]. In brief, negative photoresist (KMPR 1050, MicroChem Corp.) was patterned on silicon wafers (D=100 mm, WRS Materials) using photolithography techniques. Soft lithography was then used to fabricate polydimethylsiloxane (PDMS) devices from the patterned wafers. The devices were designed with two inlets, two outlets, a post scaffold region and three pressure ports. Holes for tubing (0.020" ID x 0.060" OD, Cole-Parmer) and blunt needles (Small Parts) were punched with 0.75 and 0.5 mm I.D. corers (Harris Uni-Core™, Ted Pella, Inc.) The main channel was comprised of two pressure ports, one upstream and one downstream of the post scaffold region. These pressure ports were used to load the post scaffold region with polymerized type I collagen ± tissue factor (TF)

following treatment with 10% bovine serum albumin (BSA). Scaffold loading was accomplished by pulling the collagen solution through the main channel pressure ports out through the scaffold outlet. The entire channel was immediately rinsed following scaffold loading to remove any remaining fibers outside of the scaffold. After the channels were rinsed and loaded, the three pressure ports (main channel upstream, main channel downstream, and scaffold exit) were hooked up to pressure transducers (Honeywell Sensing and Control). The main channel inlet was connected to a whole blood syringe that was perfused by a constant volume syringe pump (PHD Ultra, Harvard Apparatus). The downstream inlet was connected to a buffer syringe that was perfused by a controlled constant volume syringe pump (PHD 2000, Harvard Apparatus). The buffer pump was controlled via a PID controller designed in LabVIEW (National Instruments). Briefly, the controller maintains constant channel pressure by reading channel pressure measurements (NI USB-6210, National Instruments) and adjusting the buffer pump flow rate. PID settings were calculated using the Ziegler-Nichols tuning method. These settings facilitated simultaneous control over multiple channels (**Figure 4-1**).

Devices were set up on an inverted microscope (IX81, Olympus America Inc.) with a three slide holder. Anticoagulated whole blood perfused through the channel at a constant wall shear rate was labelled with fluorescent antibodies for imaging using a CCD camera (ORCA-ER, Hamamatsu). Clots were imaged from a side view prospective as they developed on the localized collagen \pm TF scaffold. Unique to this design is the ability to independently control both the inlet flow rate (wall shear rate) and the

trans thrombus pressure gradient (ΔP) as the clots developed. Wall shear rates ranged from a venous shear rate of 100 s^{-1} to an arterial shear rate of 2000 s^{-1} [23]. All trans thrombus pressure gradients were maintained within a physiologically relevant range ($\Delta P=9\text{-}30 \text{ mm Hg}$) [25, 26].

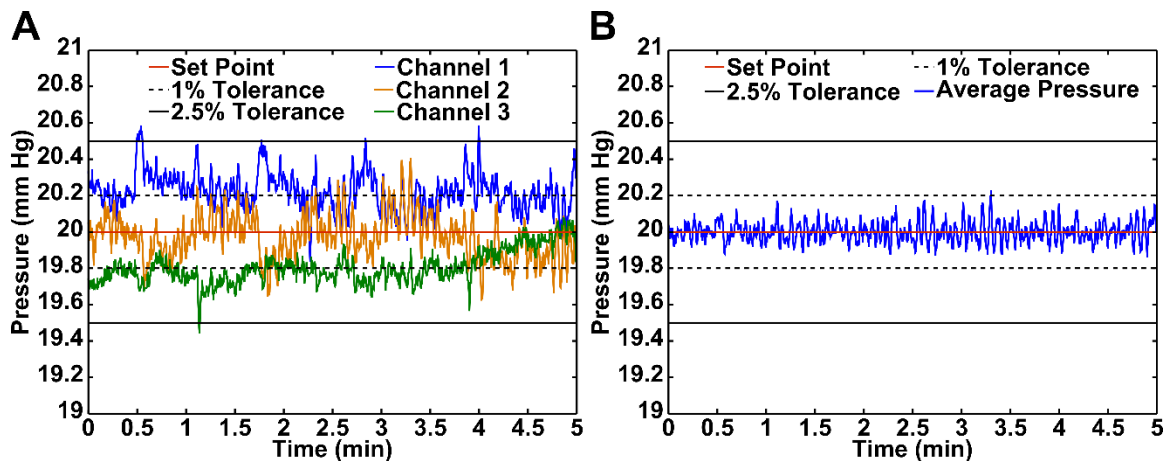


Figure 4-1 Independent pressure control was achieved in three channels simultaneously.

Dynamic pressure measurements were made using 0-1 psig pressure sensors at a constant wall shear rate. All three channel pressures were controlled within 2.5% tolerance (A). PID control was used based off of the average of all channels and was maintained within a 1% tolerance of the set point (B).

4.2.4 Fibrin polymerization and γ' fibrin(ogen) inhibition

Studies investigating fibrin polymerization were completed with GPRP. Whole blood anticoagulated with CTI or CTI/PPACK/Apixaban was incubated with HEPES (4-(2-hydroxyethyl)-1-piperazineethanesulfonic acid)-buffered saline (HBS) or 5 mM GPRP for 5 min. Two channels were then perfused simultaneously with the control (HBS) and 5 mM GPRP whole blood samples. Both channels maintained a constant wall shear rate (100 s^{-1} , 400 s^{-1} , or 2000 s^{-1}) and ΔP (20 mm Hg).

An anti-human CD32 antibody and an anti-fibrinogen γ' antibody were both used to investigate γ' fibrin(ogen)'s role in thrombin regulation. CTI whole blood was labelled with platelet, P-selectin, thrombin, and Fc γ RII antibodies for 5 min. Antibodies specific for Fc γ RII were used to prevent CD32-mediated platelet activation following incubation with anti-fibrinogen γ' antibodies. Fibrinogen γ' antibody free control buffer (0.1M Tris-glycine, pH 7.4, 0.15M NaCl, 0.05% sodium azide, 30% glycerol) was added to one sample and anti-fibrinogen γ' antibody was added at a 1:1 molar ratio with γ' fibrin(ogen) (0.3 mg/ml) [87]. Following 5 min, four channels were perfused simultaneously at a constant ΔP (16 mm Hg). Two channels were perfused at 100 s^{-1} and the other two were perfused at 2000 s^{-1} , both shear rates had one buffer control sample and one γ' fibrin(ogen) antibody sample.

4.2.5 Mouse cremaster arteriole laser injury model

Male mice 8-12 weeks of age were anesthetized with an intraperitoneal injection of sodium pentobarbital (90 mg/kg), and their jugular vein was cannulated for the introduction of fluorescent biomarkers. The mouse cremaster was exposed, cleaned of

connective tissue, opened, and prepared for viewing by intravital microscopy. The cremaster was maintained under a constant flow of bicarbonate buffer (37 °C) bubbled with 95%/5% N₂/CO₂. Mouse arterioles of 30-50 µm diameter were visualized with a BX61WI microscope (Olympus, St. Louis, MO, USA) with a 60X (0.9 NA) water immersion objective, and a CSU-X1 spinning disk confocal scanner (Yokogawa, Sugar Land, TX, USA). Fluorescence imaging was done using diode pumped solid state lasers (405 nm, 488 nm, 561 nm, 647 nm) with AOTF control as an excitation source (LaserStack, Intelligent Imaging Innovations, Denver, CO, USA), and images were captured using an Evolve digital camera (Photometrics, Tucson, AZ, USA). Endothelial cell ablation was performed with a pulsed nitrogen dye laser (SRS NL100, 440 nm) focused on the vessel wall through the microscope objective. The laser was fired between 1-10 times until red blood cells either escaped into the extravascular space or became trapped within the layers of the vessel wall. The University of Pennsylvania Institutional Animal Care and Use Committee approved all procedures. Platelets and P-selectin were labeled with fluorescent anti-GPIb α (Emfret Analytics, Eibelstadt, Germany, Clone: Xia.C3) and anti-CD62P respectively. Thrombin activity was measured using the previously described mouse thrombin sensor antibody (mThS-Ab). These fluorescent markers were imaged once per second for 3 minutes. Background fluorescence was measured within the vessel and subtracted from the images to determine staining intensities.

4.2.6 Image processing

Raw image stacks were processed by ImageJ (NIH). All stacks were background corrected using the “Subtract Background” feature in ImageJ. This feature averages the background over domains using a rolling ball approach [88]. Following background correction, images were thresholded using the triangle method [89, 90]. Binary images were then cropped to the middle 68% (first post to last post) of the clots while retaining the entire clot width. Total area was calculated for each frame and fluorescent tag.

4.2.7 Statistics

P values were calculated using paired or unpaired, two-tailed student’s *t*-tests. Statistically significance was reported if $P < 0.05$.

4.3 Results

4.3.1 Microfluidic device for investigating clot architecture at controlled wall shear rates and transthrombus pressure gradients

Thrombi were developed *in vitro* using a microfluidic device (**Figure 4-2A**). Clot formation was initiated when CTI whole blood was perfused across a post scaffold region loaded with collagen/TF (**Figure 4-2B**). The architecture of the developing clot was investigated from a side-view perspective at independently controlled wall shear rates and trans-clot pressure gradients. Clots formed within this microfluidic device, on collagen/TF scaffolds demonstrated distinct P-selectin positive and negative areas (**Figure 4-2C**). The P-selectin positive region (core) remained localized to the interior of the clot, closest to the collagen/TF surface. The P-selectin negative region (shell) enclosed the interior core region and remained exposed to the flowing whole blood. We have previously reported the ability of our device to generate these core/shell

architectures, which have only been observed *in vivo* [27, 86]. Recently, thrombin was revealed as the primary agonist responsible for core development *in vivo* during mouse arteriole laser injury [27, 73-75]. These results align with investigations we made using the soluble thrombin activity peptide, Boc-VPR-AMC where the highest thrombin activity was localized to the core region (**Figure 4-2D**). This is the first report of thrombin localization to the core region of human blood clots.

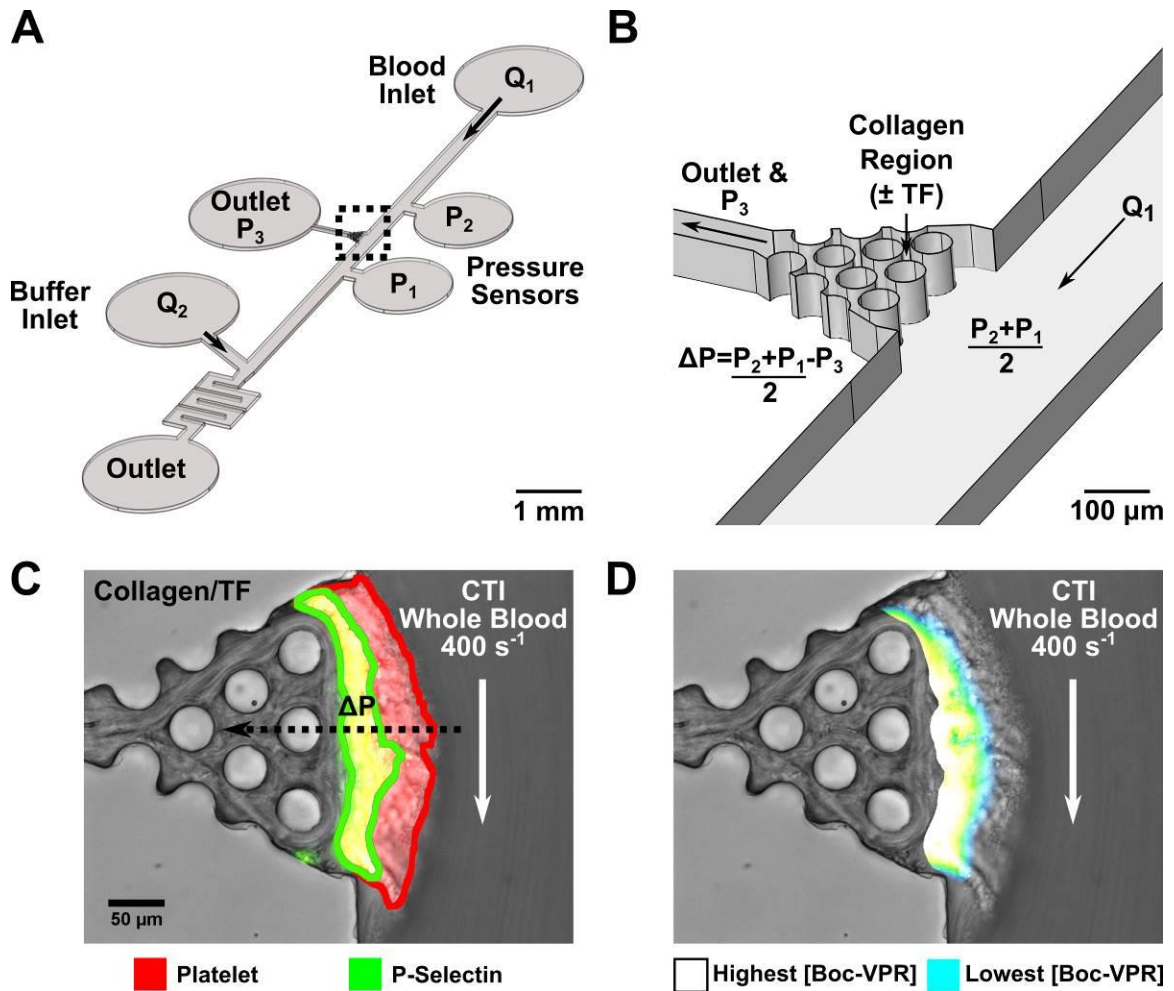


Figure 4-2 Thrombus architecture was investigated in a microfluidic device capable of independently controlling transthrombus pressure gradients and wall shear rates.

Anticoagulated whole blood was perfused at a constant wall shear rate (Q_1) while the transthrombus pressure gradients (ΔP) were independently controlled via downstream buffer infusion Q_2 (A). Polymerized collagen \pm TF was localized to a post scaffold centered between pressure ports P_2 and P_1 (B). Spatial and temporal thrombus development was monitored by side-view imaging at controlled wall shear rates and ΔP . Platelet (red) and P-selectin (green) were imaged to investigate spatial differences in platelet activation under physiologic flow conditions (C). A fluorogenic, thrombin cleavable substrate Boc-VPR-AMC was added to whole blood to demonstrate localized thrombin activity within clots developed in the presence of ΔP (D).

4.3.2 Transthrimbus pressure gradients influence thrombin mediated clot growth at 400 s^{-1}

Thrombin mediated clot growth was investigated by perfusing CTI-treated whole blood over a collagen/TF scaffold at 400 s^{-1} . Transthrimbus pressure gradients were maintained at either a low (9.0 mm Hg) or high ΔP (29.4 mm Hg). Total platelet area was calculated at each time point over the duration of the experiment ($t=10.8 \text{ min}$). Clots developing at lower ΔP (9.0 mm Hg) experienced faster initial growth (~ 3.8 fold faster, $t=0-1.8 \text{ min}$, $P<0.05$) and larger final heights (~ 1.5 fold larger, $t=10.5 \text{ min}$, $P<0.025$) than clots experiencing higher ΔP (29.4 mm Hg) (**Figure 4-3A**). The P-selectin (core) area was 57% of the total clot area for both low and high ΔP (**Figure 4-3B**). While % core remained constant, final core area was reduced by 33% ($P<0.05$) when ΔP was increased. Similar trends were observed when measurements were made with a thrombin sensing antibody. Final thrombin area was reduced by 43% ($P<0.05$) when ΔP was increased 3.2 fold (**Figure 4-3C**). This result indicates that the elution of inner clot thrombin to the surface of the clot was met with opposition by pressure-driven permeation of fluid through the clot, towards the “extravascular” space (the collagen post array). When trans-clot pressure drops were increased, the permeation-mediated transport through the clot also increased proportionately. This reduced thrombin transport towards the clot surface to result in a smaller core area. Thrombin and P-selectin area were highly correlated both spatially and temporally at low ΔP ($R^2=0.91$) and high ΔP ($R^2=0.95$) (**Figure 4-3D**). Reducing the permeation by decreasing ΔP results in greater flux of thrombin from the collagen/TF interface through the clot toward the lumen, thus resulting in a larger P-selectin positive core at lower ΔP .

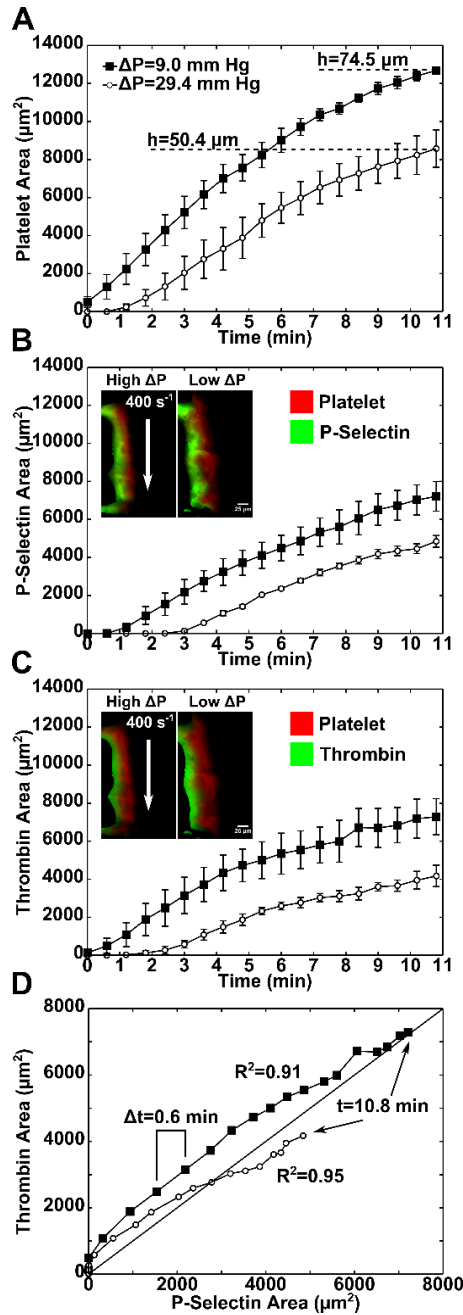


Figure 4-3 Transthrabus pressure gradients reduce clot size by diminishing thrombin boundary growth.

Platelet area was measured for clots ($n=3$) formed at a constant wall shear rate (400 s^{-1}) in the presence of either a low ($\Delta P=9.0$ mm Hg) or high ($\Delta P=29.4$ mm Hg) transthrabus pressure gradient (**A**). Clot architecture was investigated by measuring intrathrombus P-selectin (**B**) and thrombin (**C**) area for each condition. The correlation between platelet activation marker P-selectin and thrombin area were quantified for each condition over the duration of the experiment ($t=10.8$ min) (**D**).

4.3.3 Fibrin polymerization reduces both total platelet and core area at 400 s⁻¹

Fibrin polymerization has been recognized as an important step in clot stabilization and the prevention of embolic events [48]. Beyond this role, less is known about what impact fibrin polymerization may have on clot architecture and regulation of clot growth rate. In order to study these effects on thrombus growth and architecture we added GPRP, a fibrin polymerization inhibitor. Whole blood anticoagulated with CTI was incubated with and without GPRP prior to perfusion (400 s⁻¹) over a collagen/TF surface. All clots were developed in the presence of a constant transthrabus pressure gradient (Control- $\Delta P = 20 \pm 0.7$ mm Hg, GPRP- $\Delta P = 20 \pm 0.5$ mm Hg). Thrombus growth and architecture (P-selectin, fibrin) were monitored dynamically for 10.5 min of perfusion. Total platelet area and clot height grew to a greater extent when fibrin polymerization was inhibited by 5 mM GPRP (**Figure 4-4A**). Following 3 min of growth, clots formed in the presence of polymerized fibrin were statistically smaller ($P < 0.05$) than clots formed without polymerized fibrin. Disparity between clot size became even greater following 5.25 min ($P < 0.025$). Final clot height (t=10.5 min) was 67% ($P = 4.95 \times 10^{-5}$) larger when fibrin polymerization was inhibited. Accompanying total clot growth was an increase in core area (**Figure 4-4B**). P-selectin positive area grew 2-fold larger ($P = 0.003$) when fibrin polymerization was absent. As expected, fibrin polymerization, as measured by a fibrin specific antibody, was completely abolished by 5 mM GPRP (**Figure 4-4C**). The growth of fibrin slightly preceded the P-selectin positive core development in the control clots (no GPRP). This indicated that fibrin polymerization was responsible for mitigating core development and total clot growth at

400 s⁻¹, a phenomena that was not observed when thrombin was inhibited with PPACK
(Figure 4-5).

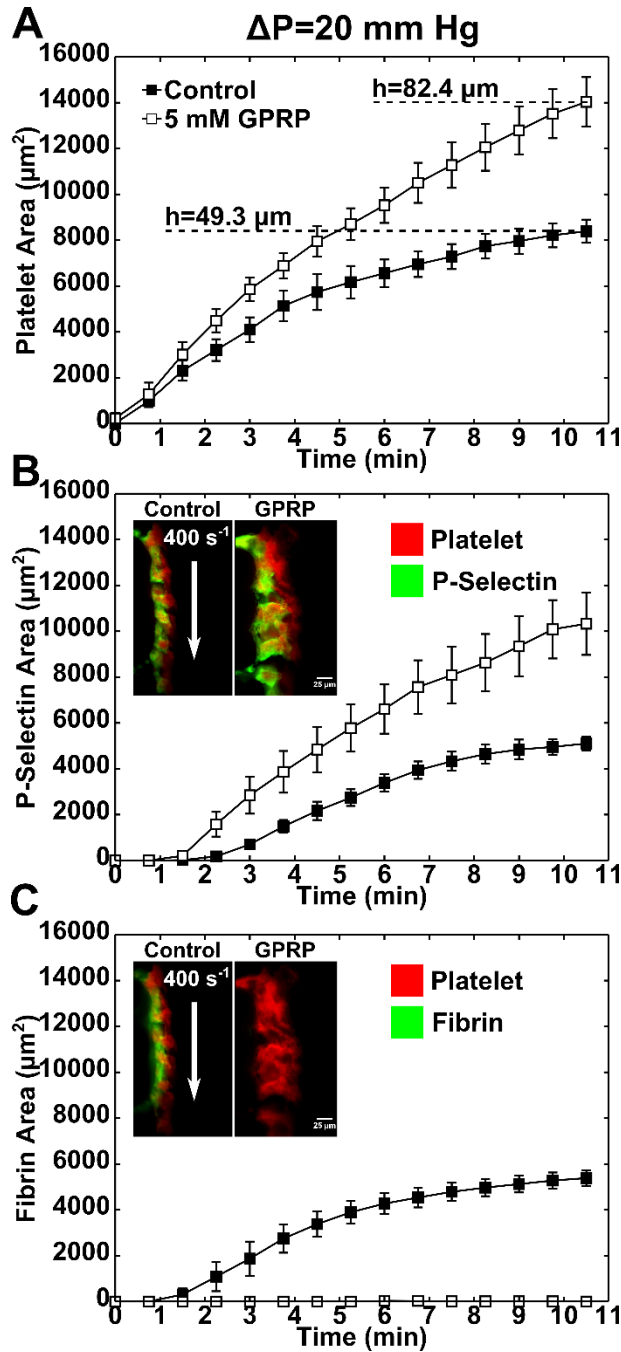


Figure 4-4 Fibrin polymerization reduces clot growth at a wall shear rate of 400 s^{-1} and $\Delta P=20$ mm Hg.

Platelet area (n=7, **A**) was measured in the absence (control) and presence (5 mM GPRP) of fibrin polymerization inhibitor Gly-Pro-Arg-Pro at a constant transthrombus pressure gradient ($\Delta P=20$ mm Hg) and wall shear rate (400 s^{-1}). P-selectin (n=7, **B**) and fibrin (n=4, **C**) area were monitored for each condition during 10.5 min of CTI whole blood perfusion.

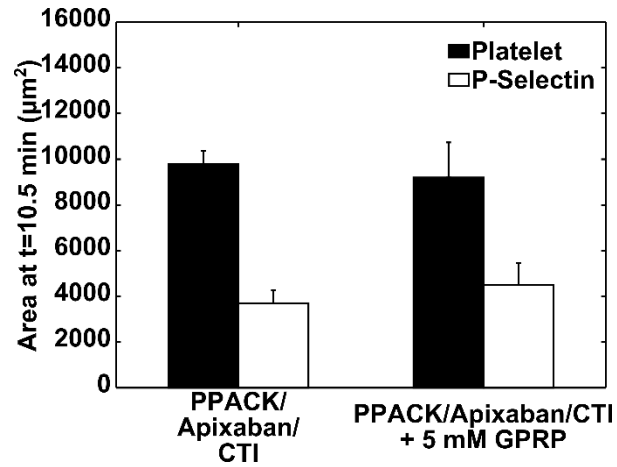


Figure 4-5 GPRP has no effect on the total clot or P-selectin (core) area when thrombin is inhibited.

Whole blood perfused at 400 s^{-1} was treated with PPACK/Apixaban/CTI to prevent thrombin generation and activity. Total clot and P-selectin (core) area were investigated in the presence and absence of 5 mM GPRP.

4.3.4 Wall shear rate does not influence the core or thrombin area but does influence the role of fibrin

Since our device facilitated independent control of both wall shear rate and transthrbus pressure gradients, we investigated clot architecture at constant ΔP (20 mm Hg) for three shear rates (100 s^{-1} , 400 s^{-1} , 2000 s^{-1}) ranging from venous to arterial flows. Total clot, core, thrombin and shell area were measured for 10.5 min of whole blood perfusion. The final area ($t=10.5\text{ min}$) for each were reported at the three distinct shear rates (**Figure 4-6A**). Interestingly, wall shear rate did not significantly alter the core or thrombin area when the trans-clot ΔP was held constant at 20 mm Hg. The only significant change that wall shear rate influenced was the shell size. The shell size was greatest at a venous shear rate of 100 s^{-1} as compared to 400 s^{-1} ($P=0.026$) and 2000 s^{-1} ($P=0.007$). This increased shell thickness resulted in an increase in total clot size at 100 s^{-1} ($P=0.009$ for 400 s^{-1} ; $P=0.015$ for 2000 s^{-1}). These outcomes indicated that shear rate only influences shell size while the transthrbus pressure gradient influences both core and thrombin boundary size (**Figure 4-3 and Figure 4-6**).

Clots in the presence of GPRP were developed in parallel with control clots for each shear rate. The blockade of fibrin polymerization on total clot, core, thrombin, and shell area was investigated at the final time point ($t=10.5\text{ min}$) (**Figure 4-6B**). Based on our previous results at 400 s^{-1} (**Figure 4-4**), we expected GPRP blockade of fibrin polymerization to enhance clot height and core area at both venous and arterial shear rates. This expectation was confirmed for an arterial shear rate of 2000 s^{-1} (**Figure 4-6C**). The addition of GPRP significantly increased total clot area (1.45-fold for 400 s^{-1} , 1.5-fold for 2000 s^{-1}) due to a drastic increase in core area (2.0-fold for 400 s^{-1} , 1.65-fold

for 2000 s^{-1}). The increase in core area was directly proportional to a significant increase in thrombin area at both 400 s^{-1} (108% increase) and 2000 s^{-1} (87% increase). Interestingly, clots developed at the venous shear rate of 100 s^{-1} did not increase in total clot, core, or thrombin area when fibrin polymerization was inhibited with GPRP. These results indicated that thrombin regulation in venous clots is not governed by fibrin polymerization.

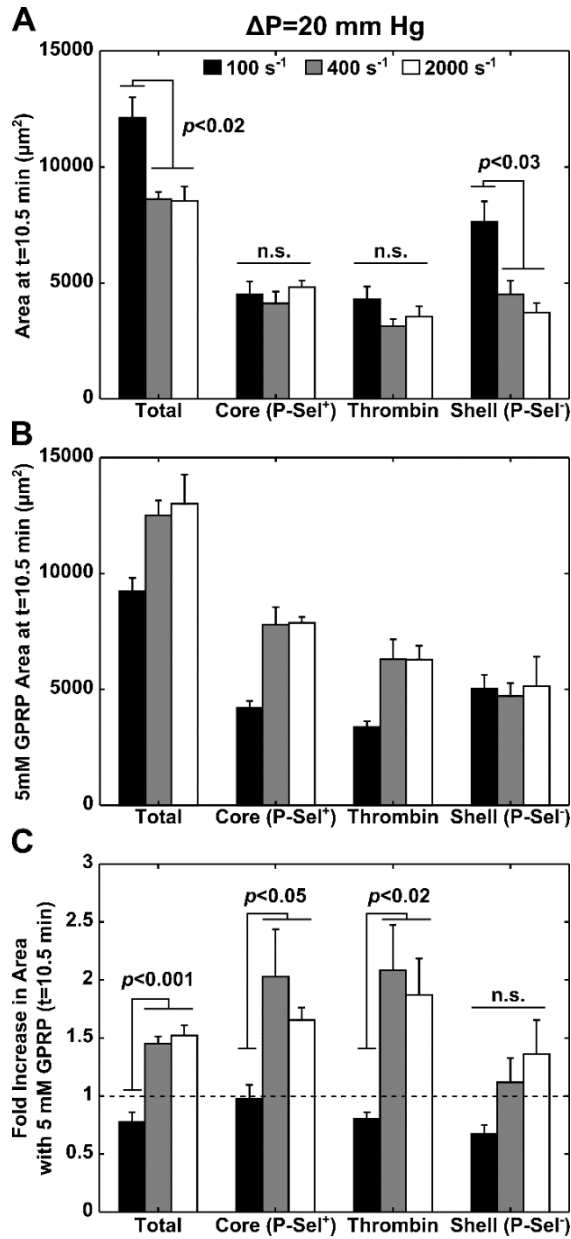


Figure 4-6 Wall shear rate does not change the core or thrombin area but does influence thrombin mediated clot growth in the absence of fibrin polymerization.

Total, core (p-sel⁺), thrombin, and shell (p-sel⁻) areas were measured, at the final time point (t=10.5 min), for clots developed at a constant pressure gradient ($\Delta P=20$ mm Hg) and varying wall shear rate (100 s^{-1} , 400 s^{-1} , 2000 s^{-1}) (n=4 for each shear rate) (A). CTI whole blood in the presence of 5 mM GPRP (fibrin polymerization inhibitor) was run in parallel at all experimental conditions (n=4 for each shear rate) (B). The fold increase in area with the addition of 5 mM GPRP was calculated for total, core, thrombin, and shell area (C).

4.3.5 γ' fibrin(ogen) reduces thrombin mediated clot growth at venous shear rates but not arterial shear rates

In order to further investigate the role of fibrin(ogen) in venous and arterial clot growth, we added a monoclonal γ' -fibrinogen specific antibody to inhibit the high affinity thrombin binding site on γ' -fibrinogen (**Figure 4-7**). Antibodies were incubated in CTI whole blood at a 1:1 molar ratio to 0.3 mg/ml γ' fibrinogen, a physiologically relevant whole blood concentration [87]. Control and γ' antibody treated samples were perfused simultaneously at both 100 s⁻¹ and 2000 s⁻¹. Total clot, core, and thrombin area were measured dynamically at a constant trans-clot ΔP (control $\Delta P=15.5$ mm Hg, γ' antibody $\Delta P=15.7$ mm Hg). Clots formed at the venous shear rate of 100 s⁻¹ had significantly increased total clot area, core area, and thrombin area when the high affinity thrombin binding site on γ' fibrinogen was blocked (**Figure 4-8, first column**). Total clot area after 11.25 min of whole blood perfusion was 2.0 fold larger ($P=0.019$) in the presence of the γ' fibrinogen antibody. This increase in total clot area was associated with faster core (1.5 min) and thrombin generation (1.25 min) and larger final areas (core-1.8 fold, thrombin-1.6 fold). Conversely, there were no significant differences between thrombi formed at the arterial shear rate of 2000 s⁻¹ (**Figure 4-8, second column**).

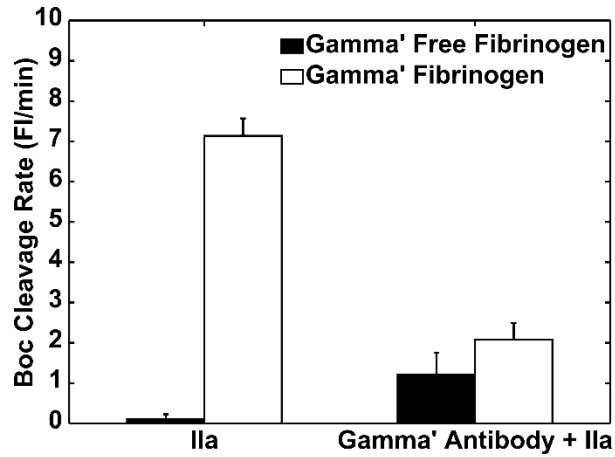


Figure 4-7 γ' -fibrinogen binds more thrombin and is inhibited to a greater extent than γ A-fibrinogen (free of the γ' -chain).

Wells in a 384 well plate were coated with either γ' -fibrinogen or γ A-fibrinogen. After rinsing and blocking non-coated surfaces with BSA, a monoclonal γ' -fibrinogen specific antibody was added to half of the γ' -fibrinogen wells and half of the γ A-fibrinogen wells. Excess antibody was removed and thrombin was incubated in each well. Following another rinse, a thrombin cleavable substrate (Boc-VPR-AMC) was added to each well and cleavage was followed using spectrofluorometry.

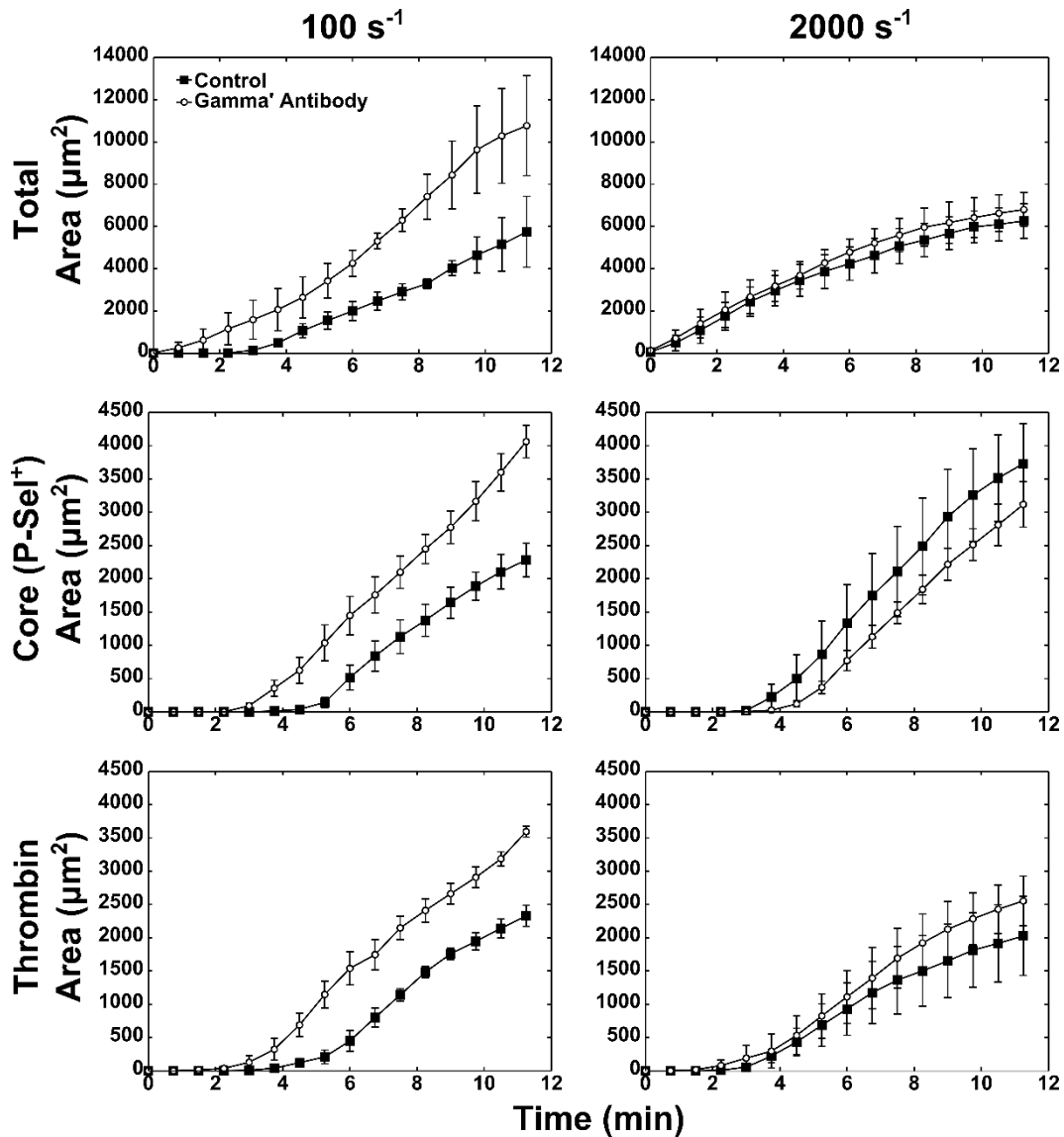


Figure 4-8 Inhibition of γ' fibrin(ogen) with a γ' specific monoclonal antibody results in larger clots at venous but not arterial shear rates.

Whole blood anticoagulated with CTI \pm γ' mAb was perfused over a collagen/TF scaffold at a constant transthrumbus pressure gradient (control $\Delta P=15.5 \text{ mm Hg}$, γ' antibody $\Delta P=15.7 \text{ mm Hg}$). Total, core (p-sel+), and thrombin area were measured dynamically at both venous (100 s^{-1} , **first column**, n=3) and arterial (2000 s^{-1} , **second column**, n=3) shear rates throughout the duration of the experiment.

4.3.6 Arterial shear rates promote increased platelet packing, greater thrombin retention, and more fibrin generation per area than venous shear rates

Since clots formed at venous and arterial shear rates demonstrated inverse growth patterns when fibrin polymerization or the high affinity thrombin binding site on γ' fibrinogen were blocked, we hypothesized that clot composition may influence fibrin(ogen)'s role in thrombin regulation. We investigated platelet packing density (**Figure 4-9A**), density corrected thrombin sensor cleavage (**Figure 4-9B**), and fibrin packing density (**Figure 4-9C**) by comparing clots formed in CTI whole blood at 100 s^{-1} to those formed at 2000 s^{-1} . Representative images at the final time point ($t=11.5\text{ min}$) demonstrated increased platelet packing at 2000 s^{-1} as compared to 100 s^{-1} . Likewise, density corrected thrombin sensor cleavage and fibrin packing density were also increased at arterial shear rates (2000 s^{-1}) as compared to venous shear rates (100 s^{-1}). The fold increase in platelet packing density as measured by platelet fluorescence intensity per area was on average 1.83 fold higher at 2000 s^{-1} than 100 s^{-1} (**Figure 4-9D**). After normalizing the thrombin sensor fluorescence intensity for platelet density, the results indicated that more sensor was cleaved in arterial clots than venous clots (1.4 fold). This provides a lower estimate for the relative increase in thrombin activity in arterial clots compared to venous clots. Supporting this estimate was the increased generation of fibrin in arterial clots (2.36-fold). These results demonstrated a drastic and important difference in the composition of clots formed at arterial or venous shear rates.

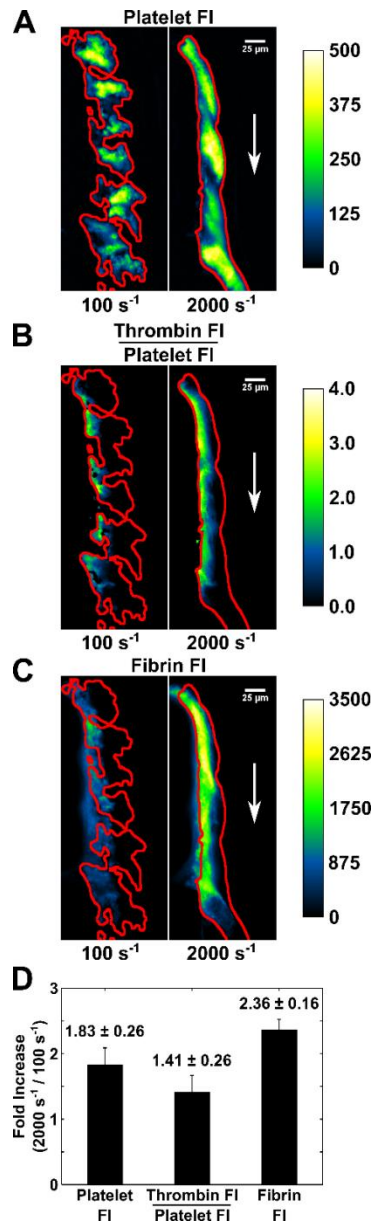


Figure 4-9 Clots formed at arterial shear rates pack tighter, cleave more thrombin sensitive peptide per area, and generate more fibrin per area than venous clots.

CTI whole blood was perfused simultaneously at a venous shear rate of 100 s⁻¹ and an arterial shear rate of 2000 s⁻¹. Platelet (A), normalized thrombin sensor (B), and fibrin fluorescence intensity (C) were imaged for 11.5 min. The fold increase in platelet fluorescence intensity per area (n=6) from clots formed at 100 s⁻¹ compared to 2000 s⁻¹ was averaged over the duration of the experiment (D). In addition, the density corrected thrombin sensor cleavage (n=6) and fibrin fluorescence intensity (n=3) were calculated and compared for venous and arterial clots.

4.3.7 Fibrin polymerization reduces clot growth at pathological shear rates

In pathophysiology, wall shear rates can reach $100,000\text{ s}^{-1}$ in stenosed vessels [24]. We investigated clot formation in a scenario similar to vessel stenosis by stepping the wall shear rate up from an initial venous shear rate of 200 s^{-1} to a pathological shear rate of $15,000\text{ s}^{-1}$. Clots were formed in PPACK whole blood at 200 s^{-1} for 7 min before stepping the shear rate up to $15,000\text{ s}^{-1}$ for an additional 7.75 min (**Figure 4-10A-C**). Following the increase to pathological shear rates, rapid platelet aggregation at the upstream edge of the clot resulted in a low shear regime prior to the trailing edge of the clot. The low shear regime facilitated the accumulation of ADP and TXA_2 agonists. This was evident by the clot contraction at the downstream edge of the clot (**Figure 4-10C**), a flow sensing mechanism that we previously documented when shear rates were reduced [46]. In this experiment, the contraction towards the center of the clot was not prevented, even at $15,000\text{ s}^{-1}$.

The role of fibrin polymerization was also investigated at pathological shear rates. Whole blood anticoagulated with either CTI or PPACK was perfused across a collagen/TF or collagen surface respectively. Experiments were performed simultaneously with both control and GPRP treated samples in order to evaluate the role of fibrin polymerization. The blood was initially perfused at an arterial shear rate of 2000 s^{-1} . After 5.4 min, the wall shear rate was increased to a pathological shear rate of $15,000\text{ s}^{-1}$ for the remaining 5.8 min of the experiment. The inhibition of fibrin polymerization with GPRP in CTI whole blood resulted in increased clot growth for both arterial and pathological shear rates (**Figure 4-10D**). The average clot height of GPRP clots was

73.2% larger after 5.4 min of flow at 2000 s^{-1} ($P=0.006$) and 152.4% larger after an additional 5.8 min of flow at $15,000\text{ s}^{-1}$ ($P=0.001$). In contrast, PPACK whole blood clots did not demonstrate a significant increase ($P>0.05$) with the addition of GPRP at either arterial or pathological shear rates (**Figure 4-10E**). This demonstrated a specific effect on clot growth due to the inhibition of fibrin polymerization and not off target effects.

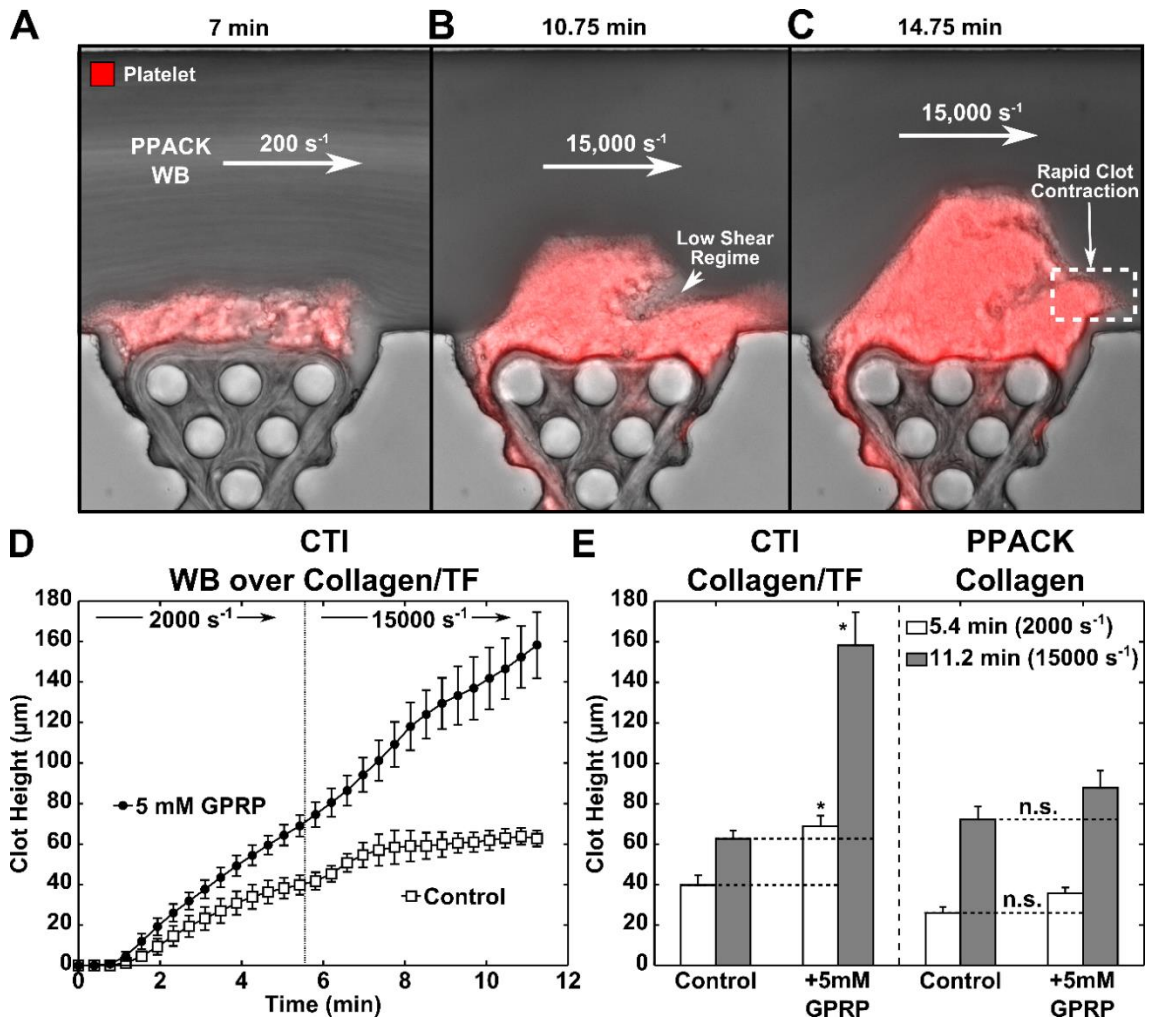


Figure 4-10 Clot growth at pathological shear rates was abated by fibrin polymerization.

PPACK whole blood was perfused across a collagen scaffold at 200 s^{-1} . Clot formation was imaged with a fluorescent platelet specific monoclonal antibody (red) (A). Following 7 min of perfusion, the shear rate was increased to a pathological shear rate of $15,000 \text{ s}^{-1}$. Images of clot formation were taken at $t=10.75 \text{ min}$ (B), and $t=14.75 \text{ min}$ (C). Zones of low shear, caused by rapid platelet aggregation upstream, often formed and contracted at the trailing edge of the developing clot. In a similar experiment either CTI or PPACK whole blood was perfused over a collagen/TF or collagen surface respectively. Perfusion was initially at 2000 s^{-1} prior to stepping the shear up to $15,000 \text{ s}^{-1}$. Control conditions were compared to GPRP treated samples with inhibited fibrin polymerization. Clot height was recorded throughout the duration of the experiment (D). Average clot heights were calculated for both the control and GPRP samples. The measurements were made for both the control and GPRP samples treated whole blood both before and after increasing the shear rate (E). (*, $P < 0.01$)

4.4 Discussion

The clots developed in our device utilizing human blood (**Figure 4-11A**), closely matched the architecture of clots developed *in vivo* (**Figure 4-11B**). When the device was operated at a constant wall shear stress, we observed that transthrombus pressure gradients could regulate the core and thrombin heights. Reducing transthrombus pressure gradients resulted in an increase in the core and thrombin heights, leading to larger total clot heights. In this scenario, pressure driven permeation through the clot towards the extravascular space was reduced when ΔP was reduced. This decrease in permeation toward the extravascular space allows for thrombin diffusion through the clot towards the lumen. As the thrombin boundary grew, the core region grew. In turn, this may result in an increase in ADP and TXA₂ release as demonstrated by P-selectin exposure. Since ADP and TXA₂ are soluble small molecules and diffuse much faster than thrombin ($D_{ADP}=50 \times 10^{-11} \text{ m}^2/\text{s} \gg D_{Thrombin}=8 \times 10^{-11} \text{ m}^2/\text{s}$), they facilitated shell growth by recruiting additional platelets to the surface of the clot (**Figure 4-11C**) [91, 92].

We demonstrated that the core/shell architecture was present throughout the development of human blood clots under physiologic conditions of hemostasis over an *ex vivo* wound of collagen/TF. The sensitivity of the core and shell development was investigated by independently controlling the wall shear rate (100 s^{-1} to 2000 s^{-1}) and transthrombus pressure gradient ($\Delta P=9.0$ to 29.4 mm Hg). Fibrin polymerization reduced thrombin mediated clot growth at arterial but not venous shear rates. This can be explained by our observation of increased platelet and fibrin packing at arterial shear rates as compared to venous shear rates. The influence of the shear rate on clot structure

and composition became more evident when γ' -fibrinogen's high affinity thrombin binding site was inhibited with a monoclonal antibody. When clots were developed at venous shear rates (decreased packing density) and the high affinity thrombin binding site on $\gamma A/\gamma'$ was inhibited, the size of the total clot, thrombin, and core increased.

We also demonstrated that the shell region is dependent on the local shear rate at the surface of the clot whereas the core region is only dependent on the transthrombus pressure gradient. These results agree with the governing role of transport rates within and around the developing clot. The low permeability of thrombi places an emphasis on both convective and diffusive transport within the clot while the transport at the surface of the clot is governed by the local wall shear rate (convection \gg diffusion) [86]. This means that thrombin, which has a much slower diffusion rate than ADP or TXA_2 , requires the protection of the clot to effectively diffuse. Conversely, the diffusive transport rates of ADP and TXA_2 are fast and can compete with larger convective forces that are present near the surface of the clot. This is why shell growth has been directly correlated with ADP and TXA_2 [27]. So when surface convection rates are low, such as venous shear rates, ADP and TXA_2 diffusion plays a larger role in platelet recruitment. This role is diminished at arterial shear rates which causes reduced shell growth. These results define the physical parameters that govern clot development and the resulting core and shell architecture of human clots.

Another important aspect of clot development is fibrin formation. In order to study fibrin's role, we examined the packing density of platelets and fibrin within human thrombi formed at venous or arterial shear rates. We found that increasing the shear from

a venous to an arterial rate results in an increase in both platelet and fibrin packing. We also found an increase in thrombin activity at arterial shears. These results supported previous work performed *in vivo*, which described the majority of fibrin formation as being contained within the densely packed core [27, 73, 75]. Complementary *in silico* investigations using the porosities of the tightly packed core and loosely packed shell illustrated thrombin retention within the core region due to the lower porosity decreasing the effective diffusion of thrombin [74].

To determine how fibrin contributes to the formation of a dense clot microenvironment we formed clots in the presence of GPRP to prevent fibrin polymerization. Our results demonstrated a drastic increase in thrombin, core, and total platelet area when fibrin polymerization was inhibited with GPRP at arterial shear rates. The same increase was not observed at venous shear rates, where clot porosity was elevated and fibrin density was reduced. At arterial shears our results are consistent with increased thrombin diffusion due to a lack of fibrin leading to an increased area of activity. However, in the case of clots generated at venous shear rates that have high porosity we propose that the reduced fibrin facilitated rapid convective removal of thrombin through the injury site. As a result, the removal of fibrin polymerization facilitated even greater thrombin removal, causing mild reductions in total and thrombin area. We hypothesized that thrombin diffusion towards the vessel lumen may also be limited by binding rather than just physical hindrance.

We investigated this hypothesis by preventing thrombin binding to the high affinity binding site on the γ' -chain of fibrinogen. The γ' -chain has been implicated as a

new clinical biomarker for acute events and chronic diseases such as myocardial infarctions, coronary artery disease, and deep vein thrombosis [87, 93, 94]. Studies have shown that thicker fibrin fibers (low thrombin concentrations) have more γ' binding sites than thinner fibrin fibers (high thrombin concentrations) [95]. These reports, coupled with our thrombin sensor cleavage results, predict greater γ' -thrombin binding at venous shear rates rather than arterial shear rates due to the differences in the fibrin network. When we blocked the high affinity binding site on the γ' -chain of fibrinogen with a monoclonal antibody we saw significant increases in total clot, thrombin and core area only at venous shear rates. This suggests that at venous shear rates, fibrinogen preferentially binds thrombin using the γ' -chain of fibrinogen to inhibit thrombosis. Conversely, the low porosity and increased fibrin present in arterial clots prevents thrombin boundary growth by physically limiting the diffusion of thrombin. While thrombin binding to $\gamma A/\gamma'$ is still present, it alone cannot prevent thrombin mediated clot growth at arterial shear rates. These results complement the requirement of fibrin polymerization at arterial and not venous shear rates.

Interestingly, clots formed at pathological shear rates were also dependent on fibrin polymerization for regulated growth. We investigated this dependence by increasing the wall shear rate from an arterial shear rate (2000 s^{-1}) to a pathological shear rate ($15,000\text{ s}^{-1}$) that might be found in a stenosed vessel. When the control samples were compared to the GPRP treated samples, the results demonstrated that fibrin polymerization was responsible for the reduction in clot growth at pathological shear rates. This regulation was in align with our results at arterial shears. Increasing the shear

rate from an arterial to pathological rate increases the dependence on platelet-vWF interactions [96]. In this case, fibrin limits thrombin mediated platelet recruitment and may also interfere with platelet-vWF interactions necessary for growth at pathological shears. This is evident by the increased growth in PPACK samples void of fibrin. This mechanism may be protective in the event of a ruptured plaque where tissue factor exposure and shear rates are high [97]. In a similar experiment, the wall shear rate was increased from a venous shear and whole blood was anticoagulated with PPACK. The clot grew rapidly, at the leading edge, when shears were increased to pathological rates. This rapid growth created a zone of low shear which facilitated the local accumulation of soluble agonists such as ADP and TXA₂, as we have previously demonstrated [46]. This enabled the downstream edge of the clot to contract, a flow sensing response to anchor the clot to the collagen scaffold. The contraction in the opposite direction of a pathological shear rate of 15,000 s⁻¹ was strong enough to prevent embolization in the absence of fibrin.

While the venous and arterial clots in this study were investigated at the same ΔP , lower vessel pressures are often found in venous circulation as compared to arterial circulation [23]. This reduction in vessel pressure may decrease the pressure drop across the developing clot, which would allow greater thrombin boundary growth and fibrin formation. The increase in fibrin formation along with the trapping of red blood cells gives venous clots the label of ‘red clot’. On the other hand, arteries often have a higher vessel pressure than veins which may increase the transthrimbus pressure gradient which would decrease clot retention of thrombin and the formation of fibrin. This reduction in

fibrin and the high concentration of platelets gives arterial clots the label of ‘white clot’. As we have demonstrated these changes in transthrbus pressure gradients would increase the role of thrombin binding via γ' fibrinogen and decrease fibrin’s role in hindering thrombin diffusion because of the resulting increase in convective removal. These observations illustrate the complex balance of both physical and biochemical parameters that influence the development of clots (**Figure 4-11C**).

These results have numerous clinical implications, particularly in venous and arterial thrombosis. Recent reports of interest have shown that IL-6 disproportionately increases the expression of γ' as compared to γ A [98]. Elevated IL-6 levels are associated with increased risk of future MI [99]. The increase in γ' -chain fibrinogen seems to be a mechanism for protection, at least in the venous circulation. Our results in this study did not indicate any protective effects within clots generated at arterial conditions but did show protective effects at venous shear rates. This may explain why lower γ' levels have been implicated as a DVT risk [94]. Future work to determine the function of the core/shell architecture and role of γ' -fibrinogen in different pathophysiologies will be required to advance and improve patient care.

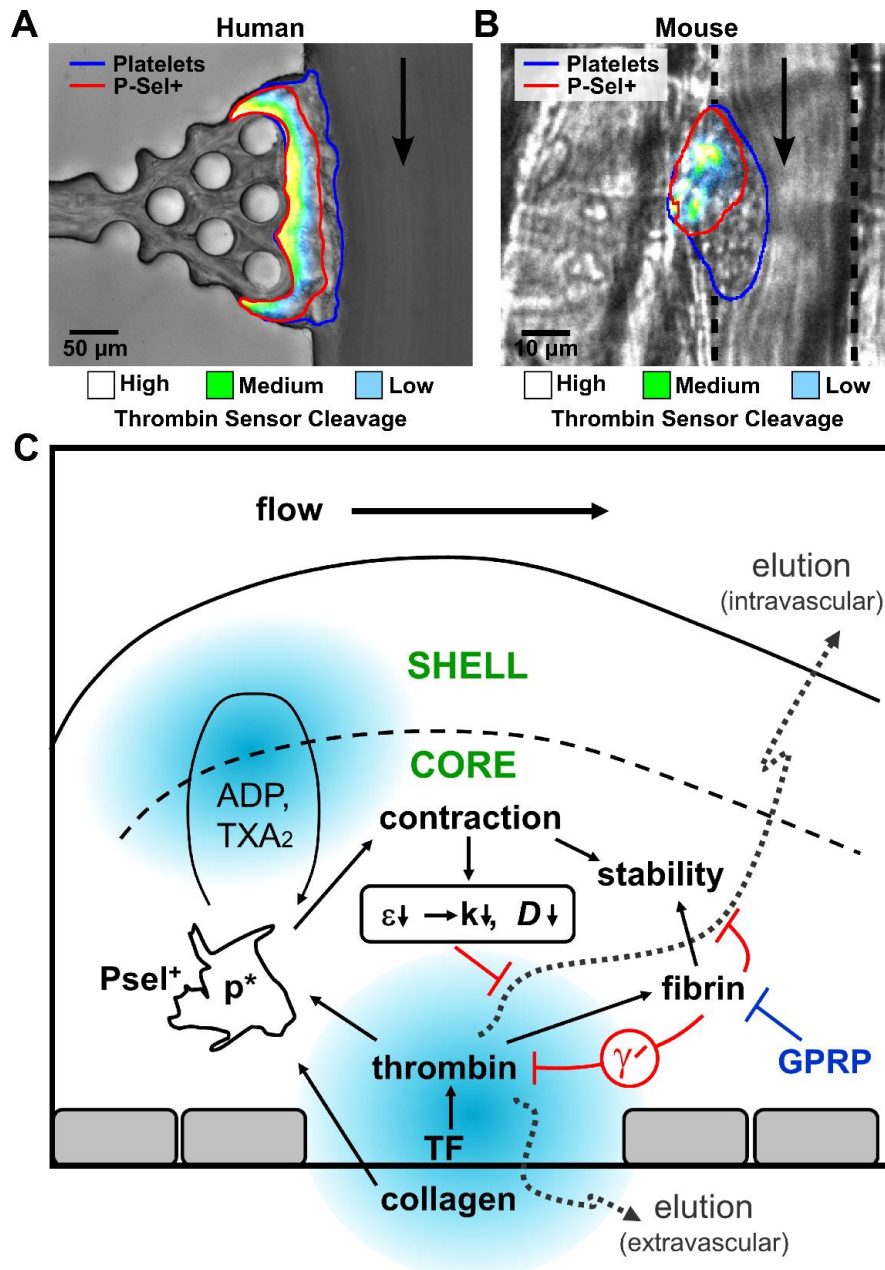


Figure 4-11 Human thrombi develop a core and shell architecture that mimic the architecture of clots developed in vivo.

Human clots developed in vitro (A) and mouse clots developed in vivo (B) were outlined by imaging the clots using platelet (blue) and P-selectin antibodies (red). A heat map was used in both images to illustrate the localization of thrombin sensor cleavage (light blue = low intensity and white = high intensity). A schematic representing the regulation of thrombin and small molecules ADP and TXA₂ demonstrates both the physical and biochemical transport regulations observed within clots (C). (ϵ , porosity; k , permeability, D , diffusivity, p^* , activated platelet)

Chapter 5 : Rapid on-chip recalcification and drug dosing of citrated whole blood using microfluidic sheath flow

5.1 Introduction

Exposure of extracellular matrix (ECM) proteins at a site of vascular injury elicits a hemostatic response from both platelets and coagulation proteins. Primary hemostasis or platelet plug formation is simultaneously accompanied by the generation of thrombin and fibrin via the coagulation cascade [1]. One factor in this response is the local wall shear stress (τ_w). Blood experiences both high (arterial) and low (venous) shear stress as it flows throughout the vasculature [23]. In cylindrical vessels, wall shear stress is uniform around the circumference of the vessel. Recreating this constant shear stress at an injury site in a rectangular microfluidic channel is difficult due to the corners. Sheathing the blood flow from the corners may result in an injury with a more physiologic architecture while offering an opportunity to diffuse small molecules into the blood via the sheathing buffer.

Platelet and coagulation assays most commonly require whole blood to be drawn directly into sodium citrate, an anticoagulant that chelates Ca^{2+} [101, 102]. Prior to most clinical assays such as PT and aPTT, citrated blood is recalcified to restore platelet and coagulation function [103, 104]. Unfortunately, many microfluidic or flow assays neglect recalcification prior to flow [105]. While previous microfluidic assays have demonstrated platelet and coagulation function under various shear rates and pressure gradients [46, 86], there have been a limited number of microfluidic studies focusing on the recalcification of citrated whole blood and the resulting platelet and coagulation

function under flow conditions. These experiments are important because of the clinical use of citrated whole blood and the recent advances in assays utilizing flow such as the PFA-100. This assay measures the time required for citrated whole blood to close a narrow opening in a collagen membrane. Without recalcification, the citrated blood used in the PFA-100 limits the system measurement to only platelet dysfunction [106]. Currently, there are no devices capable of reproducing the recalcification of citrated whole blood and evaluating the effects on platelet and coagulation function under flow conditions. A device capable of these characteristics would be important for clinically relevant flow assays utilizing citrated whole blood.

We describe the design and characterization of a converging trifurcation microfluidic device capable of recalcifying or drug-dosing whole blood under flow conditions. The device permits measurements of platelet and coagulation function at varying levels of recalcification or platelet inhibition along the length of the channel. Localized collagen or collagen/tissue factor (TF) surfaces initiated platelet and coagulation responses at a constant wall shear stress. This was produced by sheathing anticoagulated whole blood with buffer ($\pm\text{Ca}^{2+}$). During recalcification of citrated whole blood, both platelet and coagulation response demonstrated a dependence on the reconstitution of calcium. Citrated whole blood incubated for longer times prior to recalcification resulted in a priming of the intrinsic pathway (due to Factor XIIa generation in the absence of calcium). Both platelet and coagulation responses were initiated faster and magnified at the final time point. The addition of MRS-2179, a platelet P2Y₁ antagonist, to the buffer sheath flow resulted in a dose dependent inhibition

of platelet deposition in a single channel. The calculated IC50 for this dose response correlated well with previous reports. The device we report demonstrates the ability to recalcify citrated whole blood under flow as well as the ability to provide accurate single channel measurements of platelet antagonist IC50 values. This is the first device we have knowledge of that can provide both of these characteristics.

5.2 Materials and Methods

5.2.1 Fabrication

Silicon wafers (D = 100 mm, WRS Materials) were spin coated with a 60 μm layer of negative photoresist (KMPR 1050, MicroChem Corp.). Following a 20 min soft bake and UV exposure, the substrate was baked for an additional 4 min at 100 °C. The wafer was then developed using AZ® 300 MIF (AZ Electronic Materials USA Corp.). Devices were fabricated using polydimethylsiloxane (PDMS) (Ellsworth Adhesives) at a 10 : 1 ratio of base to curing agent. All inlet and outlet ports were cored using 0.75 mm I.D. corers (Harris Uni-Core™, Ted Pella, Inc.). Connections between the PDMS devices and 250 μL syringes (Hamilton Company) were made using 90°, 23 gauge x 1/2” length blunt needles (Small Parts) and 0.020” ID x 0.060” OD tubing (Cole-Parmer). Devices were reversibly sealed to the glass slides using a vacuum pump and the previously mentioned tubing.

5.2.2 Design

The trifurcation device utilized in these studies was designed to sheath whole blood with buffer flows. The device consisted of three inlets and one outlet. The center inlet is described as the blood inlet and the two side inlets are described as the buffer

inlets. The blood entrance length and buffer entrance lengths were 3 mm and 1.8 mm respectively. Channel widths were 250 μm for the blood inlet and 110 μm for the buffer inlets. At the trifurcation point, the buffer inlets were introduced at a 20° angle to the blood inlet. Following the trifurcation of the three inlets ($R_{\text{Blood}}= 1000 \mu\text{m}$, $R_{\text{Buffer}}=750 \mu\text{m}$), the channel widened to 300 μm . The channel was 44.8 mm in length and exited at a single outlet ($R_{\text{Exit}}=1000 \mu\text{m}$). Each chip was designed with two channels parallel to each other separated by 8 mm. Surrounding the channels were designed post regions ($R_{\text{Post}}=500 \mu\text{m}$) to support vacuum sealing of the chips to glass slides (75 mm x 38 mm, Fisher Scientific).

In addition to the trifurcation device, protein patterning devices were also designed. These devices used the same dimensions as the trifurcation template to provide patterned strips at consistent distances from the trifurcation point. Two patterning devices were utilized, one with 7 channels and another with 8 channels. Both the 7 channel and 8 channel devices were designed with 250 μm channels perpendicular to the direction of the trifurcation flow with one inlet ($R=1000 \mu\text{m}$) and one outlet ($R=1000 \mu\text{m}$). The channels were 11 mm in length and separated by 6 mm (7 channel design) or 5.5 mm (8 channel design). This feature allowed one device to pattern protein at one or more locations on two independent trifurcation channels. Similar to the trifurcation device, the patterning devices were designed with post regions to support vacuum assisted sealing to the glass slide.

5.2.3 Blood Collection

Phlebotomy was performed in accordance with the University of Pennsylvania's IRB. Human blood was collected from healthy volunteers, self reporting as alcohol and medication free. Blood was anticoagulated with 100 μM Phe-Pro-Arg-chloromethylketone (PPACK) (Haematologic Technologies Inc.) or concentrated citrate solution (1 part anticoagulant to 9 parts whole blood) (Sigma-Aldrich). Citrated whole blood was occasionally supplemented with 40 $\mu\text{g ml}^{-1}$ corn trypsin inhibitor (CTI) (Haematologic Technologies Inc.). Studies devoid of TF utilized PPACK whole blood and 1 $\mu\text{g ml}^{-1}$ of a fluorescently conjugated anti-CD41 monoclonal antibody (Abd Serotec). Studies including thrombin utilized citrated whole blood \pm CTI. These samples were prepared with the previously mentioned anti-CD41 monoclonal antibody as well as 0.0125 mg ml^{-1} of a fluorescently conjugated fibrinogen (Invitrogen).

5.2.4 Operation

Glass slides were treated with Sigmacote® (Sigma-Aldrich) to impede blood clotting and the adsorption of basic proteins. Following surface treatment, a patterning device was vacuum sealed to the slide. Collagen (Chrono-log Corp.) was patterned on the slides by pulling the solution through the desired channel(s). Immediately afterwards, 0.5% bovine serum albumin (BSA) was rinsed through the channel(s) to remove free collagen. In experiments requiring tissue factor (TF), the patterned collagen was incubated with TF solution (Dade Innovin Reagent, Siemens) following the BSA rinse. After incubating for 30 min, the channel was rinsed with 0.5% BSA and the patterning device was removed.

The trifurcation device was placed directly on top of the patterned collagen. The horizontal edge was aligned with the glass slide and the vertical edge was aligned to fit both flow channels perpendicular to the patterned collagen. Syringes were loaded with anticoagulated whole blood and HEPES buffer (HBS) supplemented with methyl cellulose (0.02%, Sigma-Aldrich). The addition of methyl cellulose increased the buffer viscosity to the same viscosity as whole blood (3 cP) [47]. In experiments investigating dye diffusion, fluorescein isothiocyanate (FITC) (Sigma-Aldrich) was loaded in the sheath buffer and Texas Red® conjugated albumin (BSA) (Invitrogen) was loaded in the blood or buffer in the center inlet. Recalcification experiments used buffer loaded with 30 mM Ca^{2+} while drug dosing experiments used buffer with physiologic calcium concentrations (2.4 mM Ca^{2+}) and 10 μM MRS-2179 (Tocris Bioscience), a potent P2Y_1 inhibitor [107].

A constant volume syringe pump (PHD Ultra, Harvard Apparatus) was used to perfuse the anticoagulated whole blood syringe as well as both buffer syringes. The equal flow rates set the width of each fluid to 100 μm with the center inlet containing the whole blood and the two side inlets containing buffer. Wall shear rate was controlled by adjusting the flow rate appropriately. All experiments in this study were performed at room temperature and set at a constant wall shear rate (600 s^{-1}). Glass slides with vacuum sealed devices were positioned on an inverted microscope (IX81) (Olympus America Inc.) and imaged with an ORCA-ER CCD camera (Hamamatsu).

5.2.5 Finite Element Analysis

COMSOL Multiphysics was used to simulate fluid flow and solute transport within the trifurcation device. Laminar fluid flow was modeled using the stationary Navier-Stokes equation while the solute transport was modeled using the conservation equation for chemical species. Both blood and buffer were defined with equal viscosity ($\mu=3$ cP) and density ($\rho=1060$ kg m⁻³). Diffusion coefficients were defined for FITC ($D_{FITC}= 6.4 \times 10^{-10}$ m² s⁻¹ in water) [108], BSA ($D_{BSA}= 6.1 \times 10^{-11}$ m² s⁻¹ in sodium phosphate/chloride buffer) [109], and calcium ($D_{Ca^{2+}}= 7.9 \times 10^{-10}$ m² s⁻¹ in water) [110] after they were adjusted using the Stokes-Einstein Relation to account for the increased viscosity of blood/buffer ($\mu=3$ cP). Additionally, the diffusion coefficient for MRS-2179 ($D_{MRS-2179}= 1.5 \times 10^{-10}$ m² s⁻¹, $\mu=3$ cP) (Stokes-Einstein Relation) was defined and the flow rates for blood/buffer were set ($Q=1.91$ μ L min⁻¹). The model was validated by simulating the normalized area under the curve in the middle 100 μ m of the channel for both FITC and BSA diffusion. Simulated values were collected along the length of the channel and compared to experimental measurements. The validated model was used to predict calcium and MRS-2179 diffusion along the length of the channel for a wall shear rate of 600 s⁻¹. All simulations were performed with a 2D model using a shallow channel approximation with a thickness equal to the height of the microfluidic channel ($h=60$ μ m). The approximation allowed the model to simulate the conditions at the center of the channel in the z-direction ($h=30$ μ m), where all experimental measurements of the fluorescent species were imaged.

5.3 Results

5.3.1 Diffusion controlled recalcification of citrated whole blood

We designed a trifurcated microfluidic device to analyze platelet and coagulation function at a controlled wall shear stress (**Figure 5-1A**). The center channel and two side channels were simultaneously perfused with citrated whole blood and 30 mM Ca^{2+} buffer ($\mu = 3$ cP) respectively (**Figure 5-1B**). The calcium buffer sheathed the blood flow which prevented the blood from contacting the patterned collagen/TF surface near the corners of the channel, where $\tau_w = 0$ dynes/cm². Instead, the wall shear stress experienced by the blood remained constant (**Figure 5-2**), while the buffer shear stress diminished as it approached the corners. This flow design enabled the constant wall shear stress found in cylindrical capillaries or veins to be recreated in a rectangular microfluidic device.

At the trifurcation entrance, the buffer and blood streams merged as illustrated with FITC dye (**Figure 5-1C**) and a COMSOL simulation predicting Ca^{2+} diffusion (**Figure 5-1D**). The 20° entrance angle and laminar fluid flow ($\text{Re}=0.14$) produced sharp interfaces between the blood and buffer. The low Reynolds number flows associated with microfluidic devices minimized convective mixing [111]. Therefore, diffusion controlled the concentration gradients found across the blood and buffer flows. FITC dye was added to the buffer flow stream and the concentration in the middle 100 μm of the channel was measured in whole blood or buffer. The normalized area was determined along the length of the channel (**Figure 5-1E**). At 42 mm downstream of the trifurcation entrance, 62.5% of the maximum dye area was obtained in whole blood. The COMSOL

simulation recreating this experiment predicted this measurement within 0.5%. In a similar experiment, Texas Red® conjugated BSA was added to whole blood or buffer in the center flow stream. Measurements of the normalized BSA area in the middle 100 μm of the channel were made along the length of the channel (**Figure 5-1F**). Only 17.7% of the maximum normalized BSA area was removed from the whole blood at the final measurement point ($Y=42$ mm). Again, this measurement was predicted within 0.5% using a COMSOL simulation. These experiments validated the COMSOL model used to simulate the mixing of soluble species in each of the fluid streams. Line scans of FITC dye and BSA at each position illustrated the mixing of these two tracers (**Figure 5-3**). The order of magnitude difference in their diffusion coefficients explains the disparity [108, 109].

After the model was validated, it was used to simulate the minimum concentration of Ca^{2+} in the citrated whole blood along the length of the channel (**Figure 5-1G**). The wall shear rate controlled the minimum Ca^{2+} concentration by decreasing the time the fluid remained in the channel (t_f). A 30 mM Ca^{2+} buffer solution provided a maximum centerline concentration of 20 mM Ca^{2+} . At a wall shear rate of 600 s^{-1} , a minimum Ca^{2+} concentration of 9 mM was reached prior to the first patterned collagen/TF surface. This Ca^{2+} concentration was sufficient to recover a free calcium concentration equivalent to CTI blood [112].

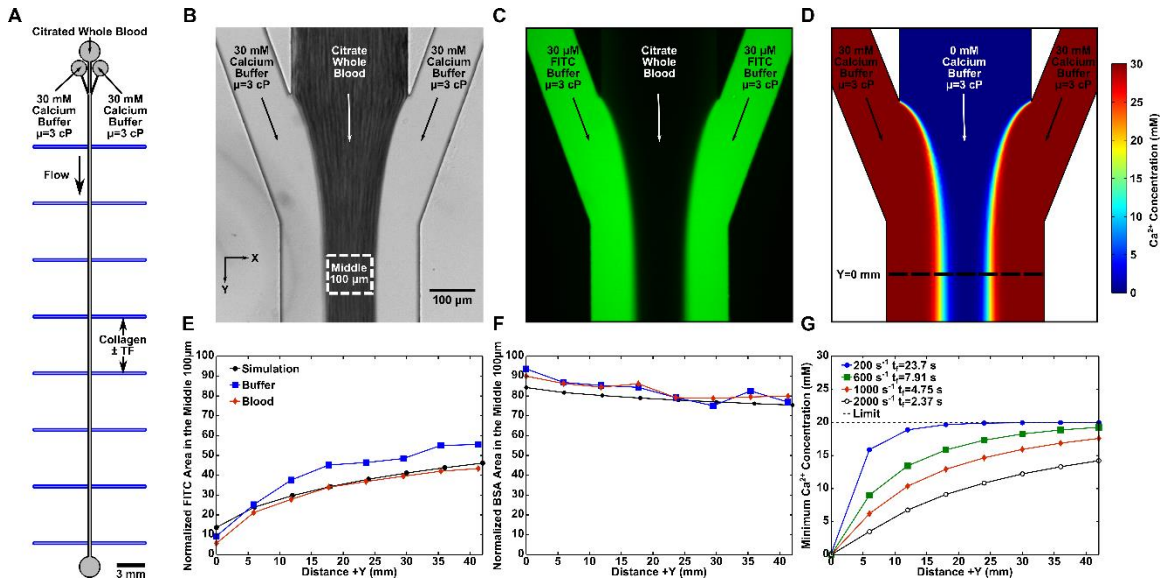


Figure 5-1 A trifurcated microfluidic device to recalcify citrated whole blood under flow.

A trifurcation microfluidic device was designed to recalcify citrated whole blood prior to contact with patterned collagen \pm TF surfaces (A). Citrated whole blood was sheathed with 30 mM calcium buffer ($\mu=3$ cP) at the entrance of the trifurcation design (B). The sharp gradients between the buffer and blood were illustrated, at the entrance, using FITC dye (C). The calcium gradients at the trifurcation entrance were simulated using COMSOL (D). The normalized FITC dye (E) and BSA (F) area were measured and simulated in the middle 100 μm of the channel at discrete points along the channel (depicted in A). Minimum calcium concentrations in the middle 100 μm of the channel were simulated in COMSOL for wall shear rates ranging from 200 s^{-1} to 2000 s^{-1} (G). Fluid transit times (t_f) along the length of the channel were calculated for each shear rate.

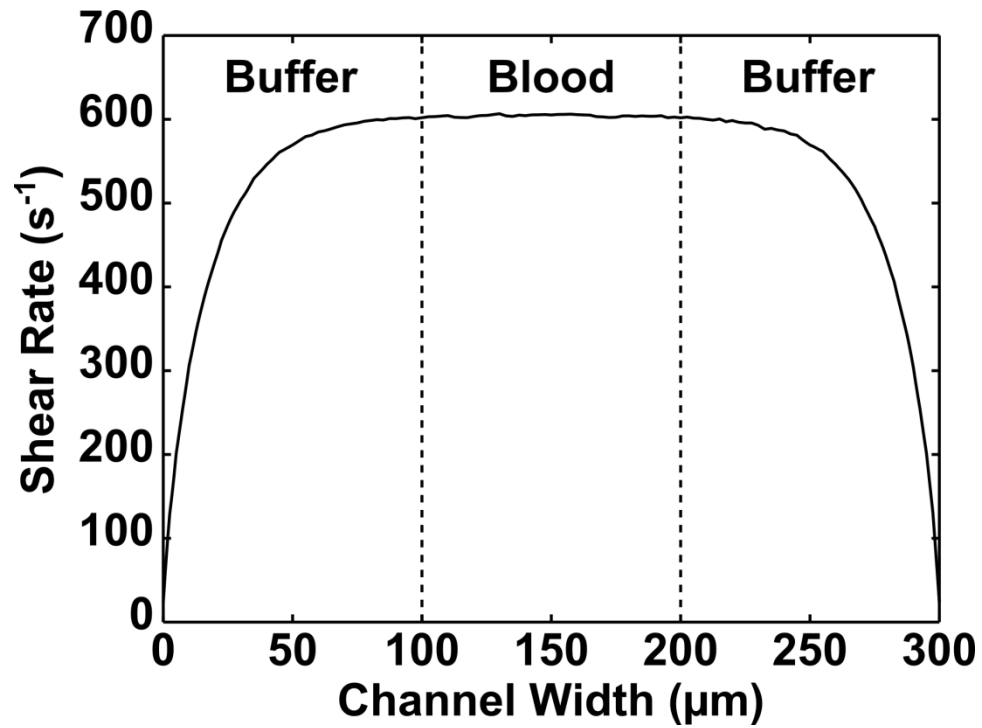


Figure 5-2 Whole blood sheathed in buffer experienced a constant wall shear rate.

COMSOL was used to calculate wall shear rate across the 300 μm trifurcation channel. In the blood region or the middle 100 μm of the channel, the wall shear rate remained constant. Alternatively, the buffer regions experienced shear rate gradients due to corner effects. Constant wall shear rates experienced by the blood region mimic *in vivo* injuries where cylindrical vessels remove corner effects.

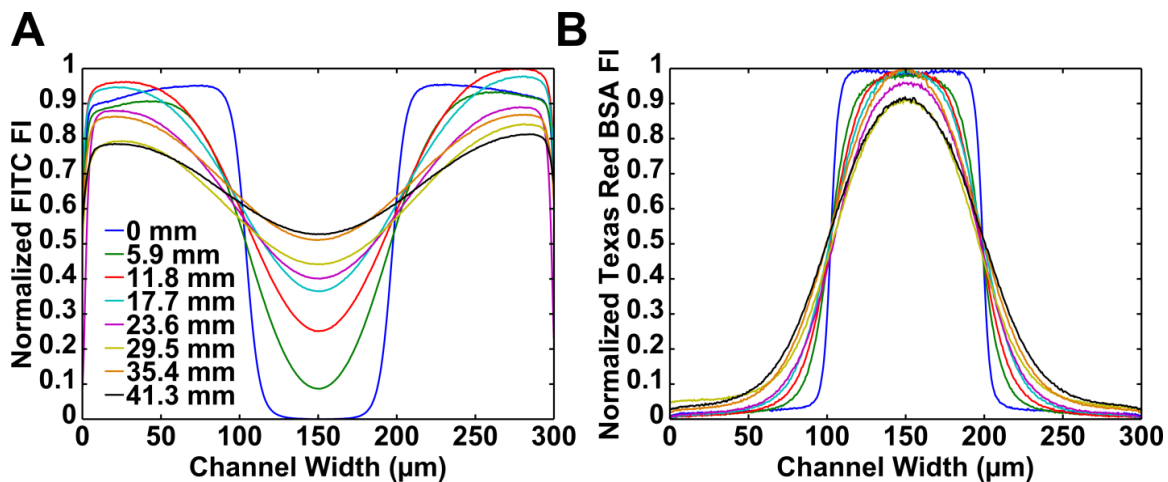


Figure 5-3 FITC and BSA line scans within the trifurcation channel.

Line scans of FITC fluorescence intensity (**A**) and Texas Red BSA fluorescence intensity (**B**) were averaged across the trifurcation channel. Measurements were made at eight locations beginning at the trifurcation point (0 mm). At a wall shear rate of 600 s^{-1} , FITC dye diffusion progressed rapidly along the length of the channel. Conversely, channel transit times limited protein diffusion (BSA).

5.3.2 Recalcification of citrated whole blood under flow recovers platelet and coagulation function

Citrated whole blood was sheathed with 30 mM Ca^{2+} buffer at a wall shear rate of 600 s^{-1} . Collagen/TF was patterned at a distance of 6 mm downstream from the trifurcation entrance. Platelet (red) and fibrin(ogen) (green) accumulation were measured dynamically at the 250 μm patterned surface (**Figure 5-4**). After 4.2 min of flow, platelet aggregation was evident while fibrin(ogen) was not (**Figure 5-4A**). Following an additional 3 min of flow, fibrin(ogen) accumulated at the downstream portions of the clot in areas free of platelets (**Figure 5-4B**). Platelet and coagulation activity continued to increase after 10 min of flow (**Figure 5-4C**). The constant shear gradient generated in the trifurcation device removed the corner effects observed during full channel flow (**Figure 5-5**).

In order to demonstrate proper recalcification, platelet and coagulation function were measured by perfusing whole blood anticoagulated with CTI and citrate with and without calcium in the sheath buffer (**Figure 5-6**). Collagen/TF surfaces were patterned at 7 positions along the length of the channel. Platelet and fibrin(ogen) fluorescence intensities were measured at each localized injury site ($L=250 \text{ m}$, $W=100 \mu\text{m}$). Both platelet and fibrin(ogen) accumulation required Ca^{2+} in the sheath buffer. Platelet aggregation with recalcification buffer began after 6 minutes of flow (**Figure 5-6A**). Similar platelet fluorescence intensities were not reached until 15 minutes without recalcification buffer (**Figure 5-6B**). On average, final platelet fluorescence intensities were reduced by $87.3 \pm 9.3\%$ when Ca^{2+} was absent. Fibrin(ogen) accumulated shortly after platelet aggregation in the recalcification experiment (**Figure 5-6C**). In the

experiment without Ca^{2+} , fibrin(ogen) accumulation was completely abolished yielding a reduction of $99.0 \pm 0.9\%$ (**Figure 5-6D**). When the $[\text{Ca}^{2+}]$ was calculated to be $>16 \text{ mM}$ in the blood, the fibrin(ogen) fluorescence intensity remained stable. Interestingly, this was the same concentration where the difference between the time to 25% of the maximum fluorescence intensity (fibrin(ogen) $t_{25\%}$ - platelet $t_{25\%}$) reached a global minimum ($\Delta t_{25\%}=0.2 \text{ min}$). These studies demonstrated the dependence of recalcification buffer for proper platelet and coagulation function on patterned collagen/TF surfaces.

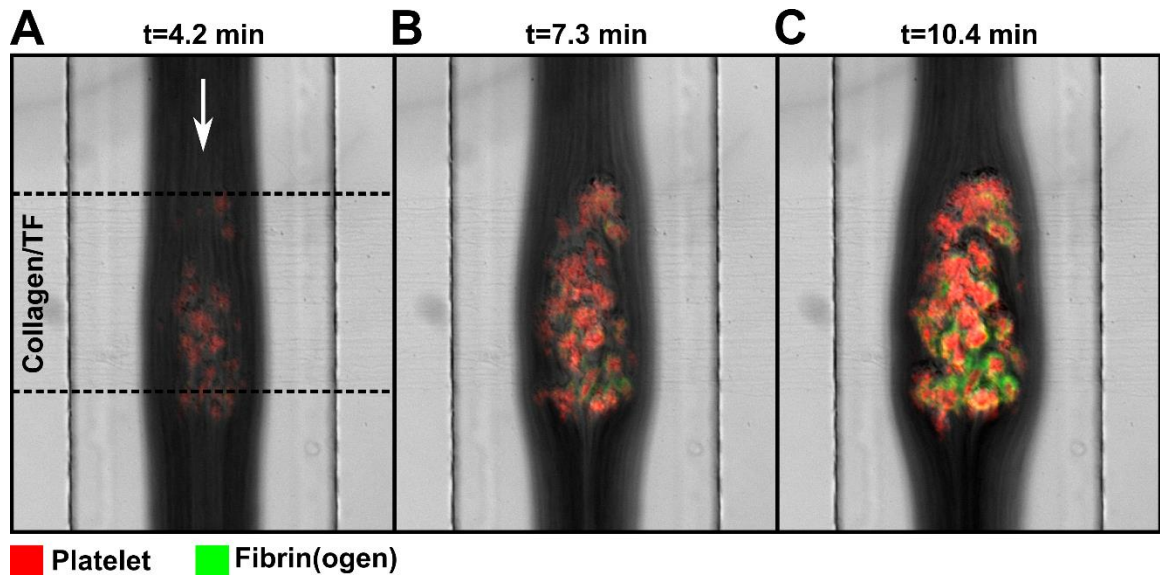


Figure 5-4 Whole blood recalcified under flow recovers platelet and coagulation function.

A strip of collagen/TF was patterned downstream ($Y=6$ mm) of the trifurcation entrance. Citrated whole blood was recalcified under flow (600 s $^{-1}$) with 30 mM Ca^{2+} buffer. Platelet (red) and fibrin(ogen) (green) accumulated at the localized injury site, illustrated at the 4.2 min (A), 7.3 min (B), and 10.4 min (C) time points.

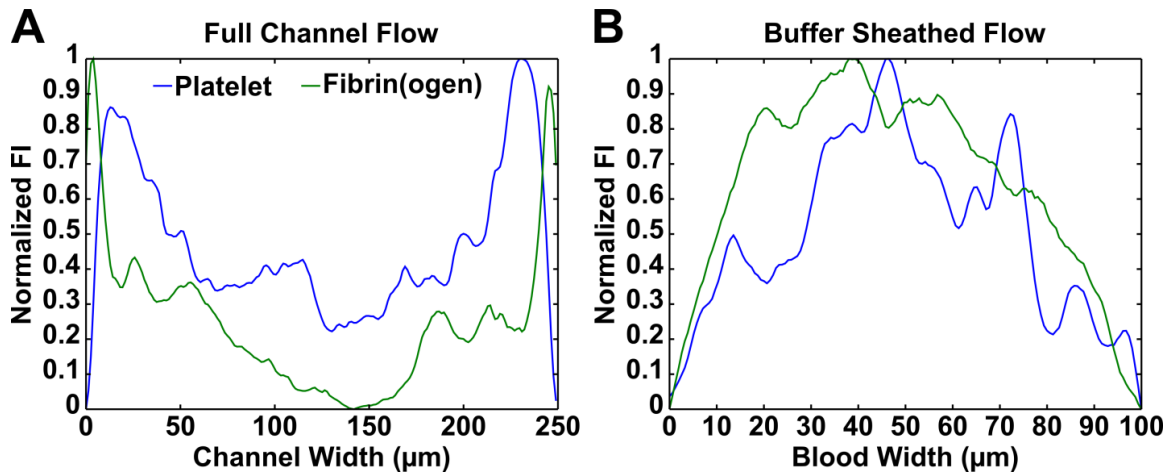


Figure 5-5 Buffer sheath flows eliminate corner effects on clot formation.

Line scans of normalized platelet and fibrin(ogen) fluorescence intensity were averaged at a patterned collagen strip (250 μm) for full channel flow (**A**) and buffer sheathed flow (**B**). The full channel flow illustrated the effects of wall shear rate dropping to zero. Both platelets and fibrin(ogen) accumulate in the corners (0 μm and 250 μm). The buffer sheathed flow yielded maximum platelet and fibrin(ogen) accumulation near the center of the flow.

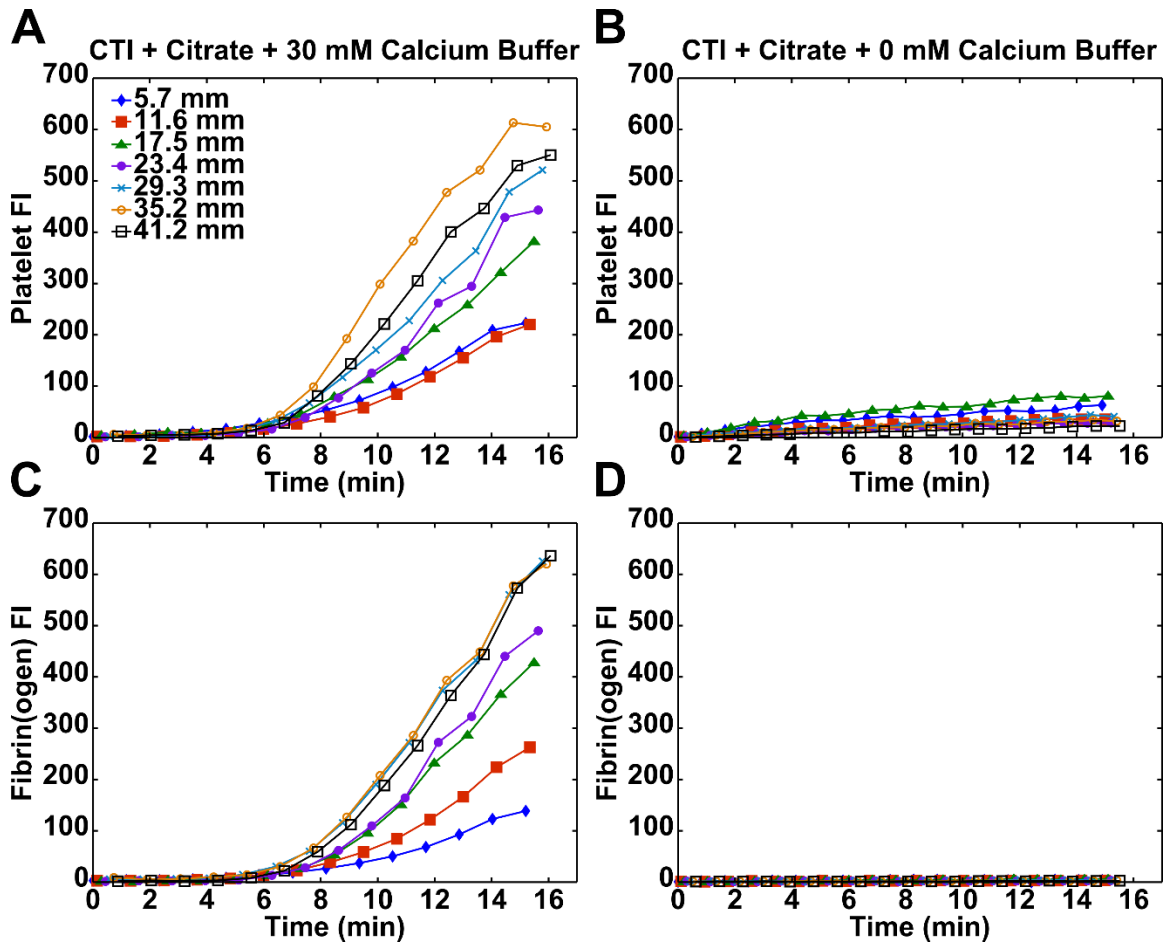


Figure 5-6 Recalcification is required for proper platelet and coagulation function.

Whole blood anti-coagulated with both CTI and citrate was sheathed in buffer ($\mu=3$ cP) \pm 30 mM Ca^{2+} . Blood and buffer \pm Ca^{2+} were perfused (600 s^{-1}) across seven, equally spaced, 250 μm collagen/TF strips each identified by the distance in millimeters from the entrance of the channel. Dynamic measurements were collected for both platelet (**A-B**) and fibrin(ogen) deposition (**C-D**) at each location.

5.3.3 Intrinsic generation of factor XIIa primed platelet and coagulation activity in citrated whole blood

The addition of CTI to whole blood provided selective inhibition of factor XIIa [113]. This impedes the initiation of the intrinsic pathway. Citrated whole blood alone does not prevent the generation of factor XIIa because factor XII is activated independently of calcium [114]. The effect of factor XIIa on platelet and coagulation activity were investigated by measuring platelet and fibrin(ogen) accumulation on a collagen/TF surface (Y= 6 mm) with citrated blood incubated for 5 min or 30 min after phlebotomy. Platelet aggregation initiated 5 min faster when citrated whole blood was incubated for 30 min rather than 5 min (**Figure 5-7A**). Final platelet aggregation, measured by final fluorescence intensity, was increased by 159%. Likewise, after a 30 min incubation fibrin(ogen) accumulation initiated 2 min faster with an 86.6% increase in final fluorescence intensity (**Figure 5-7B**). Measurements made with citrated whole blood incubated for 5 min were similar to measurements made with whole blood anticoagulated with CTI and citrate. The extra incubation time (25 min) facilitated the generation of factor XIIa. This primed the intrinsic pathway resulting in accelerated platelet and fibrin(ogen) accumulation at the injury site upon recalcification.

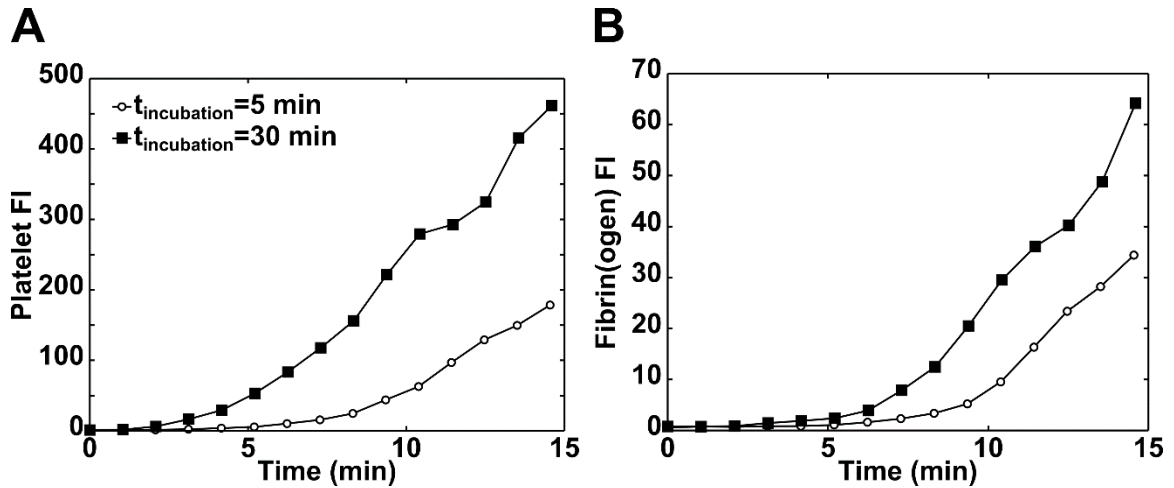


Figure 5-7 Incubation of citrated whole blood primed platelet and coagulation activity via factor XIIa.

Citrated whole blood was incubated for either $t_{\text{incubation}}=5$ min or $t_{\text{incubation}}=30$ min following phlebotomy. A 30 mM Ca^{2+} buffer sheathed and recalcified the citrated whole blood prior to the collagen/TF strip ($Y=6$ mm). Platelet (**A**) and fibrin(ogen) (**B**) deposition was measured and compared for both incubation times.

5.3.4 Single channel IC50 measurement of MRS-2179 under flow

Whole blood anticoagulated with PPACK (a potent thrombin inhibitor) was perfused through the trifurcation device. Buffer with a physiologic calcium concentration (2.4 mM) was used to sheath the blood along the length of the channel. The % hematocrit of the whole blood was calculated at each patterned collagen surface (**Figure 5-8A**). As the blood travelled down the channel the red blood cells dispersed and the % hematocrit dropped slowly. At the final collagen strip the % hematocrit was reduced by ~13% (assuming an initial % hematocrit of 45%). After the % hematocrit dropped below 38%, the platelet deposition decreased significantly (**Figure 5-8B**). While boundary depletion may not be excluded, this effect was not observed in studies with CTI and/or citrate. The presence of thrombin in those studies may have masked any observable platelet depletion.

In a related experiment, we investigated the effect of MRS-2179 (a platelet P2Y₁ antagonist) on platelet deposition. The 2.4 mM Ca²⁺ buffer was supplemented with 10 μM MRS-2179 and platelet fluorescence intensity was measured at 8 collagen strips downstream of the trifurcation entrance. The MRS-2179 drastically reduced platelet fluorescence intensity at all 8 positions as compared to buffer without MRS-2179 (**Figure 5-8B**). The % platelet inhibition was calculated at each position and compared to the simulated [MRS-2179] along the length of the channel (**Figure 5-8C**). The calculated IC50 (0.155 μM) compares favorably to previous IC50 measurements made under flow conditions (0.173 μM) [70]. The length of the channel used in this design made it possible to study MRS-2179 concentrations varying over an order of magnitude. This

facilitated accurate measurements of an IC₅₀ value below 1 μM . The trifurcation device used in this study is the first device capable of measuring platelet antagonist IC₅₀ values with a single channel. It is also the first device to accomplish these measurements using automated mixing to achieve a range of concentrations.

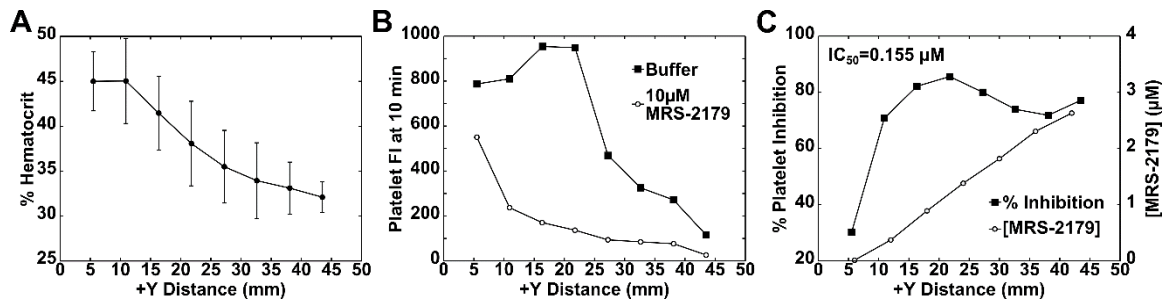


Figure 5-8 Single channel IC₅₀ measurement.

The % hematocrit of whole blood sheathed with buffer was measured in the middle 100 μm of the channel along the entire length (A). A 2.4 mM Ca^{2+} buffer \pm 10 μM MRS-2179 (platelet receptor P2Y₁ antagonist) was used to sheath PPACK whole blood prior to collagen exposure. Platelet deposition was measured at eight evenly spaced collagen strips for buffer with and without MRS-2179 (B). % Platelet inhibition and predicted MRS-2179 concentration were determined along the length of the channel (C).

5.4 Discussion

The laminar flows ($Re \sim 1$) found in microfluidic devices make convective mixing extremely difficult. Often times this characteristic mixing time is a limitation of microfluidic devices that can only be altered by the addition of active or passive mixers [115]. Rather than working against this limitation, we used long channel lengths to take advantage of diffusional mixing. We designed a trifurcation microfluidic device that utilizes differences in species diffusion coefficients to reach varying levels of concentrations along the length of a channel. Previous work with trifurcation designs have focused on concentrating or separating cells by utilizing acoustics and dextran/red blood cell affinities respectively [116, 117]. Instead, our work exploited the differences in protein and small molecule diffusion rates to recalcify or antagonize human whole blood under flow. This is the first reported device to recalcify citrated whole blood and measure platelet IC₅₀ values under flow conditions without premixed concentrations of Ca^{2+} or antagonist in whole blood. Recalcification of citrated whole blood and mixing of platelet antagonist under flow minimizes user error in measurements that may have clinical implications.

Platelet and coagulation assays currently adopted by clinicians use blood products primarily anticoagulated with sodium citrate [101, 102]. The main advantage of using citrated blood is the increased storage time and control of the initiation time (recalcification). Standard assays such as the aPTT and PT both use citrated blood but neither incorporate flow. These tests are forced to extrapolate their data in an attempt to understand how clotting occurs under flow. The device described here not only

incorporates flow but it also provides a measurement for both platelet and coagulation function. In addition, recalcification under flow maintains a constant initiation time that eliminates the generation of activated coagulation factors prior to exposure of the collagen/TF surface. This feature provides repeatable recalcification of citrated blood without the need of an expert technician. Along with proper recalcification, the designed device allows for single channel IC50 measurements. Platelet or coagulation antagonist IC50 values can be measured at submicromolar accuracy as demonstrated by our MRS-2179 measurement. This approach may be useful for future designs that desire personalized drug dosing.

The implications of this device are not limited to citrated blood recalcification and platelet IC50 measurements. This device also recreates constant wall shear stress injuries as experienced by injured cylindrical vessels *in vivo*. Corner effects in rectangular microfluidic devices cause gradients in wall shear stress that facilitate platelet adhesion to collagen during whole blood perfusion [31]. Removing this shear gradient eliminates lower shear zones where platelets and coagulation factors accumulate. Instead, as platelets accumulate at a constant wall shear stress they are forced to generate their own zones of lower shear stress to facilitate coagulation factor accumulation and fibrin generation. This represents a scenario experienced by an injury *in vivo*. In the future, studying the intrinsic and extrinsic generation of fibrin at constant wall shear stress might help distinguish their dependence on platelets at higher and lower shear stresses.

While solute diffusion was the primary means of investigation for this study, the length and mixing properties of this device make it a valuable tool for control of

temperature, pH, and hematocrit levels in future work. Investigating the effects of temperature (hypothermia), pH (acidosis), and hematocrit on platelet and coagulation function make this device suitable for studying the varying levels of trauma [118]. Current assays such as thromboelastometry overestimate the integrity of coagulation under varying combinations of these symptoms which make new assays desirable [119]. This device also has the ability to determine the influence of erythrocyte aggregation, a typical consequence of trauma [120], on clot formation. While red blood cell aggregation [121], and deformability has been studied in sepsis models [122], this system would permit further investigation on their roles in thrombosis and hemostasis. There have been very few microfluidic devices developed for addressing the severity of these symptoms and the effects on platelet and coagulation function. Using this device to investigate these symptoms in varying combinations could reveal new insights for the treatment and diagnosis of patients experiencing trauma.

5.4 Conclusions

We have demonstrated the design and novel implications of a device to rapidly recalcify citrated whole blood and dose anti-platelet drugs using buffer sheath flows. Whole blood anticoagulated with sodium citrate was recalcified under flow with buffer sheath flows containing Ca^{2+} . COMSOL simulations and measurements of platelet/fibrin(ogen) deposition with and without Ca^{2+} in the sheath buffer confirmed that recalcification was completed prior to being exposed to patterned collagen/TF surfaces downstream. The addition of CTI to citrated whole blood prevented the priming of the intrinsic coagulation protein XIIa when blood was incubated for 30 min after

phlebotomy. The long channel lengths used in this design enabled IC50 measurements for the platelet antagonist MRS-2179. Measurements made agreed with previously reported values which illustrates the devices submicromolar accuracy. The designed device provides a unique platform for studying constant wall shear stress injuries following whole blood recalcification or platelet inhibition under flow.

Chapter 6 : Future Work

6.1 Effect of platelet contraction on clot growth

The device designed in Chapter 2 has the ability to study the architecture of clots developed under physiologic conditions, as illustrated in Chapter 4. Our work in Chapter 4 defined both physical and biological conditions in which thrombin mediated clot growth was regulated. Another important aspect of clot development, which was only briefly addressed in Chapter 4, is the ability of the clot to contract. Clot contraction has an important role in preventing blood loss and anchoring the clot to the injury site to prevent embolism [59, 123]. *In vivo* results have implicated that clot consolidation via contraction aids in retaining solutes by decreasing their transport within the architecture of the clot [75]. Interestingly, human platelets are larger than mouse platelets [124]. This property may change the role of platelet contraction in human blood clots.

In order to investigate the role of clot contraction on the resulting clot architecture, we performed a preliminary set of experiments in the absence and presence of 10 μ M blebbistatin, a potent myosin IIa inhibitor (**Figure 6-1**) [68]. Whole blood anticoagulated with CTI was perfused across a collagen/TF scaffold as previously described in Chapters 2-4. The wall shear rate was set at 400 s^{-1} and the transthrombus pressure gradient was maintained at 20 mm Hg. Total clot, fibrin, and P-selectin positive area were dynamically calculated throughout the experiment. The total clot area of clots treated with blebbistatin grew to a greater extent (1.48-fold, $P < 0.01$) than control clots (**Figure 6-1A**). Their initial clot area remained unchanged until 6 min of growth ($P < 0.05$). The fibrin area did not significantly change in the presence of blebbistatin

(Figure 6-1B). % P-selectin positive area was significantly delayed ($t=1.5$ min, $P<0.025$) and reduced (15.1%, $P<0.05$) when clot contraction was inhibited (**Figure 6-1C**).

These results indicate that clot contraction is important for clot consolidation as evident by the increase in total clot area in the presence of blebbistatin. The impact on thrombin generation and localization is less clear. The fibrin polymerization data supports a claim that thrombin removal may not have been increased because the total fibrin area remained constant. In contrast, the delay in % P-selectin area and decrease in final % P-selectin positive area may have been a result of decreased thrombin retention. In order to determine the role of clot contraction, several additional experiments will need to be performed. As with our work in Chapter 4, the clot architecture will need to be examined at both venous and arterial shear rates to determine the role of clot contraction. The different platelet packing and fibrin densities could drastically influence platelet contraction. In addition, the thrombin sensor will need to be used to determine the localization of thrombin within the resulting clots. This will describe the presence of thrombin in greater detail than the fibrin polymerization results. It may also be beneficial to increase the concentration of blebbistatin to 100 μM . Previous literature has demonstrated different effects of blebbistatin at 10 μM and 100 μM [68]. These experiments are required to decipher the role that clot contraction has on thrombin mediated clot growth in human blood clots.

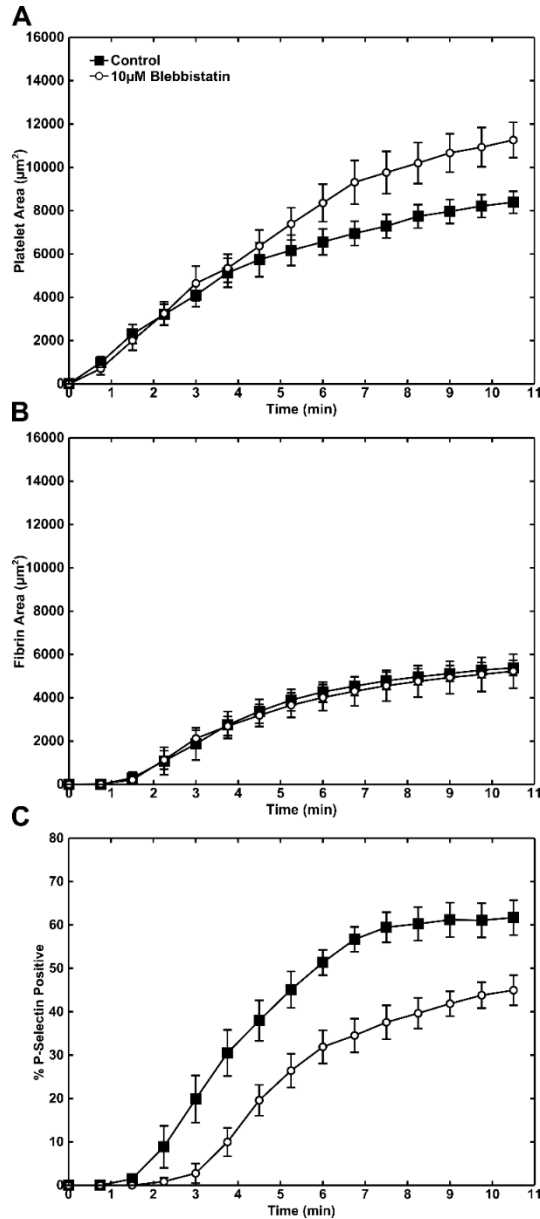


Figure 6-1 Clot contraction reduces total clot height and increases the % P-selectin positive area of the clot.

Clot growth was investigated during 10.5 min of CTI whole blood perfusion (400 s^{-1}) over a collagen/TF scaffold. Whole blood was treated with buffer or $10 \mu\text{M}$ blebbistatin prior to perfusion. Total platelet area (**A**) and fibrin area (**B**) were calculated using a fluorescently conjugated, platelet or fibrin specific antibodies respectively. % P-selectin positive area, as defined by a P-selectin antibody, was calculated based on the P-selectin positive area and total clot area for both conditions (**C**).

6.2 Model for evaluating the effect of inflammation on clotting

Throughout Chapters 2-4 we have described a microfluidic device capable of studying clot growth and architecture at controlled wall shear rates and transthrombus pressure gradients. While this device excels in models of hemostasis and thrombosis, it may also be appropriate for studying the inflammatory response, an additional phase of wound healing. To date, there are very few *in vitro* models capable of studying the interaction of flow developed blood clots and neutrophils. Neutrophils are migratory leukocytes that respond to bacterial infection at the site of injuries in a process known as chemotaxis [125]. Their migration towards the infected area is controlled by chemokines such as TNF- α and IL-8 [126, 127]. Lipopolysaccharides (LPS), an endotoxin located on gram-negative bacteria also has a prominent role in initiating the immune response. LPS is known to cause a response in both platelets and neutrophils. The toll-like receptors (TLR-4) on platelets facilitate a response to LPS resulting in increased platelet binding to fibrinogen and neutrophil extracellular trap (NET) activation [128, 129]. NET's are composed of chromatin fibers and have been implicated in increased DVT risk due to elevated thrombin generation [130]. In addition, LPS can also cause other white blood cells to release chemokines to attract neutrophils to the site of bacterial infection [131]. Understanding the migratory and NET releasing response of neutrophils, at the site of injury, may be a valuable tool for advancing patient care, specifically in DVT and sepsis.

Our preliminary investigations into neutrophil migration (**Figure 6-2**) and LPS induced activation of platelets and neutrophils (**Figure 6-3**) were performed in the device

we designed and outlined in Chapter 2. Interestingly, our first observation of neutrophil migration came when we observed a white blood cell migrating across a developed clot while studying clot permeability. In this study we perfused CTI whole blood (1000 s^{-1}) over a collagen/TF surface with a transthrombus pressure gradient of 20 mm Hg. After ~14 min of flow we turned a valve to change the whole blood to buffer to visualize the fluorescent pulse travel through the permeable structure. Throughout the experiment, we followed the migration of an adhered leukocyte (**Figure 6-2A**). The distance the leukocyte travelled remained relatively unchanged throughout the buffer pulse (**Figure 6-2B**). In contrast, there was an obvious change in distance from the starting point when the buffer pulse was perfused through the clot (**Figure 6-2C**). Prior to the buffer, the leukocyte travelled in a distinct manor towards the collagen/TF scaffold. As the whole blood transitioned to buffer ($t=14 \text{ min}$), the direction of movement dissipated with the leukocyte moving in a stochastic manner. As the blood flow was reestablished ($t=20 \text{ min}$), the leukocyte began to migrate towards and into the collagen scaffold (**Figure 6-2A**). These results lead to a hypothesis that leukocyte chemotaxis requires plasma, in the absence of endothelial cells. To further investigate this process, several experiments would need to be performed. First, the system may need to be modified to recruit additional leukocytes to the injury site. This could be accomplished by reducing the shear rate to a venous shear rate or by adding chemoattractants such as TNF- α and IL-8 to the collagen/TF scaffold. Second, the modified system could be used to observe the migration of multiple leukocytes while whole blood was transitioned to buffer or whole blood. Finally, inhibiting proteases (cathepsin G or α -chymotrypsin) or receptors (fMLP or Fc) responsible for leukocyte chemotaxis could help to define which proteases or

receptors are required for this process [132, 133]. These experiments could be used to determine which components of plasma are responsible for directing leukocyte migration.

The other inflammatory response that we investigated was the LPS induced activation of platelets and neutrophils at the site of an injury (**Figure 6-3**). In this preliminary experiment, we perfused CTI whole blood (100 s^{-1}) across a collagen/TF (**Figure 6-3A**) or a collagen/TF/LPS scaffold (**Figure 6-3B**). Average clot height (**Figure 6-3C**) and clot associated neutrophil counts (**Figure 6-3D**) were calculated throughout the duration of the experiment. Platelets were imaged with fluorescently conjugated CD41 antibodies and neutrophils were imaged with fluorescently labelled CD18 antibodies. Interestingly, the clot formed on the collagen/TF/LPS scaffold grew 2.3-fold larger than the clot formed on the collagen/TF scaffold. The growth of the clots did not begin to differentiate until after 4 min of flow. At this time, clot growth remained constant on the scaffold with LPS while clot growth on the scaffold free of LPS began to dissipate. The delay in growth rate changes may be due to the increase in clot associated neutrophils (27-fold more) in the clot formed on the LPS scaffold. Future experiments will need to be performed to evaluate the effect of LPS on both platelets and neutrophils. In order to determine the effect of LPS independently on platelets, we will inhibit neutrophil activation with proepithelin (PEPI) and secretory leukocyte protease inhibitor (SLPI) [134]. This will allow us to study clot formation dependent solely on LPS without the influence of activated neutrophils. In addition to these studies, we will also add antibodies for P-selectin expression and thrombin activity. These markers will provide insight into the regulation of thrombin in clots formed in the presence of LPS. Finally,

NET formation and influence on clot structure will be studied with Sytox green staining. These measurements will provide information regarding the influence of NET formation on platelet recruitment and thrombin generation. Further investigations of neutrophil migration and interactions with developing clots will be important for understanding the mechanisms of clot formation in patients at risk for DVT and sepsis. Moving forward, we will be able to use the device that we developed and characterized in Chapters 2-4 to study the inflammation stage of wound healing under physiologic conditions.

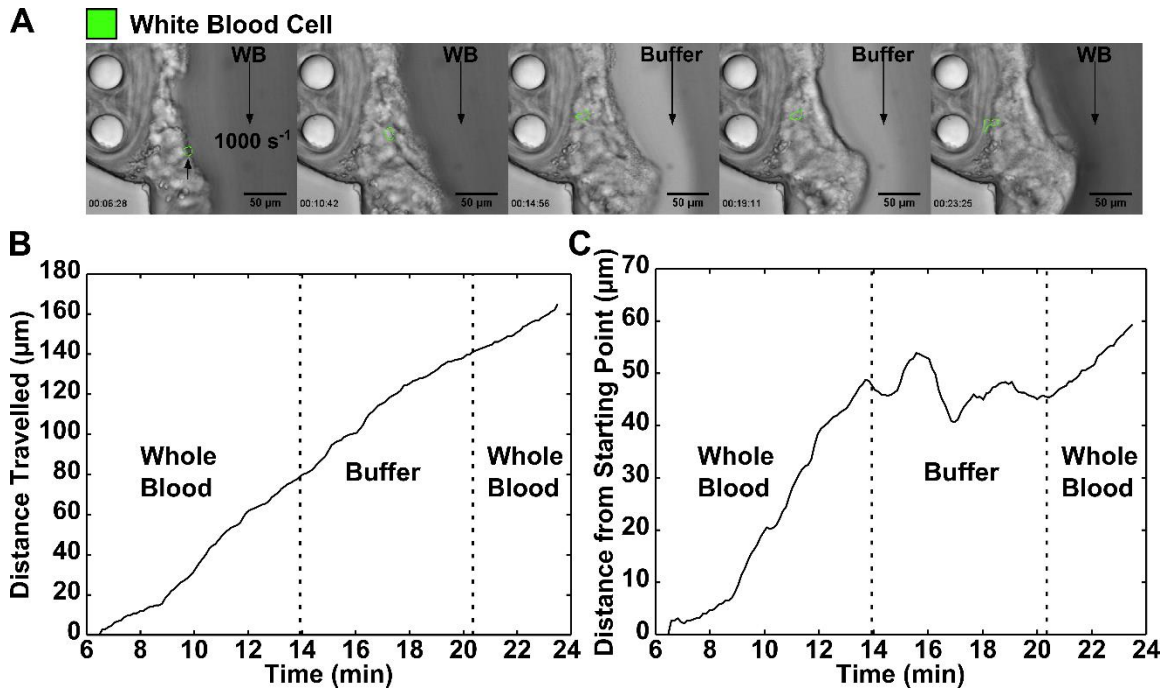


Figure 6-2 Plasma perfusion through blood clots is required for white blood cell chemotaxis towards the injury site.

CTI whole blood was perfused across a collagen/TF scaffold at 1000 s^{-1} for ~ 14 min. Following clot development, buffer was pulsed through the system (14 min-20 min) before whole blood was reestablished. A white blood cell (green) was tracked throughout the growth of the clot and the pulse of buffer (A). The total distance the white blood cell travelled (B) and the distance the white blood cell moved from the starting point (C) were tracked throughout the experiment.

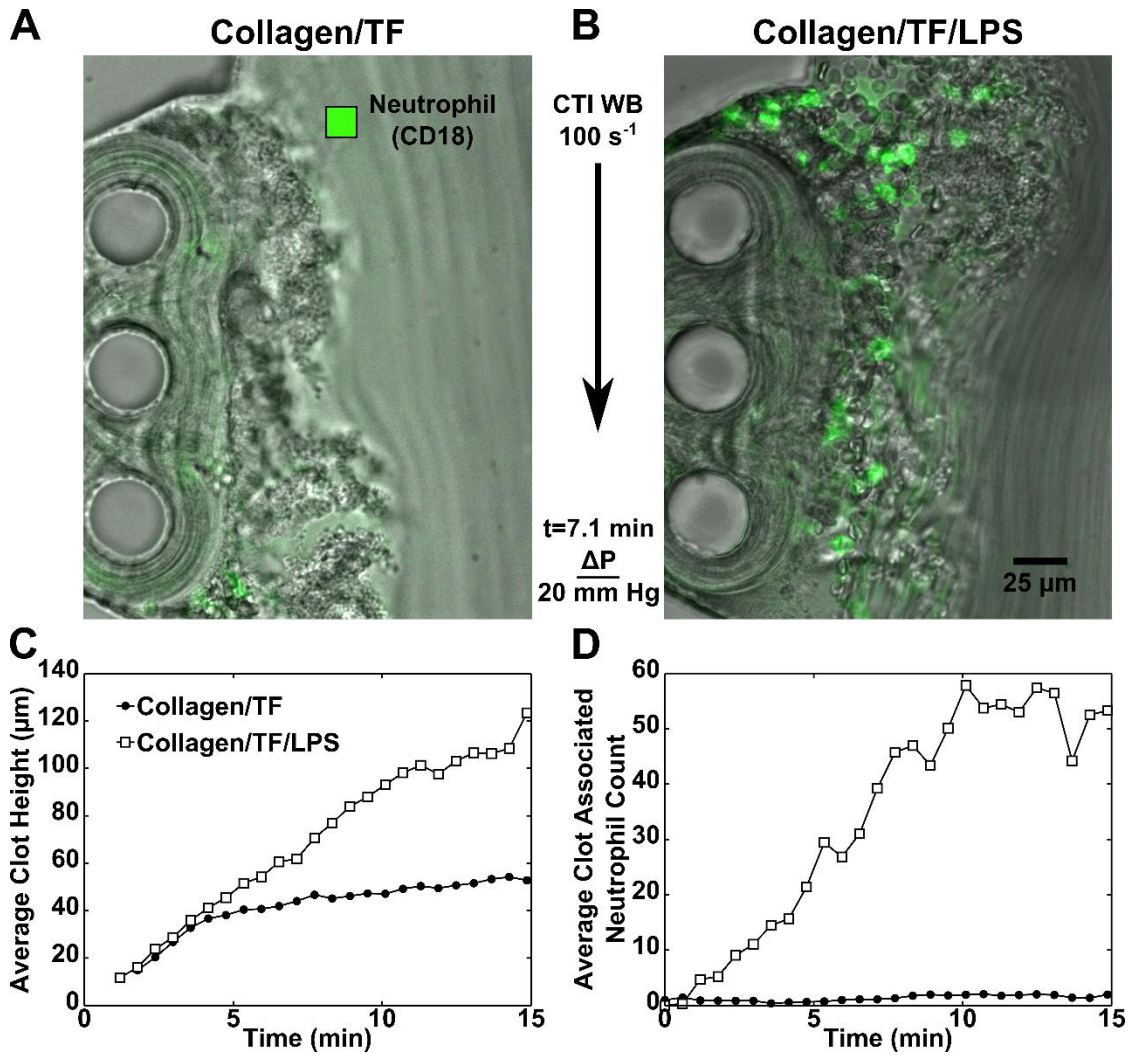


Figure 6-3 LPS embedded in a collagen/TF scaffold induces larger clot growth at venous shear rates.

Whole blood anticoagulated with CTI was perfused at the venous shear rate of 100 s⁻¹ over a collagen/TF scaffold in the absence (A) or presence (B) of 100 pg/mL LPS. Average clot height was calculated in both conditions using a platelet specific monoclonal antibody (C). Average clot associated neutrophil count was estimated by using a fluorescently conjugated CD18 antibody to calculate total neutrophil area. This area was divided by the average area of a neutrophil based on diameter.

BIBLIOGRAPHY

1. Geddis AE. 2010. Megakaryopoiesis. *Semin Hematol.* 47:212-219.
2. Giles C. 1981. The platelet count and mean platelet volume. *Br J Haematol.* 48:31-37.
3. Noris P, Klersy C, Zecca M, Arcaini L, Pecci A, Melazzini F, Terulla V, Bozzi V, Ambaglio C, Passamonti F, Locatelli F, and Balduini CL. 2009. Platelet size distinguishes between inherited macrothrombocytopenias and immune thrombocytopenia. *J Thromb Haemost.* 7:2131-2136.
4. Scholey JM, Taylor KA, and Kendrick-Jones J. 1980. Regulation of non-muscle myosin assembly by calmodulin-dependent light chain kinase. *Nature.* 287:233-235.
5. Li Z, Delaney MK, O'Brien KA, and Du X. 2010. Signaling during platelet adhesion and activation. *Arterioscler Thromb Vasc Biol.* 30:2341-2349.
6. Chen J, and López JA. 2005. Interactions of platelets with subendothelium and endothelium. *Microcirculation.* 12:235-246.
7. Yakushkin VV, Zyuryaev IT, Khaspekova SG, Sirotkina OV, Ruda MY, and Mazurov AV. 2011. Glycoprotein IIb-IIIa content and platelet aggregation in healthy volunteers and patients with acute coronary syndrome. *Platelets.* 22:243-251.
8. Lentz BR. 2003. Exposure of platelet membrane phosphatidylserine regulates blood coagulation. *Prog Lipid Res.* 42:423-438.
9. Gailani D, and Renné T. 2007. Intrinsic pathway of coagulation and arterial thrombosis. *Arterioscler Thromb Vasc Biol.* 27:2507-2513.
10. Mackman N, Tilley RE, and Key NS. 2007. Role of the extrinsic pathway of blood coagulation in hemostasis and thrombosis. *Arterioscler Thromb Vasc Biol.* 27:1687-1693.
11. Franchini M, and Mannucci PM. 2011. Inhibitors of propagation of coagulation (factors VIII, IX and XI): a review of current therapeutic practice. *Br J Clin Pharmacol.* 72:553-562.
12. Ivanciu L, Krishnaswamy S, and Camire RM. 2014. New insights into the spatiotemporal localization of prothrombinase in vivo. *Blood.* 124:1705-1714.
13. Chernysh IN, and Weisel JW. 2008. Dynamic imaging of fibrin network formation correlated with other measures of polymerization. *Blood.* 111:4854-4861.
14. de Nucci G, Thomas R, D'Orleans-Juste P, Antunes E, Walder C, Warner TD, and Vane JR. 1988. Pressor effects of circulating endothelin are limited by its removal in the pulmonary circulation and by the release of prostacyclin and endothelium-derived relaxing factor. *Proc Natl Acad Sci U S A.* 85:9797-9800.
15. Anderson FA Jr, and Spencer FA. 2003. Risk factors for venous thromboembolism. *Circulation.* 107:I9-I16.
16. Kyrle PA, and Eichinger S. 2005. Deep vein thrombosis. *Lancet.* 365:1163-1174.
17. Kanitz MG, Giovannucci SJ, Jones JS, and Mott M. 1996. Myocardial infarction in young adults: risk factors and clinical features. *J Emerg Med.* 14:139-145.

18. Antithrombotic Trialists' Collaboration. 2002. Collaborative meta-analysis of randomized trials of antiplatelet therapy for prevention of death, myocardial infarction, and stroke in high risk patients. *BMJ*. 324:71-86.
19. Legrand VM, Serruys PW, Unger F, van Hout BA, Vrolix MC, Fransen GM, Nielsen TT, Paulsen PK, Gomes RS, de Queiroz e Melo JM, Neves JP, Lindeboom W, Backx B, and Arterial Revascularization Therapy Study (ARTS) Investigators. 2004. Three-year outcome after coronary stenting versus bypass surgery for the treatment of multivessel disease. *Circulation*. 109:1114-1120.
20. Merrill EW, and Pelletier GA. 1967. Viscosity of human blood: transition from Newtonian to non-Newtonian. *J Appl Physiol*. 23:178-182.
21. Atkinson B, Brocklebank MP, Card CCH, and Smith JM. 1969. Low Reynolds number developing flows. *AIChE J*. 15:548-553.
22. Safar ME, and Lacolley P. 2007. Disturbance of macro- and microcirculation: relations with pulse pressure and cardiac organ damage. *Am J Physiol Heart Circ Physiol*. 293:H1-7.
23. Lipowsky HH. 2005. Microvascular rheology and hemodynamics. *Microcirculation*. 12:5-15.
24. Banerjee RK, Back LH, Back MR, and Cho YI. 2003. Physiological flow analysis in significant human coronary artery stenosis. *Biorheology*. 40:451-476.
25. Parazynski SE, Hargens AR, Tucker B, Aratow M, Styf J, and Crenshaw A. 1991. Transcapillary fluid shifts in tissues of the head and neck during and after simulated microgravity. *J Appl Physiol*. 71:2469-2475.
26. Wiig H. 1990. Evaluation of methodologies for measurement of interstitial fluid pressure (Pi): physiological implications of recent Pi data. *Crit Rev Biomed Eng*. 18:27-54.
27. Stalker TJ, Traxler EA, Wu J, Wannemacher KM, Cermignano SL, Voronov R, Diamond SL and Brass LF. 2013. Hierarchical organization in the hemostatic response and its relationship to the platelet-signaling network. *Blood*. 121:1875-1885.
28. Diamond SL. 1999. Engineering design of optimal strategies for blood clot dissolution. *Annu Rev Biomed Eng*. 1:427-462.
29. Liu Y, Jennings NL, Dart AM, and Du XJ. 2012. Standardizing a simpler, more sensitive and accurate tail bleeding assay in mice. *World J Exp Med*. 2:30-36.
30. Correll JT, Lyth F, Long S, and Vanderpoel JC. 1952. Some physiologic responses to 5-hydroxytryptamine creatinine sulfate. *Am J Physiol*. 169:537-544.
31. Neeves KB, Maloney SF, Fong, KP, Schmaier AA, Kahn ML, Brass LF, and Diamond SL. 2008. Microfluidic focal thrombosis model for measuring murine platelet deposition and stability: PAR4 signaling enhances shear-resistance of platelet aggregates. *J Thromb Hemost*. 6:2193-2201.
32. Sakariassen KS, Bolhuis PA, and Sixma JJ. 1979. Human blood platelet adhesion to artery subendothelium is mediated by factor VIII-Von Willebrand factor bound to the subendothelium. *Nature*. 279:636-638.
33. Turitto VT, and Baumgartner HR. 1979. Platelet interaction with subendothelium in flowing rabbit blood: effect of blood shear rate. *Microvasc. Res*. 17:38-54.

34. Heldin CH, Rubin K, Pietras K, and Ostman A. 2004. High interstitial fluid pressure – an obstacle in cancer therapy. *Nat. Rev. Cancer.* 4:806-813.
35. Fukumura D, and Jain RK. 2007. Tumor microvasculature and microenvironment: targets for anti-angiogenesis and normalization. *Microvasc. Res.* 74:72-84.
36. Vickerman V, Blundo J, Chung S, Kamm RD. 2008. Design, fabrication and implementation of a novel multi parameter control microfluidic platform for three-dimensional cell culture and real-time imaging. *Lab Chip.* 8:1468-1477.
37. Neeves KB, and Diamond SL. 2008. A membrane-based microfluidic device for controlling the flux of platelet agonists into flowing blood. *Lab Chip.* 8:701-709.
38. Duffy DC, McDonald JC, Schueller OJA, and Whitesides GM. 1998. Rapid prototyping of microfluidic systems in poly(dimethylsiloxane). *Analytical Chemistry.* 70:4974-4984.
39. Smith SA, and Morrissey JH. 2004. Rapid and efficient incorporation of tissue factor into liposomes. *J Thromb Haemost.* 2:1155-1162.
40. Colace TV, Jobson J, and Diamond SL. 2011. Relipidated tissue factor linked to collagen surfaces potentiates platelet adhesion and fibrin formation in a microfluidic model of vessel injury. *Bioconjugate Chem.* 22:2104-2109.
41. Sudo R, Chung S, Zervantonakis IK, Vickerman V, Toshimitsu Y, Griffith LG, and Kamm RD. 2009. Transport-mediated angiogenesis in 3D epithelial coculture. *FASEB J.* 23:2155-2164.
42. Ramanujan S, Pluen A, McKee TD, Brown EB, Boucher Y, and Jain RK. 2002. Diffusion and convection in collagen gels: implications for transport in the tumor interstitium. *Biophys J.* 83:1650-1660.
43. Welsh JD, Colace TV, Muthard RW, Stalker TJ, Brass LF, and Diamond SL. 2012. Platelet-targeting sensor reveals thrombin gradients within blood clots forming in microfluidic assays and in mouse. *J. Thromb. Haemost.* 10:2344-2353.
44. Litvinov RI, Gorkun OV, Galanakis DK, Yakovlev S, Medved L, Shuman H, and Weisel JW. 2007. Polymerization of fibrin: direct observation and quantification of individual B:b knob-hole interactions. *Blood.* 109:130-138.
45. Kudryk B, Rohoza A, Ahadi M, Chin J, and Wiebe ME. 1984. Specificity of a monoclonal antibody for the NH₂-terminal region of fibrin. *Mol Immunol.* 21:89-94.
46. Muthard RW, and Diamond SL. 2012. Blood clots are rapidly assembled hemodynamic sensors: flow arrest triggers intraluminal thrombus contraction. *Arterioscler. Thromb. Vasc. Biol.* 32:2938-2945.
47. Wells Jr. RE, and Merrill EW. 1962. Influence of flow properties of blood upon viscosity-hematocrit relationships. *J. Clin. Invest.* 41:1591-1598.
48. Colace TV, Muthard RW, and Diamond SL. 2012. Thrombus growth and embolism on tissue factor bearing collagen surfaces under flow: role of thrombin with and without fibrin. *Arterioscler Thromb Vasc Biol.* 32:1466-1476.
49. Falati S, Gross P, Merrill-Skoloff G, Furie BC, and Furie B. 2002. Real-time in vivo imaging of platelets, tissue factor and fibrin during arterial thrombus formation in the mouse. *Nat. Med.* 8:1175-1180.
50. Hubbell JA, and McIntire LV. 1986. Platelet active concentration profiles near growing thrombi. A mathematical consideration. *Biophys. J.* 50:937-945.

51. Flamm MH, Colace TV, Chatterjee MS, Jing H, Zhou S, Jaeger D, Brass LF, Sinno T, and Diamond SL. 2012. Multiscale prediction of patient-specific platelet function under flow. *Blood*. 120:190-198.
52. Young EW, Watson MW, Srigunapalan S, Wheeler AR, and Simmons CA. 2010. Technique for real-time measurements of endothelial permeability in a microfluidic membrane chip using laser-induced fluorescence detection. *Anal. Chem.* 82:808-816.
53. Collet JP, Montalescot G, Lesty C, Soria J, Mishal Z, Thomas D, and Soria C. 2001. Disaggregation of in vitro preformed platelet-rich clots by abciximab increases fibrin exposure and promotes fibrinolysis. *Arterioscler. Thromb. Vasc. Biol.* 21:142-148.
54. Tedgui A, and Lever MJ. 1984. Filtration through damaged and undamaged rabbit thoracic aorta. *Am J Physiol.* 247:H784-791.
55. Drake TA, Morrissey JH, and Edgington TS. 1989. Selective cellular expression of tissue factor in human tissues. Implications for disorders of hemostasis and thrombosis. *Am. J. Pathol.* 134:1087-1097.
56. Manco-Johnson MJ, Abshire TC, Shapiro AD, Riske B, Hacker MR, Kilcoyne R, Ingram JD, Manco-Johnson ML, Funk S, Jacobson L, Valentino LA, Hoots WK, Buchanan GR, DiMichele D, Recht M, Brown D, Leissing C, Bleak S, Cohen A, Mathew P, Matsunaga A, Medeiros D, Nugent D, Thomas GA, Thompson AA, McRedmond K, Soucie JM, Austin H, and Evatt BL. 2007. Prophylaxis versus episodic treatment to prevent joint disease in boys with severe hemophilia. *N. Engl. J. Med.* 357:535-544.
57. Laurens N, Koolwij P, and De Maat MPM. 2006. Fibrin structure and wound healing. *J Thromb Haemost.* 4:932-939.
58. Jen CJ, and McIntrie LV. 1982. The structural properties and contractile force of a clot. *Cell Motil.* 2:445-455.
59. Lam WA, Chaudhuri O, Crow A, Webster KD, Li T, Kita A, Huang J, and Fletcher DA. 2011. Mechanics and contraction dynamics of single platelets and implications for clot stiffening. *Nat Mater.* 10:61-66.
60. Adelstein RS. 1982. Calmodulin and the regulation of the actin-myosin interaction in smooth muscle and nonmuscle cells. *Cell.* 30:349-350.
61. Suzuki Y, Yamamoto M, Wada H, Ito M, Nakano T, Sasaki Y, Narumiya S, Shiku H, and Nishikawa M. 1999. Agonist-induced regulation of myosin phosphatase activity in human platelets through activation of Rho-kinase. *Blood.* 93:3408-3417.
62. Haling JR, Monkley SJ, Critchley DR, and Petrich BG. 2011. Talin-dependent integrin activation is required for fibrin clot retraction by platelets. *Blood.* 117:1719-1722.
63. Leisner TM, and Parise LV. 2011. Talin's second activation: retraction. *Blood.* 117:1442-1443.
64. Zidansek A, Blinc A, Lahajnar G, Keber D, and Blinc R. 1995. Finger-like lysing patterns of blood clots. *Biophys J.* 69:803-809.
65. Spero RC, Sircar RK, Schubert R, Taylor II RM, Wolberg AS, and Superfine R. 2011. Nanoparticle diffusion measures bulk clot permeability. *Biophys J.* 101:943-950.

66. Beigi R, Kobatake E, Aizawa M, and Dubyak GR. 1999. Detection of local ATP release from activated platelets using cell surface-attached firefly luciferase. *Am J Phys - Cell Physiol.* 276:C267-C278.
67. De Caterina R, Giannessi D, Gazzetti P, and Bernini W. 1984. Thromboxane-B2 generation during *ex-vivo* platelet aggregation. *J Nuclear Med Allied Sci.* 28:185-196.
68. Johnson GJ, Leis LA, Krumwiede MD, and White JG. 2007. The critical role of myosin IIA in platelet internal contraction. *J Thromb Haemost.* 5:1516-1529.
69. Ogletree ML, Harris DN, Greenberg R, Haslanger MF, and Nakane M. 1985. Pharmacological Actions of SQ 29,548, A novel selective thromboxane antagonist. *J Pharmacol Exp Ther.* 234:435-441.
70. Maloney SF, Brass LF, and Diamond SL. 2010. P2Y₁₂ or P2Y₁ inhibitors reduce platelet deposition in a microfluidic model of thrombosis while apyrase lacks efficacy under flow conditions. *Integr Biol.* 2:183-192.
71. Brass L. 2010. Understanding and evaluating platelet function. *Hematology Am Soc Hematol Educ Program.* 2010:387-396.
72. Sabovic M, Lijnen HR, Keber D, and Collen D. 1989. Effect of retraction on the lysis of human clots with fibrin specific and non-fibrin specific plasminogen activators. *J Thromb Haemost.* 62:1083-1087.
73. Welsh JD, Stalker TJ, Voronov R, Muthard RW, Tomaiuolo M, Diamond SL, and Brass LF. 2014. A systems approach to hemostasis: 1. The interdependence of thrombus architecture and agonist movements in the gaps between platelets. *Blood.* 124:1808-1815.
74. Tomaiuolo M, Stalker TJ, Welsh JD, Diamond SL, Sinno T, and Brass LF. 2014. A systems approach to hemostasis: 2. Computational analysis of molecular transport in the thrombus microenvironment. *Blood.* 124:1816-1823.
75. Stalker TJ, Welsh JD, Tomaiuolo M, Wu J, Colace TV, Diamond SL, and Brass LF. 2014. A systems approach to hemostasis: 3. Thrombus consolidation regulates intrathrombus solute transport and local thrombin activity. *Blood.* 124:1824-1831.
76. Bray PF. 2007. Platelet hyperreactivity: predictive and intrinsic properties. *Hematol Oncol Clin North Am.* 21:633-645.
77. Chan MY, Andreotti F, and Becker RC. 2008. Hypercoagulable states in cardiovascular disease. *Circulation.* 118:2286-2297.
78. Colace TV, and Diamond SL. 2013. Direct observation of von Willebrand factor elongation and fiber formation on collagen during acute whole blood exposure to pathological flow. *Arterioscler Thromb Vasc Biol.* 33:105-113.
79. Chung DW, and Davie EW. 1984. Gamma and gamma' chains of human fibrinogen are produced by alternative mRNA processing. *Biochemistry.* 23:4232-4236.
80. Lovely RS, Moaddel M, and Farrell DH. 2003. Fibrinogen gamma' chain binds thrombin exosite II. *J Thromb Haemost.* 1:124-131.
81. Wolfenstein-Todel C, and Mosesson MW. 1980. Human plasma fibrinogen heterogeneity: evidence for an extended carboxyl-terminal sequence in a normal gamma chain variant (gamma'). *Proc Natl Acad Sci U S A.* 77:5069-73.

82. Fredenburgh JC, Stafford AR, Leslie BA, and Weitz JI. 2008. Bivalent binding to gamma/gamma'-fibrin engages both exosites of thrombin and protects it from inhibition by the antithrombin-heparin complex. *J Biol Chem.* 283:2470-2477.
83. Lovely RS, Rein CM, White TC, Jouihan SA, Boshkov LK, Bakke AC, McCarty OJ, and Farrell DH. 2008. gammaA/gamma' fibrinogen inhibits thrombin-induced platelet aggregation. *Thromb Haemost.* 100:837-846.
84. Moaddel M, Farrell DH, Daugherty MA, and Fried MG. 2000. Interactions of human fibrinogens with factor XIII: roles of calcium and the gamma' peptide. *Biochemistry.* 39:6698-6705.
85. Mosesson MW, Cooley BC, Hernandez I, Diorio JP, and Weiler H. 2009. Thrombosis risk modification in transgenic mice containing the human fibrinogen thrombin-binding gamma' chain sequence. *J Thromb Haemost.* 7:102-110.
86. Muthard RW, and Diamond SL. 2013. Side view thrombosis microfluidic device with controllable wall shear rate and transthrombus pressure gradient. *Lab Chip.* 13:1883-1891.
87. Lovely RS, Falls LA, Al-Mondhiry HA, Chambers CE, Sexton GJ, Ni H, and Farrell DH. 2002. Association of gamma/gamma' fibrinogen levels and coronary artery disease. *Thromb Haemost.* 88:26-31.
88. Sternberg SR. 1983. Biomedical Image Processing. *Computer.* 16:22-34.
89. Colace T, Falls E, Zheng XL, and Diamond SL. 2011. Analysis of morphology of platelet aggregates formed on collagen under laminar blood flow. *Ann Biomed Eng.* 39:922-929.
90. Zack GW, Rogers WE, and Latt SA. 1977. Automatic measurement of sister chromatid exchange frequency. *J Histochem Cytochem.* 25:741-753.
91. Harmison CR, Landaburu RH, and Seegers WH. 1961. Some physicochemical properties of bovine thrombin. *J Biol Chem.* 236:1693-1696.
92. de Graaf RA, van Kranenburg A, and Nicolay K. 2000. In vivo (31)P-NMR diffusion spectroscopy of ATP and phosphocreatine in rat skeletal muscle. *Biophys J.* 78:1657-1664.
93. Mannila MN, Lovely RS, Kazmierczak SC, Eriksson P, Samnegård A, Farrell DH, Hamsten A, and Silveira A. 2007. Elevated plasma gamma' concentration is associated with myocardial infarction: effects of variation in fibrinogen genes and environmental factors. *J Thromb Haemost.* 5:766-773.
94. Uitte de Willige S, de Visser MC, Houwing-Duistermaat JJ, Rosendaal FR, Vos HL, and Bertina RM. 2005. Genetic variation in the fibrinogen gamma gene increases the risk for deep venous thrombosis by reducing plasma fibrinogen gamma' levels. *Blood.* 106:4176-4183.
95. Wolberg AS. 2007. Thrombin generation and fibrin clot structure. *Blood Rev.* 21:131-142.
96. Baumgartner HR, Tschopp TB, and Meyer D. 1980. Shear rate dependent inhibition of platelet adhesion and aggregation on collagenous surfaces by antibodies to human factor VIII/von Willebrand Factor. *Br J Haematol.* 44:127-139.
97. Toschi V, Gallo R, Lettino M, Fallon JT, Gertz SD, Fernández-Ortiz A, Chesebro JH, Badimon L, Nemerson Y, Fuster V, and Badimon JJ. 1997. Tissue factor

- modulates the thrombogenicity of human atherosclerotic plaques. *Circulation*. 95:594-599.
98. Rein-Smith CM, Anderson NW, and Farrell DH. 2013. Differential regulation of fibrinogen γ chain splice isoforms by interleukin-6. *Thromb Res*. 131:89-93.
 99. Ridker PM, Rifai N, Stampfer MJ, and Hennekens CH. 2000. Plasma concentration of interleukin-6 and the risk of future myocardial infarction among apparently healthy men. *Circulation*. 101:1767-1772.
 100. Furie B, and Furie BC. 2005. Thrombus formation in vivo. *J Clin Invest*. 115:3355-3362.
 101. Watson SP, and Harrison P. 2010. The Vascular Function of Platelets. In: Hoffbrand AV, Catovsky D, Tuddenham EGD, Green AR, editors. *Postgraduate Haematology*. U.K.: John Wiley & Sons; p. 772-792.
 102. Hoeltke LB. 2012. *Phlebotomy Procedures and Practices*. Connecticut: Cengage Learning.
 103. Quick AJ, Stanley-Brown M, and Bancroft FW. 1934. A study of the coagulation defect in hemophilia and in jaundice. *Am J Med Sci*. 190:501-510.
 104. Langdell RD, Wagner RH, and Brinkhous KM. 1953. Effect of antihemophilic factor on one-stage clotting tests; a presumptive test for hemophilia and a simple one-stage antihemophilic factor assay procedure. *J Lab Clin Med*. 41:637-647.
 105. Roest M, Reininger A, Zwaginga JJ, King MR, and Heemskerk JWM. 2011. Biorheology Subcommittee of the SSC of the ISTH. Flow chamber-based assays to measure thrombus formation in vitro: requirements for standardization. *J Thromb Haemost*. 9: 2322-2324.
 106. Mammen EF, Comp PC, Gosselin R, Greenberg C, Hoots WK, Kessler CM, Larkin EC, Liles D, and Nugent DJ. 1998. PFA-100 system: a new method for assessment of platelet dysfunction. *Semin Thromb Hemost*. 24:195-202.
 107. Baurand A, Raboisson P, Freund M, Léon C, Cazenave JP, Bourguignon JJ, and Gachet C. 2001. Inhibition of platelet function by administration of MRS2179, a P2Y1 receptor antagonist. *Eur J Pharmacol*. 412:213-221.
 108. Galambos P, and Forster FK. 1998. Micro-Fluidic diffusion coefficient measurement. In: Harrison DJ, van den Berg A, editors. *Micro Total Analysis Systems*. Dordrecht: Kluwer Academic Publishers; p. 189-192.
 109. Muramatsu N, and Minton AP. 1988. Tracer diffusion of globular proteins in concentrated protein solutions. *PNAS*. 85: 2984-2988.
 110. Vanýsek P. 2012. Ionic conductivity and diffusion at infinite dilution. In: Haynes WM, editor. *CRC Handbook of Chemistry and Physics*. Boca Raton: CRC Press; p. 5-77-79.
 111. Squires TM, and Quake SR. 2005. Microfluidics: fluid physics on the nanoliter scale. *Rev Mod Phys*. 77:977-1026.
 112. Mann KG, Whelihan MF, Butenas S, and Orfeo T. 2007. Citrate anticoagulation and the dynamics of thrombin generation. *J Thromb Haemost*. 5:2055-2061.
 113. Rand MD, Lock JB, van't Veer C, Gaffney DP, and Mann KG. 1996. Blood clotting in minimally altered whole blood. *Blood*. 88:3432-3445.
 114. Hanson SR, and Tucker EI. 2012. Blood coagulation and blood-materials interactions. In: Ratner BD, Hoffman AS, Schoen FJ, Lemons JE, editors.

- Biomaterials Science: An Introduction to Materials in Medicine. U.K.: Academic Press; p. 551-557.
115. Lee C, Chang C, Wang Y, and Fu L. 2011. Microfluidic mixing: a review. *Int J Mol Sci.* 12:3263-3287.
 116. Nordin M, and Laurell T. 2012. Two-hundredfold volume concentration of dilute cell and particle suspensions using chip integrated multistage acoustophoresis. *Lab Chip.* 12:4610-4616.
 117. Soohoo JR, and Walker GM. 2009. Microfluidic aqueous two phase system for leukocyte concentration from whole blood. *Biomed Microdevices.* 11: 323-329.
 118. Ferrara A, MacArthur JD, Wright HK, Modlin IM, and McMillen MA. 1990. Hypothermia and acidosis worsen coagulopathy in the patient requiring massive transfusion. *Am J Surg.* 160:515-518.
 119. Dirkmann D, Hanke AA, Görlinger K, and Peters J. 2008. Hypothermia and acidosis synergistically impair coagulation in human whole blood. *Anesth Analg.* 106:1627-1632.
 120. Baskurt OK, and Meiselman HJ. 2003. Blood rheology and hemodynamics. *Semin Thromb Hemost.* 29:435-450.
 121. Baskurt OK, Temiz A, and Meiselman HJ. 1997. Red blood cell aggregation in experimental sepsis. *J Lab Clin Med.* 130:183-190.
 122. Baskurt OK, Gelmont D, and Meiselman HJ. 1998. Red blood cell deformability in sepsis. *Am J Respir Crit Care Med.* 157:421-427.
 123. Cines DB, Lebedeva T, Nagaswami C, Hayes V, Masefski W, Litvinov RI, Rauova L, Lowery TJ, and Weisel JW. 2014. Clot contraction: compression of erythrocytes into tightly packed polyhedral and redistribution of platelets and fibrin. *Blood.* 123:1596-1603.
 124. Schmitt A, Guichard J, Masse JM, Debili N, and Cramer EM. 2001. Of mice and men: comparison of the ultrastructure of megakaryocytes and platelets. *Exp Hematol.* 29:1295-1302.
 125. Craig A, Mai J, Cai S, and Jeyaseelan S. 2009. Neutrophil recruitment to the lungs during bacterial pneumonia. *Infect Immun.* 77:568-575.
 126. Smart SJ, and Casale TB. 1994. Pulmonary epithelial cells facilitate TNF-alpha-induced neutrophil chemotaxis. A role for cytokine networking. *J Immunol.* 152:4087-4097.
 127. Li Jeon N, Baskaran H, Dertinger SK, Whitesides GM, Van de Water L, and Toner M. 2002. Neutrophil chemotaxis in linear and complex gradients of interleukin-8 formed in a microfabricated device. *Nat Biotechnol.* 20:826-830.
 128. Andonegui G, Kerfoot SM, McNagny K, Ebbert KV, Patel KD, and Kubes P. 2005. Platelets express functional Toll-like receptor-4. *Blood.* 106:2417-2423.
 129. Clark SR, Ma AC, Tavener SA, McDonald B, Goodarzi Z, Kelly MM, Patel KD, Chakrabarti S, McAvoy E, Sinclair GD, Keys EM, Allen-Vercoe E, Devinney R, Doig CJ, Green FH, and Kubes P. 2007. Platelet TLR4 activates neutrophil extracellular traps to ensnare bacteria in septic blood. *Nat Med.* 13:463-469.
 130. Fuchs TA, Brill A, and Wagner DD. 2012. Neutrophil extracellular trap (NET) impact on deep vein thrombosis. *Arterioscler Thromb Vas Biol.* 32:1777-1783.

131. Yoshimura T, Matsushima K, Oppenheim JJ, and Leonard EJ. 1987. Neutrophil chemotactic factor produced by lipopolysaccharide (LPS)-stimulated human blood mononuclear leukocytes: partial characterization and separation from interleukin 1 (IL 1). *J Immunol.* 139:788-793.
132. Lomas DA, Stone SR, Llewellyn-Jones C, Keogan MT, Wang ZM, Rubin H, Carrell RW, and Stockley RA. 1995. The control of neutrophil chemotaxis by inhibitors of cathepsin G and chymotrypsin. *J Biol Chem.* 270:23437-23443.
133. Cicchetti G, Allen PG, and Glogauer M. 2002. Chemotactic signaling pathways in neutrophils: from receptor to actin assembly. *Crit Rev Oral Biol Med.* 13:220-228.
134. Zhu J, Nathan C, Jin W, Sim D, Ashcroft GS, Wahl SM, Lacomis L, Erdjument-Bromage H, Tempst P, Wright CD, and Ding A. 2002. Conversion of proepithelin to epithelins: roles of SLPI and elastase in host defense and wound repair. *Cell.* 111:867-878.